universität wien

MASTERARBEIT / MASTER'S THESIS

Titel der Masterarbeit / Title of the Master's Thesis

„Effects of catalytic inactivation of HDAC1 on skin homeostasis and immunity“

verfasst von / submitted by

Patrick Wagner

angestrebter akademischer Grad / in partial fulfilment of the requirements for the degree of

Master of Science (MSc)

Wien, 2022 / Vienna, 2022

Studienkennzahl lt. Studienblatt / degree programme code as it appears on the student record sheet:	UA 066 834
Studienrichtung lt. Studienblatt / degree programme as it appears on the student record sheet:	Masterstudium Molekulare Biologie
Betreut von / Supervisor:	ao. Univ.-Prof. Dr. Christian Seiser

In Honour of all the mice sacrificed for science

Acknowledgement

An erster Stelle möchte ich mich bei meinem Betreuer Christian Seiser für die Möglichkeit und das Vertrauen, an diesem interessanten Projekt zu arbeiten, bedanken. Es hat mir viel Freude bereitet, Teil deiner Laborgruppe zu werden und mit dir zu arbeiten. Vielen Dank für deine durchgehende Motivation und deinen Optimismus, wenn etwas mal nicht geklappt hat – das war ansteckend. Vielen Dank an meinen hervorragenden Supervisor Heinz Fischer, der mir immer mit Geduld, Hilsbereitschaft, Verständnis und Humor zur Seite stand, wenn etwas nicht geklappt hat. Ich bin sehr dankbar für das viele fachliche, theoretische und praktische Wissen, das du mir vermittelt hast und für die gemeinsam verbrachten Mittagspausen und Gespräche zwischendurch, die mir immer viel Freude bereitet haben.

I would also like to thank the whole Seiser Lab group for being such nice people that always have an open ear and are always willing to help. Thank you to my office collegues Jelena and Gülnihal for all the fun and interesting conversations and the motivation on long days. A big thank you also goes to Martha, Terka, Natalija and Lena for always being helpful and very supportive in all regards. A special thanks goes to Kristelli, Michaela, Tom and Fatinah for their amazing friendship and the fun coffee breaks, friday evenigs and scientific and not-so scientific discussions that made this experience even more fun.

Ein großer Dank geht an meinen besten Freund, Mitbewohner und quasi schon Bruder, Janik. Danke für deine Freundschaft, deine Unterstützung, unsere fachlichen Diskussionen und die nötige Ablenkung, wenn ich festgefahren war.

Ein ganz besonderer Dank geht an Elli, meine größte Unterstüzung während des gesamten Studiums. Vielen Dank für dein großes Verständnis und deine ewige Geduld. Danke für deine immer motivierenden Worte, deine Fähigkeit mich aufzubauen und deine unendlich liebvolle Untersützung. Ohne euch wären die letzten Jahre schwerer und nur halb so lustig gewesen.

Und zu guter Letzt gilt der größte Dank meinen Eltern für ihre bedigungslose Liebe, für ihre fortwehrende Unterstützung in jeglicher Hinsicht und ihre Geduld mit mir. Vielen Dank, dass ihr mir diese tolle Zeit des Studiums ermöglicht habt und mir immer mit Rat und Tat zur Seite steht.

Abstract in English

As an important element of epigenetic expression regulation, dynamic histone acetylation and deacetylation plays a crucial role in many cellular and developmental processes such as cell-cycle regulation, stem cell pluripotency maintenance and differentiation. While acetylation is carried out by histone acetyl transferases (HATs), deacetylation is performed by so-called histone deacetylases (HDACs). Acetylation patterns on histones within the chromatin establish a dynamic code, which can be interpreted by certain reader proteins, which in turn can trigger further downstream actions like binding of chromatin remodelling complexes or co-repressor complexes. These complexes can then further enhance or downregulate the transcription of chromatin regions. The class I deacetylases HDAC1 and HDAC2 are located in the cell nucleus in distinct multiprotein complexes that are highly conserved. They are highly similar enzymes, which can deacetylate histones and non-histone targets with different biological implications and to some extent can compensate for the function of each other. Previous studies on the knockout of *Hdac1* and *Hdac2* in the murine epidermis demonstrated that a single allele of *Hdac1,* but not *Hdac2* is sufficient for correct epidermal development and that HDAC1 appears to have essential scaffolding functions for certain co-repressor complexes. Since deregulation of HDAC1 and HDAC2 has previously been shown to be involved in several different disease models, and since HDAC inhibitors are already being used to treat some tumours and certain diseases it is crucial to further dissect their specific and overlapping roles. To improve our knowledge about specific catalytic and structural functions of HDAC1, we aimed to characterize the epidermal phenotype of mice with epidermis-specific knockout of HDAC1 and mice additionally expressing different catalytically inactive variants of HDAC1 from the Rosa26 genomic locus. Mice expressing catalytically inactive HDAC1 H141A ($HDAC1^{Ci}$), which still enables co-repressor complex formation were compared with animals expressing inactive HDAC1 S421A, S423A ($HDAC1^{2S}$), which lacks the ability to be incorporated into their complexes. Here we could show that epidermal expression of $HDAC1^{Ci}$ in murine keratinocytes in the epidermal *Hdac1* knockout background resulted in an apparent skin phenotype with differentiation and proliferation defects as well as activation of the immune system, which interestingly correlates with a defective epidermal barrier. In contrast, epidermis-specific knockout of HDAC1 alone or replacement by $HDAC1^{2S}$ revealed no skin abnormalities. Thus, our data demonstrate the importance of HDAC1´s catalytic function for proliferation and differentiation processes of keratinocytes, as well as a crucial role for HDAC1 in proper epidermal barrier formation. In addition, it can be assumed, that the incorporation of inactive HDAC1 into multi-enzyme complexes is crucial for the functional impairment of epidermal homeostasis and thus for the development of a skin pathology.

Zusammenfassung

Als ein wichtiges Element der epigenetischen Expressionsregulation spielt die dynamische Histonacetylierung und -deacetylierung eine wichtige Rolle in vielen zellulären und entwicklungsspezifischen Prozessen wie der Zellzyklusregulation, der Erhaltung der Pluripotenz von Stammzellen und der Differenzierung. Während die Acetylierung von Histonen von Histonacetyltransferasen (HATs) durchgeführt wird, wird die Deacetylierung von sogenannten Histondeacetylasen (HDACs) übernommen. Die dabei entstehenden Acetylierungsmuster im Chromatin ergeben einen Code, der von bestimmten so genannten Reader-Proteinen gelesen und interpretiert werden kann. Dies kann zur Bindung von anderen Proteinkomplexen wie Chromatin-Remodelling-Komplexen oder Co-Repressor-Komplexen führen. Diese Komplexe können dann die Transkription der gebundenen Chromatinregion hoch- oder runterregulieren. Die Class I Deacetylasen HDAC1 und HDAC sind in bestimmten hoch konservierten Multiproteinkomplexen innerhalb des Zellkerns lokalisiert. Diese sehr ähnlichen Enzyme deacetylieren verschiedene Histon- und Nicht-Histon-Proteine mit unterschiedlichen biologischen Implikationen und können bis zu einem gewissen Grad die Funktionen des jeweils anderen kompensieren. Frühere Studien über den Knockout von HDAC1 und HDAC2 in der Epidermis der Maus haben gezeigt, dass ein einzelnes Allel von HDAC1, aber nicht von HDAC2, für eine korrekte epidermale Entwicklung genügt und dass HDAC1 anscheinend essentielle Gerüstfunktionen für bestimmte Co-Repressor-Komplexe hat. Da gezeigt wurde, dass die Deregulation von HDAC1 und HDAC2 eine Rolle in verschiedenen Krankheitsmodellen spielt und weil HDAC-Inhibitoren bereits zur Behandlung von bestimmten Tumoren und Krankheiten genutzt werden, ist es essentiell, ihre spezifischen und redundanten Funktionen zu untersuchen. Um unser Wissen über spezifische katalytische und strukturelle Funktionen von HDAC1 zu erweitern, war das Ziel dieser Arbeit die Charakterisierung des epidermalen Phänotyps von Mäusen mit einem epidermis-spezifischen Knockout von *Hdac1* und der zusätzlichen Expression von verschieden katalytisch-inaktiven Varianten von HDAC1 vom genomischen Rosa26-Lokus. Mäuse, die katalytisch inaktives HDAC1 H141A ($HDAC1^{Ci}$) exprimieren, welches die Formation von Komplexen noch ermöglicht, wurden mit Mäusen verglichen, die die ebenfalls katalytisch inaktive HDAC1 S421A, S423A ($HDAC1^{2S}$) Variante exprimieren, welche nicht mehr zur Komplexformation fähig ist. Wir konnten zeigen, dass die epidermale Expression von $HDAC1^{Ci}$ in Keratinozyten von Mäusen mit einem zusätzlichem epidermalen HDAC1 Knockout in Keratinozyten zu einem offensichtlichen Hautphänotyp mit Proliferations und Differenzierungsdefekten führt. Außerdem kommt es zu einer Aktivierung des Immunsystems, die mit einer defekten epidermalen Barriere korreliert. Im Gegensatz dazu zeigte der epidermisspezifische Knockout von *Hdac1* alleine oder der Austausch durch $HDAC1^{2S}$ keine

Veränderungen der Haut. Unsere Daten zeigen zum einen die Bedeutung der katalytischen Aktivität von HDAC1 für die Proliferation und Differenzierung von Keratinozyten und zum anderen die wichtige Rolle von HDAC1 in der korrekten Entwicklung der epidermalen Barriere. Zusätzlich ist anzunehmen, dass die Inkorporation von katalytisch inaktivem HDAC1 in Multi-Protein-Komplexen entscheidend für die funktionale der epidermalen Homöostase und daher auch für die Entwicklung bestimmter Hautpathologien ist.

Contents

1. Introduction

1.1 Epigenetics

In a multicellular organism the genomic DNA sequence of the vast majority of cells is identical but during development of a complex organism, a multitude of different distinct cell types with different functions and distinct gene expression patterns are necessary (Felsenfeld, 2014). How does an organism accomplish this variety of distinct cell types, tissues and organs?

The term *Epigenetics* was originally defined by Conrad Hal Waddington as "the branch of biology which studies the causal interaction between genes and their products, which bring the phenotype into being" (Waddington, 1942). Since then the knowledge about this complex cellular developmental process from genotype to a distinct phenotype has greatly improved and has led to a new working definition of epigenetics as "the study of mitotically and/or meiotically heritable changes in gene function that are not caused by changes in DNA sequence" (Waterland, 2006). Epigenetic alterations enable cells to establish lineage type-specific gene transcription profiles by different modifications on DNA bases, DNA-associated proteins and histone protein complexes that can be inherited throughout mitosis (Dupont et al., 2009). Recent research has shown an influence of a broad range of environmental factors (e.g. stress, diet, infections, chemicals, drugs and even social environment) on the epigenetic landscape of cells as well as a heredity of certain acquired epigenetic modifications across generations (Cavalli & Heard, 2019). Furthermore, it was shown that dysregulations in the epigenome can contribute to the emergence of pathologies and have been implied in a variety of different diseases including cancer, autoimmune diseases, neurological disorders and cardiovascular diseases (Portela & Esteller, 2010a). Especially in cancer it was shown that epigenetic changes can culminate in tumour development (Dawson & Kouzarides, 2012). Epigenetic modifications are reversible and can therefore be valuable targets for therapeutic approaches using drugs targeting epigenetic mechanisms. The FDA approved the first epigenetic drug in 2006 (Vorinostat) and has since then approved several other epigenetic drugs mainly to treat certain types of cancer. With the development of more specifically targeted epigenetic therapies it might be possible to reverse or prevent pathological phenotypes in the future (Heerboth et al., 2014). However, the complex interplay of epigenetic mechanisms, their influence on the development of a specific phenotype and their involvement in pathogenesis are still far from being completely understood. Therefore, more basic and applied medical research is needed in order to fully understand and utilize epigenetics to develop novel therapeutical approaches.

1.2 Chromatin structure

Chromatin describes the complex of DNA and its associated protein scaffold. Epigenetic modifications form a complex network that can modulate the packaging of the genome and the accessibility of DNA by changing the chromatin structure (Bernstein et al., 2007). In eukaryotes, the main components of chromatin are called nucleosomes. They are composed of 147 bp of DNA which wrap around an octamer of histone proteins. Every octamer comprises two copies of each of the highly conserved, positively charged histone proteins H3, H2A, H2B and H4 (Volle & Dalal, 2014). The positive charge allows the negatively charged phosphate groups of the DNA's nucleotides to bind to the histone complex. These nucleosomes can then be stacked on another by help of a fifth histone protein, the linker histone H1. H1 engages with the "free" DNA between the nucleosomes and the histone octamers, enabling them to form stacks of nucleosomes and compacting the size of the DNA (Alberts et al., 2014). However, this level of compaction is not sufficient to fit the entire DNA into the nucleus of a cell. With help of other non-histone proteins, the stacked nucleosomes can be further folded into secondary and tertiary structures to form a 30nm thick, so called, chromatin fibre. During mitosis these chromatin fibres can be further condensed to form the highest level of chromatin compaction, a mitotic chromosome (Klug et al., 2019).

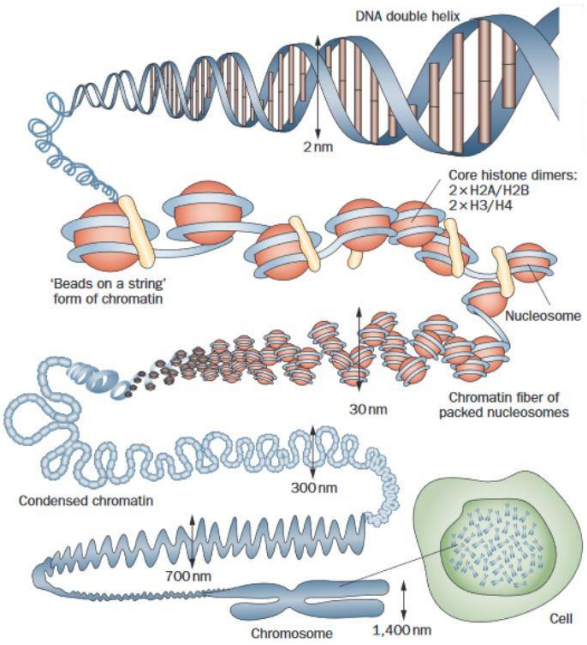

Figure 1: Structural organisation of eukaryotic chromatin. Double helical DNA wraps almost twice around a nucleosome, forming a "beads on a string" structure. Further compaction and stacking of nucleosomes results in 30nm thick chromatin fibre which can be even more condensed to finally form to most compacted form chromatin, the chromosome. (Tonna et al., 2010)

The loosening and compaction of chromatin is a highly dynamic process and is altered according to the individual requirements of the cell. For instance, in proliferating cells the condensation level changes throughout the cell cycle progression with loosely packed chromatin during interphase and maximally condensed during mitosis (Saksouk et al., 2015). Besides cell cycle related changes in chromatin condensation, chromatin states also vary between cell-types to establish a specific transcriptional program (Kouzarides, 2007).

However, there are two main chromatin condensation states describing the transcriptional activity of a certain chromosomal domain. Euchromatin describes loosely packed and therefore more accessible regions of DNA and is mainly associated with transcriptional activity. Heterochromatin on the other hand consists of tightly packed nucleosomes restricting access to the DNA rendering these regions transcriptionally inert (Allis & Jenuwein, 2016). Some regions of chromatin are always highly condensed regardless of the cell type. These regions are called constitutive heterochromatin and function as silencers of gene poor areas and repetitive sequences at pericentromeric regions and telomeres and provide structural chromosomal stability (Saksouk et al., 2015). The dynamic process of condensing and opening the chromatin is influenced and regulated by many different epigenetic mechanisms acting on DNA or histones to control the accessibility of the DNA (Kouzarides, 2007).

1.3 Epigenetic mechanisms

Over the past decades four different groups of epigenetic mechanisms have been identified, each capable of stably altering gene expression patterns and/or transmitting the alterations during mitosis. DNA methylation, RNA-based mechanisms, histone modifications and chromatin remodelling processes (Gibney & Nolan, 2010). All these mechanisms form a highly interconnected regulatory network to control cellular processes like transcription, differentiation, DNA replication and DNA-repair (Kouzarides, 2007).

1.3.1 DNA methylation

One of the best understood and most widely studied epigenetic alterations is the methylation of the 5`-position of a cytosine within the DNA to 5-methylcytosine (5mC). In mammals inheritable DNA methylation is restricted to cytosines preceding guanine nucleotides or CpG sites (Gibney & Nolan, 2010). In general, the mammalian genome is highly depleted from CpG dinucleotides (~1%) which might be due to 5mCs high mutagenic potential (Moore et al., 2013) . Additionally, in mammalian somatic tissue around 80% of all CpG sites within the DNA are methylated (E. Li &

Zhang, 2014). The remaining CpG`s tend to form clusters in regions called CpG islands (CGIs) which are sections of DNA with an overall higher density of CpG`s and a G+C content of at least 50% and an observed to expected ratio higher than 60%. These CGIs are often not methylated and are associated with about 60-70% of gene promotors of the mammalian genome and seem to generate a chromatin structure favourable for gene expression (Portela & Esteller, 2010a). However, during development and differentiation some CGIs are highly methylated which results in stable silencing of gene expression, which is important for processes like X-chromosome inactivation in females and parental imprinting (J. K. Kim et al., 2008). In general, DNA methylation is associated with silencing of genomic regions by interfering with the binding of transcription factors or recruiting methyl-CpG-binding domain (MBD) proteins, which in turn can recruit other co-repressor complexes (Portela & Esteller, 2010a). Another function of DNA methylation is the silencing of transposable and viral elements that reside in the intergenic regions of mammalian genomes and are potentially harmful when they are expressed (Moore et al., 2013).

Methylation marks on DNA are established during embryonic development by *de novo* methyl transferases DNMT3a and DNMT3b. During replication these methylation marks must be copied onto the newly synthesized daughter strand of DNA to stably inherit silenced regions throughout cell division. This task is accomplished by another methyltransferase called DNMT1 which has a preference for hemimethylated DNA and copies the methylation pattern from the parental strand to the newly synthesized strand. Dysregulations in DNA methylation patterns are associated with many diseases and are especially common in cancer (E. Li & Zhang, 2014).

1.3.2 RNA based mechanisms

RNA based mechanisms for epigenetic modifications are less well understood but are also key regulators of chromatin structure and transcription in eukaryotic cells. Most of the known mechanisms are carried out via non-coding RNAs (ncRNAs) but it was shown that even some mRNAs seem to be able to recruit chromatin modifying complexes (Holoch & Moazed, 2015). There are small ncRNAs that can target gene expression at post-transcriptional level via RNA interference pathways like microRNAs (miRNAs) or short interfering RNAs (siRNAs) and they can act as scaffolds for large chromatin remodelling complexes like the RNA-induced transcriptional silencing (RITS) complex (Gibney & Nolan, 2010) (Holoch & Moazed, 2015). Long ncRNAs (lncRNAs) can also act as scaffolds for chromatin modifiers like the lncRNA *Xist,* which play a crucial role in the inactivation of the X-chromosome in mammals by recruiting the polycomp repressive complex 2 (PCR2) to the inactive X-Chromosome in females (Holoch & Moazed, 2015). Recent research found that lncRNAs can also have activating roles via recruitment of co-activator complexes and

by mediating chromatin looping to bring the enhancers and promotors into proximity (Holoch & Moazed, 2015).

1.3.3 Histone variants

Another layer of epigenetic transcription control is based on the nucleosomal structure of chromatin. Besides the four core histones H3, H2A, H2B and H4 a range of variants of these histones were found that have specialized properties for certain tasks. These histone variants are synthesized independently of replication and only vary in a few amino acids (Biterge & Schneider, 2014). Furthermore, they differ in their mode of integration into the chromatin. The normal core histones are incorporated between old nucleosomes during replication whereas histone variants replace a histone in an already assembled nucleosome. This has the potential to change the local chromatin state and therefore potentially changing transcriptional activity, altering the pattern of posttranslational modifications or changing the epigenetic memory (Volle & Dalal, 2014) (Henikoff & Smith, 2015). Some histone variants are known to be incorporated at specific genomic sites like the H3 variant CENP-A which is exclusively present in centromeric regions of chromosomes and is essential for propagation and maintenance of the centromere (Henikoff & Smith, 2015). In mammals there are three major H2A variants. H2A.X occurs at DNA damage sites and has a serine residue which can be phosphorylated upon DNA damage signalling and subsequently recruits the DNA damage repair machinery as well as chromatin remodellers (Biterge & Schneider, 2014). H2A.Z regulates nucleosomal depletion by destabilizing the interaction of the histone proteins and promotes gene activation in differentiating cells (Zhaoyu Li et al., 2012). MacroH2A is associated with more stable, digestion resistant nucleosomes and more compact chromatin (Biterge & Schneider, 2014).

1.3.4 Histone post-translational modifications and chromatin remodelling complexes

Histones can not only be switched out for more specialized variants but they can also be covalently modified at their flexible N- or C-terminal tails by a plethora of posttranslational modifications (PTMs) like acetylation, methylation, phosphorylation, ubiquitination and many more (Biterge, 2016). These PTMs can alter the chemical nature of the histones and therefore change the histone interactions with DNA and other nucleosomes to increase the dynamic accessibility of DNA. The chemical modifications can be dynamically added and removed by specific histone modifying enzymes (Bowman & Poirier, 2015). Additionally, PTMs serve as signals or binding platforms for other non-histone protein complexes which can have chromatin remodelling properties that recognize and bind the specific histone marks via designated domains. The epigenetic landscape established by the histone marks is crucial for the correct distribution of the non-histone proteins

to further modify the chromatin structure (Kouzarides, 2007). These chromatin remodelling complexes are large multiprotein complexes which hydrolyse ATP to manipulate the chromatin structure by sliding, ejecting, exchanging or restructuring nucleosomes. This process is essential to permit or restrict transcription factor binding sites and the assembly of the transcription machinery (Portela & Esteller, 2010). Therefore, PTMs can not only influence site specific transcription profiles but can also affect many other nuclear processes like DNA-repair, replication or recombination and are responsible for the right assembly of higher chromatin structures via recruitment of chromatin remodelling complexes. It is important to note that not a single mark determines the chromatic changes, but the sum of modifications at a certain site to a certain time, determine which kind of proteins are recruited to modulate the chromatin at that specific site (Kouzarides, 2007) (Bannister & Kouzarides, 2011).

1.3.4.1 Histone methylation

The addition of methyl groups onto lysine, arginine or histidine residues of histones is one of the most prominent histone PTMs resulting in transcriptional silencing or activation. Another layer of complexity is added to this modification since the different residues can have multiple different methylation sites e.g. lysine can be mono,-di- or tri-methylated, whereas arginine can be mono-, and symmetrically or asymmetrically di-methylated (Bannister & Kouzarides, 2011). The transfer of the methyl group(s) is facilitated by histone methyltransferases that utilize S-adenosyl methionine (SAM) as the methyl-group donor. Recent research also found demethylases removing methyl groups from histones implicating methylation to also be a dynamic mark (Biterge, 2016). Compared to other PTMs histone methylation does not act by changing the chemical charge of the histone residues but by establishing a specific methylation code which can act repressive or activating. For instance, while the trimethylation at lysine 4 on histone 3 (H3K4me3) is an active mark the same modification on lysine 9 (H3K9me3) and 27 (H3K27me3) marks repressed expression (Biterge, 2016). These specific methylation marks can be bound by effector proteins containing chromodomains that can “read” the methylation pattern and then further recruit chromatin modifying complexes and amplify repressive or activating processes (Greer & Shi, 2012).

1.3.4.2 Histone phosphorylation

The phosphorylation of histones mainly takes place on serine, threonine and tyrosine residues on the N-terminal histone tails (Sawicka & Seiser, 2012). The phosphate groups are added by kinases hydrolysing ATP and removed by phosphatases. The covalent binding of a phosphate group adds a significant negative charge to the histone which can directly influence the chromatin structure

around it (Bannister & Kouzarides, 2011). Since the DNA backbone is negatively charged an additional negative charge on a histone loosens the association of DNA with the histone. Histone phosphorylation has been associated with multiple different cellular processes like apoptosis, cell cycle progression, DNA repair, developmental gene regulation and chromosome condensation (Ramazi et al., 2020). The phosphorylation of histone can also have both, repressive or activating properties for transcription. For instance, the phosphorylation of histone 3 on serine 10 (H3S10ph) can disrupt the interaction of the repressive heterochromatin protein 1 (HP1) with the repressive mark H3K9me3 and therefore activate transcription but H3S10ph has also been associated with chromatin condensation during mitosis (Sawicka & Seiser, 2014).

1.3.4.2 Ubiquitination and sumoylation

Compared to the small chemical changes of histones by mechanisms like phosphorylation, methylation and acetylation, ubiquitination and sumoylation add larger polypeptides to the histones resulting in a larger covalent modification (Bannister & Kouzarides, 2011). Ubiquitin and SUMO are relatively small proteins with high resemblance in their three-dimensional structure and can bind on lysine residues of their target proteins. Both proteins attach to their targets *via* an enzymatic cascade involving three enzymes: an activating enzyme (E1), a conjugative enzyme (E2) and a ligating enzyme (E3). This histone modification is also highly dynamic and reversible as SUMO can be detached by a sumo-specific protease and ubiquitin can be removed by deubiquitinating enzymes (Ramazi et al., 2020). Histone ubiquitination was shown to play an important role in both transcriptional silencing and activation, whereas histone sumoylation is mainly associated with transcriptional repression (Bannister & Kouzarides, 2011).

1.3.4.3 Histone acetylation and deacetylation

Dynamic histone acetylation and deacetylation adds another important element to epigenetic expression regulation. The addition or removal of a positively charged acetyl-group to lysine residues of a histone results in a change of the net histone charge. Adding an acetyl group to the histone residue can lead to the repulsion of the negatively charged DNA and thereby to the opening of the chromatin structure, whereas removal of an acetyl-group leads to a tighter bond between the histone and the DNA as illustrated in figure 2. This directly changes the accessibility of the DNA for the RNA polymerase II, transcription factors and co-factors (Chen et al., 2015). Histone acetylation also contributes to the epigenetic code established by all the different modifications on DNA, histones and other associated proteins. Acetylated lysine's can be recognized and bound by bromodomain containing chromatin remodelling complexes to further establish the desired chromatin state (B. Li et al., 2007) (Bannister & Kouzarides, 2011). This highly

dynamic process is facilitated by two different protein families. Histone acetyltransferases (HATs) catalyse the transfer of an acetyl group onto a histone, utilising acetyl-CoA as a cofactor. Nuclear A-type HATS include three different families GNAT, MYST and CBP/p300 which are classified based on their sequence homology (Hodawadekar & Marmorstein, 2007). They are similar in their core for substrate binding but otherwise display distinct differences in substrate specificity and biologic activities. Many HATS are recruited and guided by multiprotein complexes with chromatin remodelling properties (Hodawadekar & Marmorstein, 2007). The removal of acetyl groups from the histone tails is facilitated by Histone deacetylases (HDACs). HDACs are subdivided into four classes based on their homology with yeast enzymes: Class I includes the Rpd3-like HDAC1, 2(discussed in detail in 1.4) 3 and 8; class II consists of the Hda-related enzymes HDAC4, 5, 6, 7 and 9; class III are structurally and mechanistically unrelated to the other HDACs and play an important role in metabolic processes while class IV only consists of HDAC11 (Zhiming Li & Zhu, 2014).

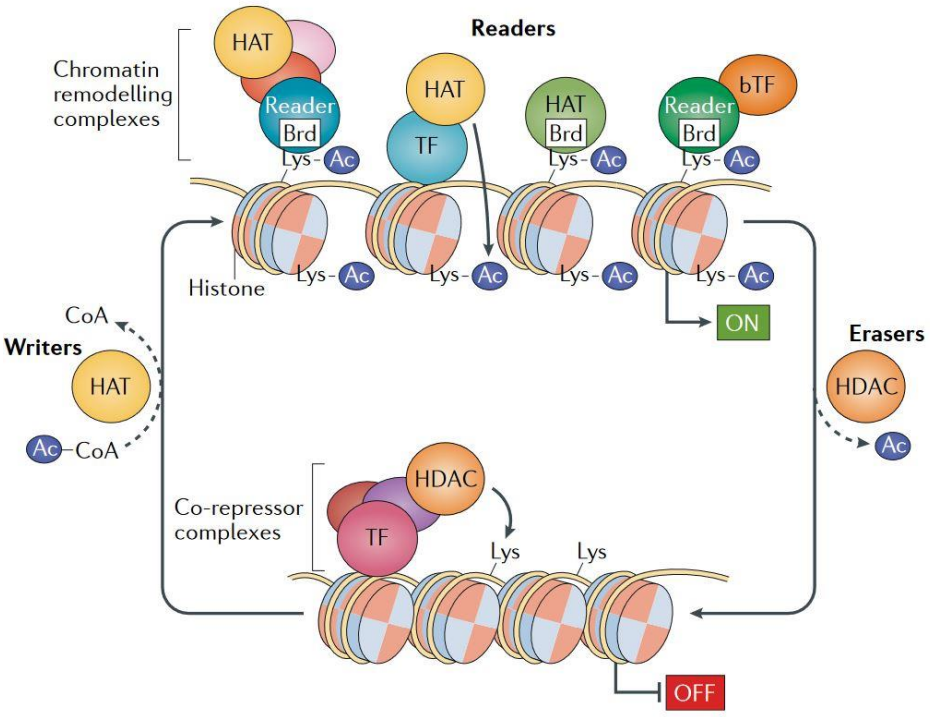

Figure 2: Schematic of dynamic histone acetylation and deacetylation by HATs and HDACs. The acetylation (Ac) of lysine residues on histone via Histone Acetyl Transferases (HATs) (writers) correlates with the active state of chromatin. Acetylation of positively charged lysine residues electrostatic interactions between DNA and histone proteins therefore loosening the association of DNA and nucleosomes. This allows other proteins like transcription factors (TF) and other multi-protein complexes to access the DNA. Specific acetylation marks can be "read" by epigenetic reader proteins which can recruit chromatin remodelling complexes. Erasing the acetylation mark on a histone is facilitated by co-repressor complexes containing histone deacetylases (HDACs) which leads to compaction and therefore silencing of the region. Figure from (Ellmeier & Seiser, 2018)

1.4 HDAC 1 & 2 in detail

1.4.1 Class 1 HDACs

Class I of histone deacetylases comprises HDAC1, 2, 3, and 8. They are classified by their homology with the yeast Rpd-protein and ubiquitously expressed in all tissue types (Chiocca & Segré, 2011). HDAC1, HDAC2 and HDAC3 are found in distinct multiprotein complexes (Sin3, NuRD, CoREST and NCor/SMRT) which are highly conserved and are important for distinct cellular processes like, cell-cycle regulation, stem cell pluripotency maintenance and differentiation (Nakayama & Hayakawa, 2011). HDAC1 and HDAC2 are highly similar proteins and located in the nucleus were they deacetylate both histone and non-histone targets. They can act as hetero- or homodimers with each other and are incorporated into larger multiprotein complexes. The two deacetylases show some distinct functions as well as redundant functions (Brunmeir et al., 2009). It was previously shown that if one of the paralogues of either HDAC1 or HDAC2 is deleted, the transcription of the other is upregulated and can partially compensate for the loss (Jurkin et al., 2011).

HDAC3 can localize in the nucleus as well as in the cytoplasm since it has both, a nuclear localization domain (NLS) and nuclear export signal (NES). HDAC3 can either form homo-oligomers or associate with Class II HDACs (Mirjam Andrea Moser et al., 2014). HDAC8 is the least studied histone deacetylase. It has been described to localize both in the nucleus and in the cytoplasm and to form homodimers. Compared to the other Class I HDACs, which enzymatic functions are dependent on other multiprotein complexes, HDAC8 is then only enzymatically independent Class I HDAC (Mirjam Andrea Moser et al., 2014).

1.4.2 Structure and functional domains of HDAC1 & 2

HDAC1 and HDAC2 are two highly homologues enzymes which are expressed ubiquitously over all mammalian tissue and localize predominantly in the nucleus (Ma & Schultz, 2016). It is suggested that the two enzymes evolved from a relatively recent gene duplication event in a common ancestor (Khier et al., 1999). The amino-acid sequence of HDAC1 and HDAC2 is 86% identical in mice and in humans, which indicates a high functional redundancy (Brunmeir et al., 2009). However, they also comprise specific domains for both enzymes. The first N-terminal domain of the enzymes is the HDAC association domain (HAD) which is essential for dimerization of HDAC1 and HDAC2. It partially overlaps with the catalytic domain of the enzyme witch constitutes the largest domain of the protein with more than 300 amino acids (Brunmeir et al., 2009). The catalytically active site is comprised of a Zn^{2+} ion, a tyrosine, two aspartic acid residues and two histidine residues. The catalytic centre of HDAC1 shows two additional amino acids enabling

HDAC1 interaction with the Chfr ubiquitin ligase. The catalytic domain is followed by and IAC (E/D)E motif which enables pocket protein (P107, p130, pRb) binding. The C-terminal domains are specific for HDAC1 and HDAC2. HDAC2 has a coiled-coil domain which might be involved in protein-protein interactions, whereas HDAC1 has a nuclear localisation signal (NLS) (Brunmeir et al., 2009). In addition to their functional domains both enzymes exhibit multiple sites for post-translational modifications. These sites can be dynamically modified and are important to regulate and direct specific HDAC functions (Chiocca & Segré, 2011). Like PTMs of histone proteins, these modifications can be small chemical moieties (acetylation, phosphorylation, methylation etc.) or longer amino acid chains like ubiquitin or SUMO proteins (Ma & Schultz, 2016).

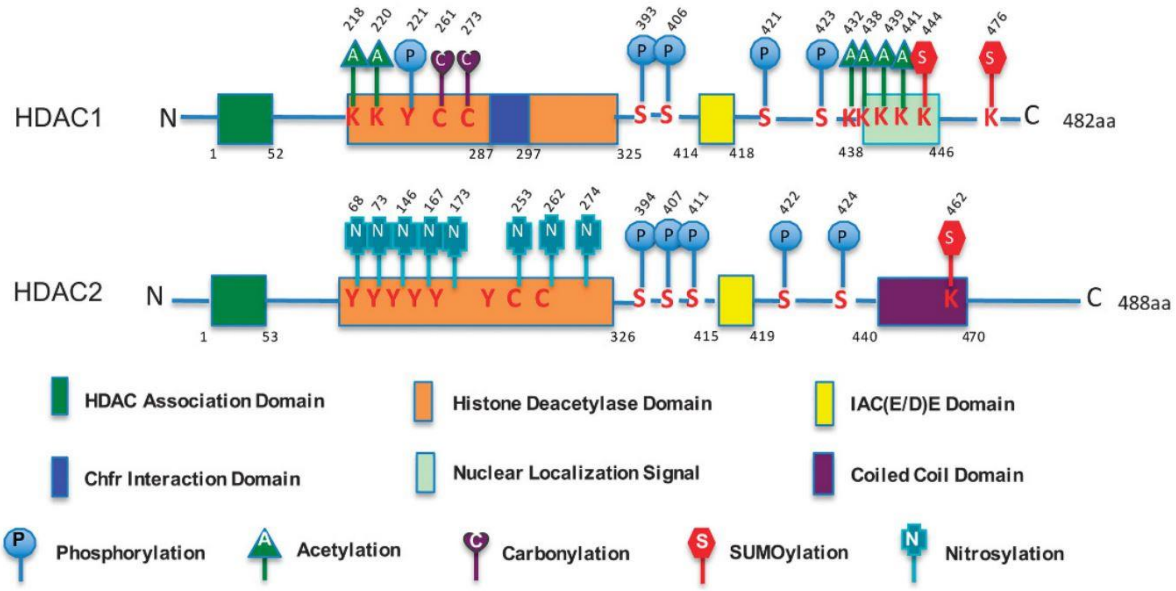

Figure 3: Illustration of functional domains and PTMs of mammalian HDAC1 and HDAC2. On the N-terminal side both proteins harbour a HDAC association domain followed by their catalytic domain. HDAC1 also harbours a Chfr interaction domain within its catalytic domain. Towards the c-terminus HDAC1 contains a IACEE motif whereas HDAC2 carries a IACDE domain. HDAC1 also has a nuclear localization signal domain on the c-terminus while HDAC2 contains a coiled-coil domain. HDAC1 and HDAC2 have several residues on which they can be modified via PTMS like phosphorylation, acetylation, carbonylation, SUMOylation and nitrosylation. (Figure from (Ma & Schultz, 2016))

1.4.3 HDAC1/2 in co-repressor complexes

As mentioned before, HDAC 1 and 2 can form hetero and homodimers and can partially compensate for each other. HDAC1/2 dimers form an enzymatic subunit that is incapable of binding DNA or histones itself. Therefore, the dimer has to be either, bound by transcription factors or incorporated into larger multiprotein co-repressor complexes to gain its deacetylase

activity. These large protein complexes are comprised of multiple different subunits that can have chromatin remodelling properties. Some HDAC1 and 2 carrying co-repressor complexes like Sin3A/B, CoREST and NuRD have already been well characterized and were shown to be involved in several different cellular processes like differentiation, apoptosis and cell cycle regulation (Brunmeir et al., 2009). In addition to their enzymatic activity previous studies also showed a scaffolding function of HDAC1/2 dimers for the stability of co-repressor complexes (Winter et al., 2013a)

1.4.4 Non histone targets of dynamic acetylation

Recent studies showed that posttranslational chemical modifications such as acetylation not only occur on histone proteins but also on amino-acid residues of other proteins. A high-resolution mass spectrometry analysis was able to identify lysine acetylation sites on 1750 human proteins with a partial upregulation of acetylation marks upon Class I HDAC inhibition (Choudhary et al., 2009). Consequently, HDACs also have been shown to deacetylate lysine residues on non-histone proteins influencing a variety of biological processes (Table 1.)

Biological implication	*Affected proteins*
Protein stability	Acetylation increases stability: p53,p73,c-myc, Runx3, H2A.z,E2F1, NF-E4 Acetylation decreases stability; GATA1, HIF-1α, pRb, SV40 T-Ag
DNA binding	Increases DNA binding: p53, SRY, STAT3, E2F1, p50, p65, AML1, BETA2 Decreased DNA binding: YY1, HMG-A1, HMG-N2, p65, DEK, KLF13
Protein interactions	Enhanced: STAT3, AR, EKLF, Importin A, STAT1, TFIIB, α-Tubulin, actin Decreased: p65, Ku70, Hsp90
Localisation	To nucleus: PCAF, SRY, CtBP20, POP-1, HNF-4, PCNA To cytosol: c-Abl, P300, PAP
mRNA stability	Increased: p21, Brm Decreased: Tyrosinhydrolase (th), eNOS
Enzymatic activity	Enhanced: p300, ATM Decreased: PTEN, HDAC1, Mdm2, ACS, Neil2, Polβ

Table 1: Selection of functional consequences of acetylation of some non-histone target. Table modified from (Spange et al., 2009)

For instance, dynamic acetylation and deacetylation can influence protein-protein interactions by blocking or releasing the lysine residue for other substrates or by directly creating or blocking a binding pocket for other proteins. It can also directly influence DNA-protein interactions by changing the chemical charge on transcription factors. Besides protein-protein and DNA-protein interactions, lysine acetylation and deacetylation are considered to influence cell signalling, protein stability, DNA damage response, steroid receptors, chaperones and subcellular

localisation. The biological outcome of the dynamic acetylation is dependent on the target and the biological context (Spange et al., 2009) (Mirjam Andrea Moser et al., 2014).

1.4.5 HDAC in disease and HDAC inhibition

Since HDACs have a wide variety of functions in many different biological processes the deregulation of HDAC1/2 has been previously implicated in various diseases including neurodegenerative diseases, inflammatory disorders, cardiovascular diseases and various different types of cancer (Yoon & Eom, 2016). Neurodegenerative and other neurological disorders are generally linked with hypoacetylation due to deregulation of HAT and HDAC activity (Mirabella et al., 2016).Various cancer cell types were shown to overexpress class I HDACs. In prostate, gastric, colon, lung and breast cancer an overexpression of HDAC1 was observed whereas HDAC2 was overexpressed in cervical, colorectal and gastric cancers. In general, increased HDAC levels can lead to the increased repression of tumour suppressor genes (e.g.: p21), increasing angiogenesis and the alteration of metabolic and apoptotic pathways resulting in tumour progression (Hrabeta et al., 2014). HDAC inhibition has shown beneficial effects for the treatment of non-solid tumours like myelogenous leukaemia (AML), cutaneous T-cell lymphoma (CTCL) and other lymphomas. Besides cancer the reversible nature of HDAC activity makes HDACs promising targets for the treatment of several other diseases. For instance in cardiovascular diseases like atherosclerosis, myocardial, cardiac hypertrophy and cardiac fibrosis the chemical inhibition of HDACs has shown promising results for preventing disease progression (Yoon & Eom, 2016). Studies in mice indicate a key role for HDAC1 in the pathogenesis for rheumatoid arthritis (RA), which is a chronic inflammatory autoimmune disease. Mice with a T cell specific deletion of HDAC1 showed resistance to the development of collagen-induced arthritis. Fittingly the analysis of human patient RA tissue samples revealed a subset of CD4+ cells with enhanced HDAC1 expression, suggesting HDAC1 inhibition as a promising target for RA treatment (Göschl et al., 2019). To date there are several clinical trials running for different specific and broad-spectrum HDAC inhibitors while the FDA has already approved a few HDAC inhibitors. For instance the pan-inhibitor SAHA (vorinostat) and the class I specific inhibitor romidepsin have been approved for the treatment of CTCL and peripheral cell lymphomas (Hrabeta et al., 2014). Given that broad-spectrum HDAC inhibitors are associated with many different side effects and new evidence of non-catalytic HDAC functions is being discovered, in order to improve clinical applicability, it is necessary to further research the redundancy and specificity of HDACs and their inhibition in different biological contexts

1.5 The epidermis

The epidermis together with the dermis comprise the two functional compartments of the largest organ of the body, the skin. It envelopes the whole organism to form a bi-directional barrier to the environment. As the inside-outside barrier it protects the body from unregulated loss of water and solutes, whereas the outside-inside barrier function protects it from invasion of pathogens or other harmful insults (Baroni et al., 2012). The dermis and epidermis are separated by a extracellular matrix- and growth factor-rich basement membrane (Fuchs & Horsley, 2008). The main barrier function is provided by the epidermis, which is the outermost layer of the skin that interacts directly with the environment. The structure of the epidermis itself provides a physical barrier whereas the presence of lipids, acids, hydrolytic enzymes and antimicrobial peptides also provides a chemical and biochemical barrier (Baroni et al., 2012). Besides its barrier function the epidermis also provides several appendages including hair follicles, sebaceous glands, sweat glands and nails which are important for other functions of the skin like skin lubrication and thermoregulation (Fuchs & Horsley, 2008). The innate immune system additionally provides an immunological defence to the epidermis via cellular and humoral components (Baroni et al., 2012). The epidermis is also a highly regenerative organ showing rapid turnover and a renewing cycle of approximately 28 days in humans. Deregulation of the precisely balanced process of proliferation and desquamation can lead to the development of skin disorders (Baroni et al., 2012).

1.5.1 Structure and development of the epidermis

The epidermis is a stratified epithelium established by multipotent stem cells (SCs) by differentiating into the interfollicular epidermis (IFE), the hair follicle (HF) and the sebaceous gland (SG) linages. After development these SCs reside in the epithelial tissue (Blanpain & Fuchs, 2009). The IFE is comprised of several layers of mostly keratinocytes which are the main cell type of the epidermis. The first basal layer (stratum basale) sits right on top of the basement membrane which separates epidermis and dermis. The stratum basale contains SCs that keep their proliferation and self-renewing potential and are responsible for the renewal of the skin and are crucial of epidermal homeostasis. Most of these cells (~75%) are in a quiescent state and can be activated when enhanced proliferation is needed for instance during wound healing (Baroni et al., 2012) (Alonso & Fuchs, 2003). In addition to keratinocytes the stratum basale also hosts some other cell types like, pigment producing melanocytes protecting the skin from ultraviolet light or Merkel cells and dendritic epidermal T-cells for mechanosensory and immune surveillance

purposes(Heath & Carbone, 2013) (Wickett & Visscher, 2006).

The other layers of the epidermis are developed during differentiation toward the surface, ending in a process called terminal differentiation. During normal differentiation the basal keratinocytes detach from the basement membrane, loose their self- renewing properties and start migrating toward the surface. While migrating outward during the differentiation process the keratinocytes undergo morphological and biochemical changes defining the three outer layers (Baroni et al., 2012)(Alonso & Fuchs, 2003).

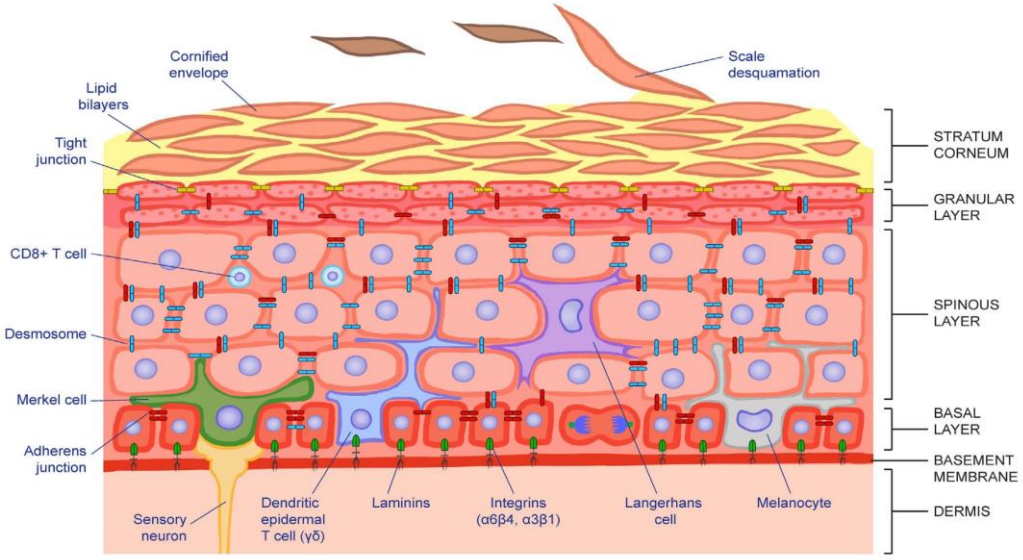

Figure 4: Schematic illustration of the structure of the epidermis. The epidermis is separated from the dermis by the basement membrane and can be separated into four main layers defined by degree of keratinocyte differentiation. The basal layer of keratinocytes stays connected to the basement membrane which maintains their proliferative potential. Differentiating keratinocytes move outward towards the surface through the spinous layer and the granular layer culminating in terminal differentiation generating the strateum corneum. It consists of dead, enucleated, squamous cells surrounded by a lipid bilayer and forms the direct barrier to the environment. The epidermis additionally hosts immune cells (dendritic epidermal T-cells and Langerhans cells), sensory cells Merkel cells) and melanocytes. Image taken from (Gonzales & Fuchs, 2017)

The spinous layer starts right after the basal layer and consists mostly of keratinocytes expressing a special set of keratin filaments that provide mechanical support by strengthening the cytoskeletal and intercellular connections (Gonzales & Fuchs, 2017). This layer additionally contains sensory nerve endings for temperature and pain sensing as well as specialized dendritic Langerhans cells which are the antigen-presenting cells of the skin (Wickett & Visscher, 2006). Keratinocytes in the granular layer are interconnected by tight junctions which play an important role in the barrier function of the skin. In this layer, cells produce lipid-rich granules and lysine- and glutamine-rich proteins. These proteins are irreversibly cross linked by transglutaminases which provides the base to form the cornified envelope (Fuchs & Horsley, 2008). As keratinocytes transit from the granular stage to the last epidermal layer, the strateum corneum, they undergo

several changes. They start expressing late differentiation markers like loricrin, filaggrin and involucrin. The cells are flattened by rearrangement of keratin filaments into tight bundles and they release lamellar granular by exocytosis to form a water-inpermeable seal (Fuchs & Horsley, 2008). Finally in the last step of terminal differentiation the keratinocytes undergo a special programmed cell-death called cornification. They stop all metabolic and transcriptional activity and lose all cytoplasmic organelles including the nucleus. This results in flat enucleated squamous cells that are enveloped by cornified proteins and a lipid bilayer. Eventually this layer of the epidermis is shed of and replaced by differentiating cells of the preceding layers undergoing the terminal differentiation process (Fuchs & Horsley, 2008), (Baroni et al., 2012).

1.5.2 Immune system of the epidermis

As the organ with direct exposure to the environment and its hazards the skin has to have additional protection against invading pathogens besides the physical cornified barrier. One structural mechanism to protect the deeper layers of the epidermis from invasion is the regular shedding of the cornified cells. The exposed surface is also covered with microbes competing for nutrients and providing a microbial protective layer (Baroni et al., 2012). Furthermore antimicrobial peptides and lipids are secreted onto the surface of the skin within sweat and sebum, which is produced in sebaceous glands, as protection from pathogenic organisms (Chambers & Vukmanovic-Stejic, 2020). On a molecular level the epidermis is equipped with several components of the innate and adaptive immune system. As mentioned earlier the epidermis harbours several different immune cells. In the murine epidermis dendritic epidermal T-cells are the most abundant T-cell population. These cells are important for monitoring “stress” of the epidermis and have been shown to participate in wound healing, inflammation signalling during viral infections and tumour surveillance (Heath & Carbone, 2013). The epidermal-environmental border is also under surveillance by dendritic Langerhans cells, which are mononuclear phagocytes that constantly expand and retract their dendrites to sample the environment. They can activate the local immune response by taking up and processing lipid antigens and microbial fragments which they then present to local T-cells or by migrating to the lymph nodes (Chambers & Vukmanovic-Stejic, 2020). Keratinocytes also contribute to the regulation of the innate immune response in various ways. They can express various pattern recognition receptors including Toll-like receptors, which can recognize many pathogenic components. By expressing these different pattern recognition receptors keratinocytes are capable of sensing and responding to viral RNAs, microbial components and fungal infections. As a direct response a microbial threat they can produce several antimicrobial peptides (e.g: LL-37,

ß-defensins, RNAses, S100 family members). Keratinocytes are also capable of expressing different chemokines and cytokines (e.g.: CXCL10, CCL10, IL-1ß, IL-6) to attract T-cells and monocytes upon encountering a pathogen. To control recurrent infections after a pathogen encounter the immunity and immune memory is generated by CD8+ tissue resident memory T-cells and circulating CD4+ cells which mainly reside in the dermis (Heath & Carbone, 2013). The immune system of the skin also extends further into the dermis with several different mechanisms and cell types involved, which are beyond the scope of this work. Deregulations in the activity of the immune system can lead to several immune mediated diseases of the skin including psoriasis, systemic lupus erythematosus, cutaneous T-cell lymphoma and atopic dermatitis (Nestle et al., 2009).

1.5.3 Function of HDAC1 in epidermal mouse models

Murine global germline knockouts of *Hdac1* are embryonically lethal showing severe developmental and proliferation defects. Other class I HDACs like HDAC2 and HDAC3 were upregulated upon HDAC1 ablation but could not fully compensate for HDAC1 suggesting unique functions of the enzyme (Lagger et al., 2002a). In order to further investigate the specific functions of HDAC1, tissue or cell type specific conditional knockout models were designed by utilizing the cre-mediated recombinase system. The conditional knockout of *Hdac1* in various different cell lines only caused a mild effect and was accompanied by an upregulation of the HDAC2 paralog as a compensatory mechanism. (Mirjam Andrea Moser et al., 2014). Similarly, the tissue specific loss of HDAC1 or HDAC2 in the epidermis had no obvious consequence for epidermal development and only showed correlation with a higher incidence of scar formation in HDAC1-defiecient epidermis (Winter et al., 2013a). Whereas the conditional deletion of both *Hdac1* and *Hdac2* in the epidermis leads to perinatal lethality and impairment of epidermal stratification (LeBoeuf et al., 2010). To further examine the redundant and non-redundant functions of HDAC1 our lab generated mice expressing different allelic combinations of HDAC1 or HDAC2 in the epidermis utilizing the cre-recombinase under control of the K5-cre promotor (Winter et al., 2013a) Mice with no functional epidermal *Hdac2* allele but a single *Hdac1* allele as well as mice carrying only one allele of each enzyme showed normal development with no distinct phenotype. However, mice deficient for *Hdac1* with a single *Hdac2* allele displayed severe developmental abnormalities. This demonstrates that a single *Hdac1* allele can compensate for the loss of *Hdac2* whereas a single allele of *Hdac2* can not rescue HDAC1 deficiency (Winter et al., 2013a).

Mice haploinsufficient for HDAC2 in the absence of HDAC1 were smaller, gained less weight and exhibited progressive alopecia. Adult animals had reduced bodyweight, little body hair, shorter whiskers and scaly tail regions. On a microscopic level these mice showed disturbed hair follicle

(HF) morphogenesis and failure to enter the hair cycle accompanied with degeneration of HFs due to increased p53 expression and apoptosis. They also exhibited hyperkeratosis and epidermal hyperproliferation caused by deregulated expression of the epidermal differentiation complex (EDC), which is a genomic region containing gene clusters important for keratinocyte differentiation. Furthermore, the study showed changes in lineage determination induced by enhanced apoptosis in the HFs, increased proliferation in the IFE and redirection of stem cells. These findings correlate with studies of mice overexpressing *c-myc*, suggesting a deregulation of C-MYC activity directly or indirectly via HDAC1. Consistently, *c-myc* was also found to be strongly expressed in tumours that spontaneously formed in older mutant mice. Lastly, they found that the loss of *Hdac1* and the expression of only one allele of *Hdac2* in the epidermis led to the destabilization of certain components of Co-repressor complexes like Sin3a and NuRD indicating essential scaffolding functions of HDAC1 for the stability of epidermal co-repressor complexes (Winter et al., 2013a).

1.6 Background and aim of the project

Our lab is interested in elucidating the specific and overlapping functions of HDAC1 and HDAC2 and their domains to further improve knowledge about specific HDACs which may ultimately help to design more specific inhibitors that can help combat cancer and other diseases. Our lab previously investigated mice with catalytically inactive endogenous versions of HDAC1 and HDAC2, which carry point mutations within the catalytic centre, abolishing the deacetylase activity but keeping its scaffolding functions in tact (Hagelkruys et al., 2016a). Models, studying catalytical inactivation of HDACs which can still fulfil their structural functions, are especially interesting since they mimic isoform specific HDAC inhibition. No mice homozygous for catalytically inactive *Hdac1* were born, whereas heterozygous mice were born at the expected frequency and showed no phenotype. Mice carrying one allele of catalytically inactive *Hdac2* show a severe developmental phenotype whereas complete deletion of *Hdac2* showed no obvious defect (Hagelkruys et al., 2016a). As described above, the lab also investigated the functions of HDAC1 and HDAC2 in the epidermis since, as a self-renewing tissue, it is an excellent model to study proliferation and differentiation. Deregulation of these processes can cause different pathological responses including cancer. Therefore it is crucial to further elucidate the influence of HDAC inhibition on the different pathways and mechanisms during proliferation and differentiation (Winter et al., 2013a). For this project we combined the epidermal specific deletion of endogenous HDAC1 ($Hdac1^{\Delta/\Delta ep}$) with the introduction of a catalytically inactive HDAC1 (HDAC1 CI, $Hdac1^{ci/+}$)

transgene expressed from the Rosa26 locus in an inducible manner using the cre-recombinase system. Additionally, we investigated a HDAC1 mutant called HDAC1 2S (HDAC1 S421A S423A, *Hdac1* $^{2S/+}$) which can not be phosphorylated at S421 and S423 rendering them incapable of forming complexes as well as abolishing its enzymatic activity (Hess, 2017). The aim of this thesis was the characterization of mice epidermally depleted for endogenous HDAC1 carrying either a HDAC1 Ci (*Hdac1* $^{ci/+}$ *Hdac1*$^{\Delta/\Delta ep}$) or a HDAC1 2S (*Hdac1* $^{2S/+}$ *Hdac1*$^{\Delta/\Delta ep}$) transgene version of HDAC1 in order to further improve knowledge about specific catalytic and structural functions of HDAC1.

2.Material & Methods

2.1 Mouse models

All experiments involving mice were approved by the Austrian Animal Care Committee and conducted in accordance with the guidelines for the use and care of laboratory animals. Mice were held in the animal facilities of the Centre for Anatomy and Cell Biology at the Medical University of Vienna and at the Max Perutz Laboratories at the University of Vienna. The used mouse strains were bred to a mixed genetic background of C57BL/6J x 129SV.

2.1.1 Epidermis specific deletion of endogenous *Hdac1* and expression of HDAC1 Ci

The mutation of the histidine 141 to an alanine (H141A) in the catalytic centre of the HDAC1 enzyme dramatically decreases its deacetylase activity without affecting the incorporation into co-repressor complexes (Hassig et al., 1998). In order to conditionally delete endogenous HDAC1 while simultaneously overexpressing this catalytically inactive HDAC1 variant from the ROSA26 locus the cre-loxP system was utilized. To ensure epidermis specific deletion and expression, the cre recombinase was expressed under the control of the bovine Keratin 5(K5) promotor. In the epidermis the K5 promotor is active in the basal epidermal layer starting on embryonic day 9.5 (E9.5). Since the progenitor cells in the basal epidermis give rise to all epidermal cells, the whole epidermis and its appendages are affected. Only males carrying the K5-cre transgene were used for crossing, since female transmission can lead to non-epidermis unspecific recombination of loxP sites during embryogenesis. These mice were a generous gift from Maria Sibilia (Medical University Vienna, Austria). Male K5-cre mice were first crossed with females carrying the catalytically inactive *Hdac1* transgene at the ROSA26 locus. This transgene also comprises a Geo-stop-cassette flanked by two loxP sites upstream of $Hdac1^{Ci}$. Upon cre-mediated recombination the stop-cassette is floxed out, allowing transcription of $Hdac1^{Ci}$(Figure 5.).

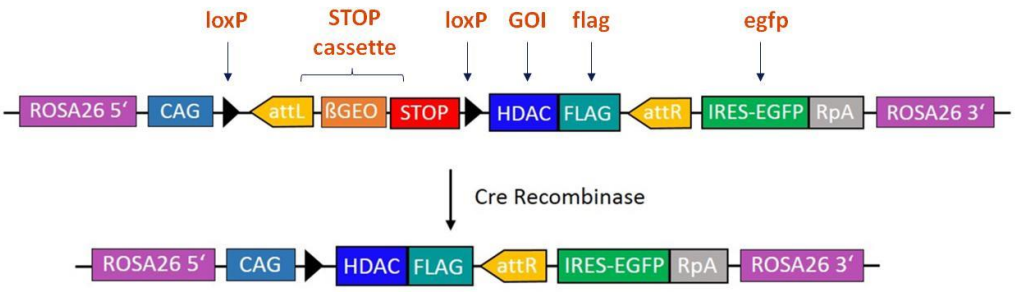

Figure 5: Vector used for conditional $Hdac1^{Ci}$ knock-in at the ROSA26 locus. The flag tagged gene of interest (GOI), $Hdac1^{Ci}$, was inserted together with a ß-geo stop cassette conferring neomycin resistance for selection and preventing the GOI to be expressed. The stop-cassette is flanked by two loxP sites. Cre-recombinase expression leads to the excision of the ß-geo stop cassette and allows transcription of the GOI

via the CAG promotor. Additionally, an IRES-EGFP tag is expressed allowing visual confirmation of GOI expression. Figure modified from (Hess, 2017)

The offspring carrying the K5-cre and the *Hdac1*^{Ci} transgene were then crossed with mice harboring one or two endogenous *Hdac1* alleles with loxP sites flanking exon 6 (E6) (Figure 6). When K5-cre becomes active, in successfully crossed mice carrying both the deletion of endogenous *Hdac1* and the catalytically inactive mutant, the recombinase simultaneously excises E6 of the endogenous *Hdac1*alleles and the Geo-Stop cassette in the *Hdac1*^{Ci} transgene. This results in a knockout of endogenous *Hdac1* while expressing the catalytically inactive *Hdac1* transgene. Mice expressing the transgene from one *Rosa26* allele were labelled *Hdac1*$^{Ci/+ep}$ *Hdac1*$^{\Delta/\Delta ep}$.

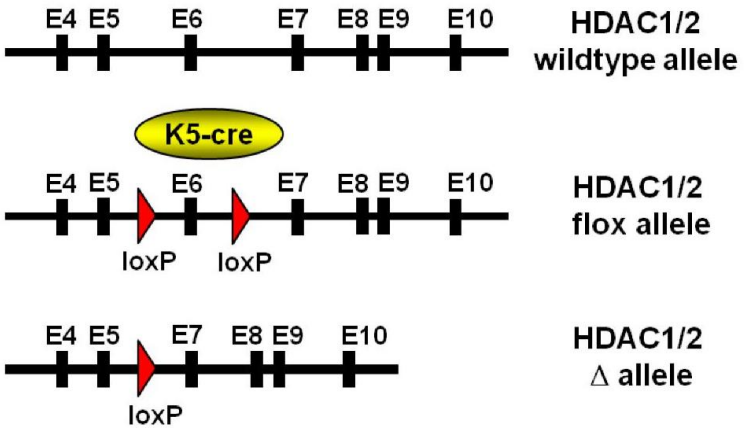

Figure 6: Conditional knockout of endogenous *Hdac1*. Exon 6 from the endogenous *Hdac1* alleles was flanked by two loxP sites. Upon K5-Cre expression the recombinase targets the loxP sites, excising exon 6 and consequently stopping the expression of endogenous *Hdac1*. (Mirjam A. Moser, 2011)

2.1.2 HDAC1 2S mice

Additionally, another HDAC1 variant was investigated in the epidermis namely HDAC1 2S. This mouse strain also harbors two floxed endogenous *Hdac1* alleles but expresses the 2S variant of HDAC1 from the Rosa26 locus. This HDAC1 variant can not be phosphorylated anymore at S421 and S423 due to mutations of the serine residues to alanine's. This mutation renders HDAC1 catalytically inactive and additionally disrupts its complex formation capabilities. The CRE-loxP system under control of the K5 promotor as described above was utilized to introduce the transgene at the ROSA26 locus. Mice carrying the 2S transgene at the Rosa26 locus were crossed with mice harboring two floxed *Hdac1* alleles, resulting in a *Hdac1*$^{2S/+ep}$ *Hdac1*$^{\Delta/\Delta ep}$ genotype.

2.1.3 Control strains

As a control we utilized wildtype mice that were cre-negative and were therefore normally expressing wildtype endogenous HDAC1. Additionally, we also used an *Hdac1* knockout mouse strain *Hdac1*$^{\Delta/\Delta ep}$ as a second control which harbours two floxed HDAC1 alleles.

2.1.4 Genotyping of mice

Isolation of genomic DNA

For genotyping of the mice toe clips were used. The tissue was digested in 96µl Tail lysis buffer and 4µl proteinase K (20mg/ml; *PanReac AppliChem*) over night at 56°C while slightly shaking at 350 rpm. The next day, the samples were incubated for 5 minutes at 95°C to inactivate the proteinase K. Subsequently, the samples were diluted with 400µl nuclease free dH_2O and stored at 4°C.

Tail Lysis Buffer

- 100mM Tris-HCl pH 8.0
- 5mM EDTA pH 8.0
- 200mM Sodium chloride
- 0.1% SDS

Genotyping PCR for tissue lysates

The genotypes of the samples were determined by Polymerase Chain Reaction (PCR) with gene-specific primers (Table 2). For these PCRs the OneTaq Hot Start Quick-Load 2x Master mix (*New England Biolabs*) was used and the samples were processed on a T100 Thermal Cycler (*Bio-Rad*) using the program below. Positive and negative controls were always included for each gene.

Genotyping PCR reaction mix

- 12.5µl 2x OneTaq Hot Start master mix (*New England BioLabs*)
- 1µl genomic DNA lysate
- 0.5µl 10µM forward primer
- 0.5µl 10µM reverse primer
- filled up to 25µl with dH_20

PCR Programs & Primers

Cre PCR program

95°C	5 minutes	
95°C	30 seconds	40 cycles
58°C	30 seconds	
72°C	100 seconds	
72°C	3 minutes	
20°C	∞	

HD1 floxed PCR program

95°C	5 minutes	
95°C	30 seconds	40 cycles
54°C	30 seconds	
72°C	100 seconds	
72°C	5 minutes	
12°C	∞	

HD1 delta PCR program

95°C	5 minutes	
95°C	30 seconds	35 cycles
54°C	30 seconds	
72°C	120 seconds	
72°C	5 minutes	
12°C	∞	

HD1 Screen1 PCR program

95°C	5 minutes	
95°C	30 seconds	35 cycles
56°C	30 seconds	
72°C	120 seconds	
72°C	5 minutes	
12°C	∞	

R26 wildtype

95°C	5 minutes	
95°C	30 seconds	40 cycles
56°C	30 seconds	
72°C	40 seconds	
72°C	5 minutes	
12°C	∞	

Primer	Sequence 5' —> 3'	Product length
Cre_F	TAATCGCCATCTTCCAGCAG	no product (Cre-)
Cre_R	CAATTTACTGACCGTACAC	1000bp (Cre+)
Hdac1_screen_F	GCATCGCCTTCTATCGCCTTC	no product (TG-)
Hdac1_screen_R	CTTGGTCATCTCCTCAGCATTGG	1241bp (TG+, Cre-)
HDAC1_LoxF	CGTAGTTCACAGCATAGTACTT	Δ 600bp
HDAC1_Δ_R	GTTACGTCAATGACATCGTCTT	
HDAC1_lox_F	GGTAGTTCACAGCATAGTACTT	850bp (wt)
HDAC1_lox_R	CCTGTGTCATTAGAATCTACTT	900bp (flox)
Rosa26wt_F	GCACTTGCTCTCCCAAAGTC	445bp (wt)
Rosa26wt_R	GGCGGATCACAAGCAATAAT	no product (homozygous KI)

Table 2: Primers used genotyping PCRs

Agarose gel electrophoresis

For visual verification the PCR products were ran on a 2% agarose gel. The gel was prepared by adding the appropriate amount of agarose to 1x TAE buffer and boiling to mixture until the agarose dissolved. After cooling, 1.2µl peqGreen DNA stain (*VWR*) were added and the gel was cast. After polymerization half of the genotyping PCR reaction was loaded directly onto the gel and the gel was run at 120V until the separation of bands was sufficient. As a reference standard 4µl of the 1 kb Plus DNA Ladder and/or the 100bp DNA Ladder (*New England Biolabs*) were also loaded on the gel.

10x TAE

- 400mM Tris-Acetate
- 20mM EDTA
- diluted in dH_2O, adjusted pH to 8.5

2.1.5 Transepidermal water loss (TEWL)

TEWL was measured on shaved nape skin immediately after euthanizing mice using a Tewameter from Courage and Khazaka, model TM300 (Cologne, Germany). Measurement was performed at least three times for each mouse and the average value for was calculated.

2.1.6 Isolation of skin and epidermal tissue

Mice were anesthetized with isoflurane and subsequently sacrificed *via* cervical dislocation. Back and belly of the mice were shaved and skin including the ears were cleaned with 70% ethanol. For the histological analysis the ears and a piece of whole back-skin were isolated and fixed in 4% Paraformaldehyde (PFA) for 24 hours before further processing as described in 2.2.1. For molecular analysis of the epidermal tissue, dermis and epidermis of the tail were separated using Dispase solution (5mg/ml in 1x PBS; *Roche*). The tail skin was isolated from the bone, washed once in cold 1x PBS containing 0.1µl/ml Protector RNase Inhibitor (*Roche*) and subsequently placed on the Dispase solution which also contained the RNAse inhibitor. After incubation at 4°C for 2 hours the epidermis was carefully separated from the dermis using two forceps and subsequently washed again in cold 1x PBS. For protein analysis, the epidermal samples were transferred into tube containing small ceramic beads (*Precellys CK14 Lysing kit, VWR*), snap frozen in liquid nitrogen and stored on -80°C before further processing. Samples dedicated for RNA isolation were also transferred into ceramic bead tubes containing 1ml of Trizol (*Invitrogen*). The tissue was incubated for 1 minute at room temperature before being snap-frozen in liquid nitrogen and stored on -80°C.

10x PBS

- 137mM Sodium chloride
- 2.7mM Potassium chloride
- 10mM Disodium hydrogen phosphate
- 1.8mM Monopotassium dihydrogen phosphate
- diluted in dH_2O, adjusted pH to 7.4

2.2 Histology

2.2.1 Embedding of histology samples

The skin was isolated from the mice as described in 2.1.6 and fixed in 4% PFA for 24 hours at 4°C. PFA was removed and the tissue samples were briefly washed with 1x PBS. 70% ethanol was added to the samples for storage at 4°C for up to one week. For the preparation of the paraffin samples, they first were dehydrated using the tissue processor (*Leica*) running the protocol indicated in Table 3. The dehydrated tissue was embedded in paraffin using the TBS88 paraffin embedding system (*Mediate*) embedding unit. The paraffin samples were stored at room temperature. Before further processing, the samples were cooled down to -20°C and subsequently cut into 4µm thin tissue sections with the Thermo Shandon Dinesse ME microtome (*Thermo Fisher Scientific*) and placed in a 40-45°C warm water bath to flatten them out. For standard H&E staining the sections were mounted onto standard glass slides. Samples used for immunofluorescence staining were placed onto SuperFrost glass slides (*Thermo Fisher Scientific*). The slides were dried overnight at room temperature before further processing. Unstained samples were kept at room temperature for long term storage.

Step	Solution	Duration	Temperature
1	70% Ethanol I	1h	30°C
2	70% Ethanol II	1.5h	30°C
3	80% Ethanol I	1h	30°C
4	96% Ethanol	1.5h	30°C
5	100% Ethanol I	1h	30°C
6	100% Ethanol II	1.5h	30°C
7	100% Ethanol/Xylene (5:1)	2h	30°C
8	Xylene I	0.5h	30°C
9	Xylene I	1h	30°C
10	Xylene III	1.5h	30°C
11	Paraffin I	1.5h	57°C
12	Paraffin II	1.5h	57°C
13	Paraffin III	2h	58°C
14	Paraffin IV	2.5h	58°C

Table 3: tissue processor protocol for embedding of histology samples

PFA for fixation

- 4g PFA
- 100ml 1xPBS
- Add few drops 1M NaOH and stir at 60°C to facilitate dissolving
- Cool down to 4°C, filter and adjust pH to 7.4
- store aliquots at -20°C.

2.2.2 Hematoxylin and eosin (H&E) staining

The slides were incubated at 60°C for one hour prior to staining in order to melt the paraffin of the section. Subsequently, the samples were immersed twice in xylene for 10-15 minutes. Staining with hematoxylin and eosin (H&E) was performed on the COT 20 Linear Slide Stainer (*Mediate*) according to the protocol indicated in Table 4. After the last step of the staining protocol the slides were kept in xylene to prevent desiccation and were immediately mounted with the EUkitt Quick-hardening mounting medium before being sealed with glass coverslips.

Step	Solution	Duration
1	Histolab-Clear	
2	100% Ethanol I	
3	100% Ethanol II	
4	96% Ethanol	
5	70% Ethanol	
6	Distilled water	
7	Mayer'sHematoxylin (*Histocom*)	
8	Tap water (running)	
9	Tap water (running)	
10	Tap water (running)	
11	Tap water (running)	
12	Tap water	
13	1% aqueous Eosin I (*Morphisto*)	
14	1% aqueous Eosin I] (*Morphisto)*	
15	Tap water (running)	
16	70% Ethanol	
17	96% Ethanol	
18	100% Ethanol I	
19	100% Ethanol II	
20	Histolab-Clear I	
21	Histolab-Clear II	
22	Histolab-Clear III	
23	Xylene	
15	Tap water (running)	
16	70% Ethanol	
17	96% Ethanol	
18	100% Ethanol I	
19	100% Ethanol II	
20	Histolab-Clear I	
21	Histolab-Clear II	
22	Histolab-Clear III	
23	Xylene	

Table 4: COT 20 Linear Slide Stainer protocol for H&E staining

2.3.3 Immunofluorescence staining of paraffin sections

The slides with the paraffin sections were incubated at 60°C for at least one hour to melt the paraffin. Subsequently the samples we completely deparaffinised and rehydrated using the following incubation protocol. All steps were performed at room temperature

Rehydration of paraffin slides

Step	Solution	duration
1	Xylene I	15 minutes
2	Xylene II	15 minutes
3	100% Ethanol I	2 minutes
4	100% Ethanol II	2 minutes
5	80% Ethanol I	30 seconds
6	80% Ethanol II	30 seconds
7	30% Ethanol I	30 seconds
8	30% Ethanol II	30 seconds
9	dH_20 I	2 minutes
10	dH_20 II	2 minutes
11	1xPBS	storage

Table 5: incubation protocol for rehydration of paraffin slides

To prevent drying out, the samples were kept in 1xPBS after the rehydration protocol. Depending on the Antibody, the slides were then transferred into either 10mM citrate buffer (pH 6) or in Dako Target Solution (pH 9; *Agilent*) and booiled for 20 minutes in the 2100 Antigen Retriever (*Aptum biologics*) at 121°C to unmask the antigen. Afterwards the samples were washed twice with 1xPBS.

Citrate buffer

- 10 mM Sodium citrate
- Adjust to pH 6.0

Subsequently, the tissue samples on the slides were encircled with the Dako Sample Pen S2002 (*Aligent*) to create a fatty barrier for liquids around the sample. Prior to primary antibody incubation, the samples were blocked with a 2% BSA and 10% goat serum containing 1x PBS solution for 20 minutes at room temperature. 1x PBS containing 2% BSA was used to dilute the different primary antibodies as indicated in Table 6. The antibody solutions were carefully pipetted onto the samples before incubating the slides overnight at 4°C in a moisture chamber. The next day, the slides were washed three times in 1x PBS for 5 minutes. Afterwards, the samples were incubated with the secondary fluorophore-labelled antibody (diluted 1:500 in 1x PBS with 2% BSA and 10% goat serum) for 30 minutes at room temperature in the dark. Depending on the origin of the primary antibodies, either goat IgG anti-rabbit, goat IgG anti-mouse or goat IgG anti-rat coupled to an Alexa Fluor Dye (*Thermo Fischer Scientific*) were used as secondary antibodies (Table 7.). After incubation, the slides were washed three times with 1x PBS. The samples were counterstained with PicoGreen (*Thermo Fisher Scientific P7581*) and/or DAPI (1mg/ml; *Thermo Fisher Scientific*). The two dyes were diluted (Picogreen 1:000; DAPI 1:2000) in 10mM aqueous Tris/HCl pH 7.4 buffer with 1mM EDTA and incubated for 20 minutes at room temperature in the

dark. A final washing series was performed in which samples were washed twice with 1xPBS for 5 minutes and finally once with dH_20. Subsequently the slides were mounted with Pro Long Gold Antifade (*Thermo fisher Scientific P36930*) and stored at room temperature for at least 2 hours to dry.

Antibody	Species	Dilution	Retrievel	Company
FLAG (#M2, F1804)	Mouse	1:500	pH6	Sigma-Aldrich
H2A.Xph (#JBW301, 05-636)	Mouse	1:500	pH6	Sigma-Aldrich
H3S10ph (SC8656-R)	rabbit	1:2000	pH6	Santa Cruz Biotechnology
Cgas (D3080)	Rabbit	1:500	pH6	Cell signalling
Krt10	Rabbit	1:2000	pH6	Covance
H3K56ac (ab76307)	Rabbit	1:1000	pH6	Abcam
KI67 (SolA 15)	rat	1:500	pH6	Thermo fisher scientific
Keratin 6	rabbit	1:1000	pH9	Covance
Loricrin	rabbit	1:1000	pH9	Covance
CD45 (C-10558)	rabbit	1:1000	pH9	Abcam
CD3 (A045229-2)	Rabbit	1:800	pH9	Agilent

Table 6: Primary antibodies used for immunofluorescence staining's of histology samples

Secondary Antibody	Species	Dilution	company
Alexa Fluor 546	anti-mouse	1:500	Thermo Fisher Scientific (A-11010)
Alexa Fluor 488	anti-rabbit	1:500	Thermo Fisher Scientific (A-32731)
Alexa Fluor 546	Anti-rat	1:500	Thermo Fisher Scientific (A-11006)

Table 7: secondary fluorescence antibodies used for IF

2.3 Human keratinocyte cell culture

All cell lines used were derived from the NHEK/SVTERT3-5 cell line, which is a human immortalized keratinocyte cell line. They were cultivated in Keratinocyte Growth Medium 2 (KGM2, *Promo cell*) supplemented with 1% penicillin/streptomycin (*Sigma-Aldrich, P4333*), 50 pg/ml G418 *(Sigma-Aldrich 4Z2Z878007*) and the supplements mix delivered with the KGM2 kit (see Table 8). All reagents were preheated to 37°C before use. All working steps with cells were conducted under sterile conditions in a Laminar Flow Hood. Incubation conditions were 37°C at 5% CO_2.

KGM2 Supplement	Final concentrations
Bovine Pituitary Extract	0.004 ml/ml
Epidermal Growth Factor (recombinant human)	0. l25 ng/ml
Insulin (recombinant human)	5 pg/ml
Hydrocortisone	0.33 pg/ml
Epinephrine	0.39 pg/ml
Transferrin (recombinant human)	10 pg/ml
CaC1	0.06 mM

Table 8: List of Supplements in the supplement mix and their concentration in KGM2

Cell lines (clone)	Genotype/features
HD1 WT (3-5, A7)	HDAC1 wildtype cell line (SV-TERT 3-5)
HD1 Ci (H1)	Knock-in of catalytically inactive HDAC1 ($HDAC1^{ci/+}$)
HD1 wt+ (A9)	Knock-in of wildtype HDAC1 ($HDAC1^{wt/+}$)
HD1 WT+ eKD (3II)	Knock-in of wt HDAC1 & knockdown of endogenous HDAC1 (HDAC1kd, $HDAC1^{wt/+}$)
HD1 Ci+ eKD (4III)	Knock-in of catalytically inactive HDAC1 & knockdown of endogenous HDAC1 (HDAC1kd, $HDAC1^{ci/+}$)

Table 9: List of cell lines and their features

2.3.1 Thawing, passaging and freezing of keratinocytes

Thawing of cells

Cells were quickly thawed and added to a 15ml falcon containing 10 ml of cold medium. The cells were centrifuged for 5 minutes at 300 rcf. Subsequently, the supernatant was removed, the pellet was resuspended in fresh preheated medium and transferred into a T-25 Flask. For freshly thawed cells, the medium was changed one day after thawing.

Passaging of cells

Cells were split and passaged at 60-80% confluency. Therefore, the medium was removed from the dish and the cells were washed once with 1x PBS. After removing the PBS, Trypsin-EDTA(*Sigma-Aldrich T3924)* was added to the dish to detach the cells (3ml for 10-cm dish). Subsequently, the cells were incubated for 5 min at 37°C. Due to the strong adherence of keratinocytes the detachment of the cells was supported by tapping the side of the dish. Then, an equal amount of KGM2 was added to the dish and the cells were washed off the dish and pipetted into a 15ml flacon tube. The cell suspension was centrifuged for 3 minutes at 300rcf. After removing the supernatant, the cells were resuspended in KGM2 and split onto new culture dishes in the desired ratio (usually 1:3 to 1:5).

Freezing of cells

The cells from a 15-cm dish were washed and trypsinized as described in 2.1.2. After the centrifugation the pellet was resuspended in 1 ml of KGM2. The cells were counted using the *Countness 2 Cell counter* (Thermo Fisher Scientific) and diluted to $2*10^6$ cell/ml. Subsequently the cell suspension was mixed in a 1:2 ratio with pre-cooled freezing medium [80% KGM2, 20% DMSO *(Merck)*] to achieve a final concentration of $1*10^6$ cell/ml and transferred to cryo-tubes. The vials were frozen at -80°C using Mr. Frosty freezing container (Nalgene, Sigma Aldrich) and then transferred into the liquid nitrogen tank for long term storage.

Trypsin/ EDTA

- 0.1% trypsin
- 2% EDTA
- Diluted in PBS, sterile filtrated

Freezing medium

- 80% GIBCO DMEM high glucose 1x (*Thermo Fisher Scientific*)
- 20% DMSO

10x PBS

- 8% sodium chloride
- 0.2% potassium chloride
- 0.2% monopotassium phosphate
- 1.11% disodium hydrogen phosphate
- Diluted in dH_2O and pH adjusted to 7.4 with NaOH

2.3.2 Seeding & harvesting cells

Seeding cells for Immunofluorescence staining

At 60-80% confluency cells were washed, trypsinized and centrifuged. After resuspending the pellet in 1 ml of KGM2 the cells were counted. Subsequently the desired number of cells were added to 12 – or 6- well plates containing sterile coverslips.

Harvesting cells for protein analysis

Cells were washed once with 1xPBS and then scraped off the plates using a cell-scraper. The suspension was transferred into a Falcon tube, centrifuged for 5 minutes at 1,200 rpm and the supernatant was discarded. After one more washing step with PBS, the cell pellet was either stored at -80°C or immediately used for further experiments.

2.3.3 Treatment with HDAC inhibitors

To induce hyperacetylation of the histones and other target proteins of HDAC1, different human keratinocyte cell lines were treated with the class I HDAC inhibitor MS-275. This inhibitor has an especially high affinity for HDAC1 and HDAC3. 10mM stocks of MS-275 in DMSO were diluted in fresh KGM2 media to a final HDAC inhibitor concentration of 2µM. The cells on multi-well plates were treated once for 24h and a second time if they were treated for 48h. As a control, cells were treated with an equal volume of DMSO. After 24h or 48h hours the cells were harvested for protein/RNA extraction or fixed for immunofluorescence staining.

2.3.4 Immunofluorescence staining of keratinocytes

Treated and untreated control cells were cultivated on sterile coverslips in 12 or 6 well dishes for 2-4 days. After washing the cells briefly with 1xPBS, they were fixed with 4% PFA in 1x PBS and incubated for 20 minutes at 4°C for. The cells were then washed twice with 1xPBS and subsequently permeabilized by adding 0.1% Triton-X in PBS for 20 minutes at room temperature. To prevent unspecific binding of antibodies, cells were blocked with 2% BSA and 10% goat serum

in 1x PBS for 30 minutes at room temperature. The primary antibodies were diluted in 1x PBS containing 2% BSA as depicted in Table 10 and incubated overnight at 4°C. To remove the primary antibody, the cells were washed three times for 5 minutes with 1x PBS. The secondary fluorophore-labelled antibody was diluted 1:500 in 1x PBS with 2% BSA and 10% goat serum and added onto the cells. Depending on the origin species of the primary antibody different secondary antibodies were used (Table 10). After 1 hour incubation in the dark the cells were washed again three times with 1x PBS. The super sensitive DNA stain PicoGreen (*Thermo Fisher Scientific P7581*) and/or DAPI were used for nuclear counterstaining. Both dyes were diluted in 10mM aqueous Tris-HCl pH 7.5 with 1 mM EDTA and incubated for 30 minutes at room temperature in the dark (PG 1:1000; DAPI: 1:2000). Subsequently, the cells were washed another three times with 1x PBS and once shortly with dH_2O. Finally, the coverslips were mounted on microscopy slides using Prolong Gold Antifade reagent (*Thermo Fisher Scientific P36930*).

Antibody	Species	Dilution	Company
Histone H3S10ph (SC8656-R)	Rabbit	1:2000	Santa Cruz Biotechnology
cGas (D1D3G)	Rabbit	1:200	Cell signalling
M2 FLAG (F 1804)	Mouse	1:500	Sigma Aldrich
H3K56ac (ab76307)	Rabbit	1:1000	Abcam
γH2ax (JBW301)	Mouse	1:1000	Millipore

Table 10: Primary antibodies used for immunofluorescence staining of keratinocytes

2.4 Microscopy

Image acquisition of the slides stained with H&E or immunofluorescent dyes was performed with the *Olympus BX61VS* slide scanner. The whole slide was pre-scanned with the 2x objective for sample detection. Subsequently, the whole sample or only selected areas were scanned in detail using 20x, 40x, or 100x objectives depending on the desired resolution. Single images were chosen and analyzed with the accompanying *Olympus OlyVIA* software. Figures were prepared with *Adobe Photoshop*, *Image J* and *Adobe illustrator*.

2.5 Work with proteins

2.5.1 Total protein extraction from mouse epidermis

The ceramic bead tubes containing the epidermal samples were supplemented with approx. 200µl of Hunt lysis buffer containing a set of protease inhibitors, which were added directly before use. Using the FastPrep-24 homogenizer (*MP biomedicals*) the tissue was processed twice for 6m/s for 30 seconds. In between homogenization runs the samples were kept on ice for 1-2 minutes. The samples were then centrifuged for 5 minutes at 14000rpm and 4°C. The supernatant which contains the extracted proteins was transferred to a fresh tube and centrifuged again for 30 minutes at 140000rpm and 4°C. Afterwards, the supernatant was collected and put into a new tube. The concentration of the samples was measured using the Bradford protein assay (*Bio-Rad*). The Bradford protein dye reagent concentrate (*Bio-Rad*) was diluted in dH_2O 1:5. 1ml of the diluted Bradford solution was mixed with 1µl of sample. The absorbance of the samples was measured at 595 nm using polystyrene cuvettes with the NanoDrop UV-vis spectrophotometer using 1ml diluted Bradford solution mixed with 1µl of Hunt buffer as blank. Samples were always measured in duplicates and the average concentration was calculated. The lysates were either directly used or snap frozen and stored at -80°C

2.6.2 Protein extractions of keratinocytes

The harvested cell pellets were resuspended in the appropriate amount of Hunt buffer with freshly added protease inhibitors. To extract the protein from the cell suspension the tubes were snap-frozen in liquid nitrogen and then thawed at room temperature. This process was repeated three times. The third thawing step was performed during centrifugation for 30 minutes at 14000rpm and 4°C. The protein containing supernatant was transferred to a new tube, measured and stored as described in 2.4.1

Hunt Buffer

- 20 mM Tris/HCl pH 8.0
- 100 mM Sodium chloride
- 1 mM EDTA
- 0.5% NP-40

Protease inhibitors

- 1x Complete Protease Inhibitor Cocktail (*Roche*)
- 10mM Sodium fluoride (1M stock)
- 10mM -glycerophosphate (1M stock)
- 100µM Orthovanadate (activated 5min at 95°C; 100mM stock)
- 100µM Phenylmethylsulfonyl fluoride (PMSF; 100mM stock)
- 10µM Sodium molybdate (10mM stock)

2.6.3 SDS-PAGE

Sodium Dodecyl Sulfate Polyacrylamide Gel Electrophoresis (SDS-PAGE) was used to separate proteins according to their molecular weight. For this, a 10% separation gel and a 5% stacking gel were prepared in a chamber consisting of 2 glass plates (*BioRad*) with the separation gel in the bottom and the stacking gel on top. After polymerization the glass chamber containing the gel was placed into an electrophoresis chamber.

After adding an appropriate amount of SDS loading dye containing SDS to the samples they were heated for 5 minutes at 95°C. The samples and a protein marker (pre-stained Precision Plus All Blue Protein Standard, *Bio-Rad*) were then loaded onto the stacking gel and ran in 1x running buffer at 15-20mA. When the samples reached the separation gel the current was increased to up to 30mA.

10% SDS separation gel (2 gels)

- 3.45ml 30% acrylamide
- 3.9ml 1M Tris, pH 8.8
- 3.06ml dH_2O
- 52.5µl 20% SDS
- 112µl 20% APS
- 7.5µl TEMED

5% stacking gel (2 gels)

- 510µl 30% acrylamide
- 375µl 1M Tris/HCl, pH 6.8
- 2.1ml dH_2O
- 15µl 20% SDS
- 28µl 20% APS
- 7.5µl TEMED

SDS loading dye

- 100 mM Tris/HCl pH 6.8
- 20% Glycerol
- 0.01% Bromophenol blue
- 10% β - Mercaptoethanol
- 5% SDS
- diluted in dH_2O

10x Running Buffer (pH 8.3)

- 14.4% Glycine
- 3% Tris base
- 1% SDS
- diluted in dH_2O

2.6.4 Western Blotting (Wet Transfer)

After SDS-PAGE the separated proteins were transferred from the gel onto a nitrocellulose membrane by wet blot transfer. For this, the stacking gel was removed and a "blotting sandwich" was assembled in the following order from cathode to anode in a transfer cassette: sponge, Whatman paper, separation gel, nitrocellulose membrane, Whatman paper, sponge. Before use, all components were soaked in 1x transfer buffer. After placing the cassette into a blotting tank (*BioRad*), it was filled with cold 1x transfer buffer. The proteins were blotted at 4°C for 2 hours at 250mA. To check if the transfer was successful, the nitrocellulose membrane was briefly stained with 1xPonceau staining solution for 5 min to check if the transfer was successful and afterwards distained with dH_20.

Wet Transfer Buffer

- 3.024 g/L Tris/HCl, pH 8.0
- 14.42 g/L Glycine
- 20% Methanol (optional)
- diluted in dH_2O

10x Ponceau stain solution

- 2% Ponceau S
- 30% Trichloroacetic acid
- 30% Sulfosalicylic acid
- diluted in dH_2O

2.6.5 Antibody incubation and immunodetection

In order to prevent non-specific binding of antibodies, the membrane was incubated in blocking solution for 30 minutes, shaking and on room temperature. After blocking, the membrane was rolled over night and incubated at 4°C with the primary antibody diluted in 5ml blocking solution according to Table 11. Subsequently, the membrane was washed three times for 5 minutes each with 1x PBS-tween (0,1% Tween-20). The blot was then incubated with the secondary antibody (diluted 1:10000) for 1 hour at room temperature while shaking. Depending on species of origin species of the primary antibody, either goat igG anti-rabbit or goat igG anti-mouse secondary antibodies (see Table 12.) were used. Afterwards, the blot was washed again three times with 1x PBS-tween before the chemiluminescent ECL Western Blotting Detection Reagent (*GE Healthcare*) was added. Detection reagents 1 and 2 were mixed 1:1 and pipetted onto the membrane. After a

couple of seconds of incubation, the Fusion FX (Vilber Lourmat) detection system was then used to visualize the antibody-antigen signals.

Blocking Solution

- 1% Milk powder
- 1% Polyvinylpyrrolidone
- 0.1% Tween-20
- 0.02% Sodium azide
- diluted in 1xPBS
- pH adjusted to 7.4

Antibody	Animal	Source	Dilution
HDAC1 Sat 208	rabbit	Seiser Lab	1:10000
HDAC2 #3F3	mouse	Seiser Lab	1:1000
HDAC1 #10E2	mouse	Seiser Lab	1:1000
FLAG #M2	mouse	Sigma (F 1804)	1:1000
beta-actin	mouse	Abcam (ab8226)	1:1000
yH2AX	mouse	Millipore (JBW301)	1:1000

Table 11: Primary antibodies for Protein detection

Antibody	Animal	Source	Dilution
Anti-mouse-HRP	goat	Jackson Laboratories (124594)	1:10000
Anti-rabbit-HRP	goat	Jackson Laboratories (129411)	1:10000

Table 12: secondary antibodies for protein detection

2.7 Expression analysis

Before working with RNA, the workbench as well as all of the equipment used were cleaned using 1M NaOH/1mM EDTA to prevent RNA degradation caused by RNase contamination.

2.7.1 RNA extraction from mouse epidermis

The isolated epidermal tissue for RNA extraction was snap-frozen in a tube containing 1ml of Trizol *(Invitrogen)* and ceramic beads by liquid N2. The samples were slowly thawed on ice before being processed using the FastPrep-24 homogenizer (*MP Biomedicals*). The homogenization process was repeated twice at 6m/s for 30 seconds. Between runs, the samples were cooled on ice for 1 minute. Subsequently, the tubes were centrifuged at 12000rpm at 4°C for 10 minutes. The RNA containing Trizol solution was aspirated and transferred to a fresh tube. Next, 200µl chloroform was added and the samples were shaken vigorously for 15 seconds before being incubated for 2 minutes at room temperature. After incubation, the samples were centrifuged for 15 minutes at 12000rpm at 4°C. The upper aqueous phase containing the RNA was carefully aspirated and transferred into a new tube. For the first precipitation step, 500µl of isopropyl alcohol and 1µl glycogen (20mg/ml) were added and mixed with the samples by inverting the tubes. After 10 minutes incubation on room temperature, the samples were centrifuged for 10 minutes again at 12000rpm and 4°C. To wash the RNA pellet, the supernatant was removed and 1 ml 75% ethanol was added to the tube. After vortexing the samples until the pellet detached from the bottom of the tube, the tubes were centrifuged for another 5 minutes at 7500rpm at 4°C. Next the ethanol was removed and the pellets were air-dried. Depending on their size the pellets were dissolved in 30-100µl nuclease free dH_20 (supplemented with 0.1pl/ml Protector RNase Inhibitor; *Roche*) and incubated at 55°C for 10 minutes while shaking slightly (300rpm). For the second precipitation 1/10 vol. 3M sodium acetate (pH 5.2), 1µl of glycogen (20mg/ml) and 2.5 vol. 96% ethanol were added and the samples were kept at -20°C overnight. The next day, the RNA was pelleted by centrifugation for 30 minutes at 12000rpm at 4°C and the supernatant was discarded. Another washing step was performed using 75% ethanol as described above. Finally, the pellet was resuspended in 30µl nuclease free dH_2O (supplemented with 0.1µl/ml Protector RNaseInhibitor; *Roche*) and the samples were incubated at 55°C slightly shaking for 10 minutes to properly dissolve the RNA. The RNA concentration was measured using a NanoDrop UV-Vis spectrophotometer (*VWR*) and RNA integrity was assessed by gel electrophoresis.

2.7.2 RNA extraction from immortalized human keratinocytes

Cells for RNA extraction were cultivated on 6 or 12 well plates. The cells were washed once with cold 1x PBS before adding 500µl Trizol reagent (*Invitrogen*) to each well. To detach the cells from the surface, the reagent was pipetted up and down a couple of times. The cells were then transferred to a 1.5 ml tube and either stored in Trizol at -80°C or directly used for RNA extraction. First, 150µl of chloroform were added to the samples. After vortexing the samples for 15 seconds, they were centrifuged for 5 minutes at maximum speed at room temperature to allow phase separation. The upper aqueous phase containing the RNA was aspirated and pipetted into a new tube. For precipitation of the RNA 300µl isopropyl alcohol, 30µl sodium chloride (4M in nuclease free dH_2O) and 1µl glycogen(20mg/ml) were added to the samples. After 10 minutes of incubation on room temperature the samples were centrifuged at 4°C and maximum speed for 30 minutes. Subsequently, the supernatant was discarded and the RNA pellet was washed by adding 1ml 75% ethanol, mixing and centrifuging the samples for 5 minutes at 4°C and 7500rpm. The samples were washed twice before air-drying them by opening the lid for the ethanol to evaporate. Subsequently, the dry pellet was resuspended in 30µl nuclease free dH_2O and incubated at 55°C for 10 minutes while shaking. The RNA concentration was measured using a NanoDrop UV-Vis spectrophotometer (*VWR*) and RNA integrity was assessed by gel electrophoresis.

2.7.3 RNA gel electrophoresis

The quality of the RNA was assessed by denaturing gel electrophoresis on a 1.2% MOPS agarose gel. 500ng of RNA from each sample were diluted with nuclease free dH_2O and 2µl RNA loading buffer. Before loading the samples on the gel, the RNA was denatured on a shaking heating block at 65°C for 5 minutes and subsequently cooled on ice for 1 minute. After loading the samples onto the MOPS gel, electrophoresis was run in cold 1x MOPS buffer at 90 V for approximately 30-40 minutes. If the gel showed clearly defined 28S and 18S rRNA bands showing a 2:1 intensity ratio, RNA integrity is confirmed.

RNA loading buffer

- 15ml Formamide (deionized)
- 4.8ml 37% Formaldehyde
- 3ml 10 x MOPS
- 2ml 87% Glycerol
- 2ml dH_20
- 10mM EDTA
- 1.6ml 10% Bromophenol blue
- 100µl Ethidium bromide

10x MOPS buffer

- 0.2M MOPS
- 50mM Sodium acetate pH 5.0
- 10mM EDTA
- in dH_2O, adjusted to pH 7 with 1M NaOH, autoclaved

MOPS gel

- 1.2g Agarose
- 90ml sterile dH_20
- 10m] 10x MOPS
- 5.2ml 37% Formaldehyde (added after heating)

2.7.4 Reverse transcription

RNA was reversely transcribed using the iScript cDNA synthesis Kit (*Bio-Rad*). For each transcription, 500-1000ng of total RNA was used per sample and mixed with 4µl 5x iScript reaction mix, 1µl iScript reverse transcriptase and filled up to a total volume of 20µl with nuclease free dH_2O. The iScript reaction mix consists of reverse transcriptase with RNase H activity, RNase inhibitor, dNTPs, oligo(dT) and random hexamer primers. The mixed samples were put on a thermocycler (T100 Thermal Cycler; *Bio-Rad*) and reversely transcribed using the program below. Subsequently, the cDNA was diluted 1:10 with nuclease free water to a total volume of 200µl.

Reverse transcription program

25°C	5 minutes
46°C	20 minutes
95°C	1 minute
4°C	∞

2.7.5 Quantitative real time PCR

For quantitative real-time PCR (qRT-PCR), the SSo Advanced Universal SYBR Green Supermix (*Bio-Rad*) and the CFX96 or CFX284 Real-Time PCR Detection System (Bio-Rad) were used. The reaction set-ups for the samples were calculated as indicated below. Each reaction was performed in duplicates. For every primer pair an internal dilution series of combined cDNA from all samples was included to obtain a standard curve. All primers are listed below and were designed with a desired annealing temperature of approx. 60°C. Hypoxanthine-guanine-phosphoribosyl transferase (Hprt) was used as a reference gene to normalize mRNA expression for mouse samples. For human keratinocytes the housekeeping gene ß2-Microglobulin (B2m) was used as a reference gene.

qRT-PCR reaction mix

- 5µl cDNA template
- 0.24µl forward primer (10M)
- 0.24µl reverse primer (10M)
- 0.52µl dH_2O
- 6µl Sso Advanced Universal SYBR Green Supermix (*Bio-Rad*)

qRT-PCR program

95°C	2minutes	
95°C	10 seconds	40 cycles
60°C	30 seconds	
65-95°C	melt curve generation	
20°C	∞	

Primer	Sequence 5' — 3'
mRT_Hprt_for	GCTGGTGAAAAGGACCTCT
mRT_Hprt_rev	CACAGGACTAGAACACCTGC
mRT_Isg15_for	CCAGTCTCTGACTGTGAGAGC
mRT_Isg15_rev	GCATCACTGTGCTGCTGGGAC
mRT_Cxcl10_for	TTCTGCCTTCATCCTGCTG
mRT_Cxcl10_for	AGACATCTCTGCTCATCATTC
mRT_Oasl1_for	ACGATGATGGTGAGCCTTGTC
mRT_Oasl1_rev	CAGGAAGAGCAGGTCAGAGATG
mm_Ccl5_ex1F1	CCCTCACCATCATCCTCACT
mm_Ccl5_ex2R1	GAGCACTTGCTGCTGGTGTA
mm_Tnf_F1	CCACCACGCTCTTCTGTCTA
mm_Tnf_R1	CACTTGGTGGTTTGCTACGA

mRT_Ifit1_F2	GCTCTGCTGAAAACCCAGAG
mRT_Ifit1_R2	CCCAATGGGTTCTTGATGTC
m_cGas_F2	ACGAGAGCCGTTTTATCTCGTACCC
m_cGas_R2	GCTCCGGAAGATTCACAGCATGTTT
mRT_Krt1_F1	GCTCTGCTGAAAACCCAGAG
mRT_Krt1_R1	CCCAATGGGTTCTTGATGTC
mRT_Krt6A+B_F	ACAACAACCGTAGCCTGGAC
mRT_Krt6A+B_R	TGGCACACTGCTTCTTAACG
mRT_Cers4_F	CCGGTCCTATTTCCTCCCTC
mRT_Cers4_R	ACCAGTATGTCTCCTGCC
mRT_Sphk1_F	CGGGACCTGGCTATGGAA
mRT_Sphk1_R	ATGGTTCTTCCGTTCGGTGA
mRT_Fdps_F	TCCGCGTTGAAGAACAGGGAG
mRT_Fdps_R	GTAGGAAACCAAGCCACCTCT
mRT_Hmgcs1_F	CACAGTCTGGGGTCTCCTTG
mRT_Hmgcs1_R	GCATGGTGAAAGAGCCAAAGG
mRT_Lef1_F	AGCGAATGTCGTAGCTGAGT
mRT_Lef1_R	GAGCTTCTCTTACCACCTGAA
mRT_Runx1_F	GAGCGGTAGAGGCAAGAG
mRT_Runx1_R	AGTGGAGTGGTTCAAGGAG
mRT_Ior_F	TCCCTGGTGCTTCAGGGTAAC
mRT_Ior_R	TCTTTCCACAACCCACAGGA
mRT_Clau3_F	CCGGTCCTATTTCCTCCCTC
mRT_Clau3_R	ACCAGTATGTCTCCTGCC
mRT_Epgn_F	TCCGCGTTGAAGAACAGGGAG
mRT_Epgn_R	GTAGGAAACCAAGCCACCTCT
mRT_DNase2L_F	GACGCGTCTACGATGTGTA
mRT_DNase2L_R	ATCCGGTCATAGGCACAGTC
mm_Spink5-F	TGGGAGGACACATGGCAATA
mm_Spink5-R	CACAGAGGGCACACTTGTTC
mm_Ly6d_F	ACTTCTGCAAAACCGTCACC
mm_Ly6d_R	TTGCATAGGTCAGTCTGGCA
mm_Ly6g6_F	ACCCTGTCTGCCCTACTCTA
mm_Ly6g6_R	TTTCGTTGAAGACCTCCCGA
mm_Prdm1_F	TCCCAAGAATGCCACAGGA
mm_Prdm1_R	GGTTGGCAGGGATAGGCTTA
Krt10	GAGCGGTAGAGGCAAGAG
Krt10	AGTGGAGTGGTTCAAGGAG
Ifng	AGCGAATGTCGTAGCTGAGT
Ifng	GAGCTTCTCTTACCACCTGAA

Table 13: Primers used for qRT-PCR with mouse samples

2.8 Single Cell RNA Sequencing (scRNAseq) and data analysis

ScRNAseq was performed in cooperation with Michael Mildner (Department of Dermatology, Medical University of Vienna) as previously described (Klas et al, 2021; Figure 7). Briefly, three punch biopsies (6 mm) were taken from the nape skin of shaved mice and pooled for each genotype. Subsequently, tissues were eenzymatically digested using GentleMACS whole skin dissociation kit (Miltenyi Biotec) according to the manufacturer protocol. For further processing of the samples, the GentleMACS OctoDissociator (Miltenyi Biotec) was utilized. Using 100µm and 40µm filters, the cell suspension was filtered and subsequently washed with 0.04% bovine serum albumin (Sigma Aldrich) in PBS. After assessing cell viability and concentration, the concentrations were adjusted to the 1.2 x 10^6 cells/mL. Next, gel beads-in-emulsion (GEMs) were generated. In accordance to the protocols of the manufacturer of Chromium Next GEM Single Cell 3'GEM, Library and Gel Bead Kit v3.1, Chromium Next GEM Chip G Single Cell Kit and Single Index Kit T Set A (10x Genomics) GEM generation, barcoding, sample clean-up, cDNA amplification as well as library construction were performed. Final RNA-sequencing, demultiplexing and counting were performed by the Biomedical Sequencing Facility (BSF) of the Centre for Molecular Medicine (CeMM, Vienna, Austria). Data analyses were carried out using R-studio desktop application and the R-Package "Seurat" (Seurat v4.0.3,) according to Klas et al. 2021. Gene ontology enrichment analyses was done using the free-version of the enrichment tool Metascape (https://metascape.org/gp/index.html#/main/step1).

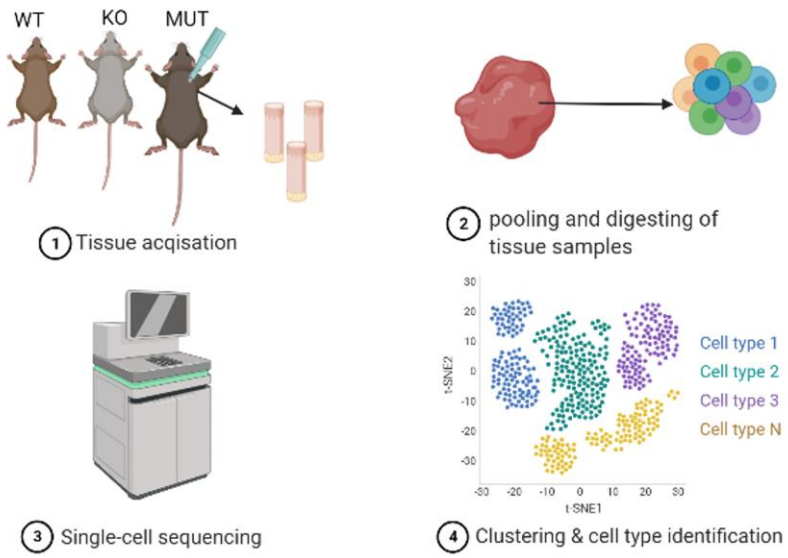

Figure 7: Schematic of ScRNAseq procedure. (1) Tissue samples are isolated from each mouse of the different genotype. (2) The whole tissue samples for each genotype are pooled and digested. (3) Afterwards, single cell sequencing is performed and cell types are identified as clusters bioinformatically (4).

2.9 Statistical analysis

GraphPad Prism software was utilized for statistical analysis and for the generation of visual representations. Relative mRNA expression levels of qRT-PCR analyses of murine epidermal skin samples were normalized to wildtype control mice with *Microsoft Excel*. Expression Data was analysed using ordinary one-way ANOVA. Sidak multiple comparison tests were used to determine p-values. Gaussian distribution of samples was assumed.

The TEWL was measured at least three times for each individual, the mean was calculated and compared to the other genotypes using ordinary one-way ANOVA under the same conditions as described above.

To quantify the abnormal mitotic cells after HDAC inhibitor treatment in human wildtype keratinocytes and in keratinocytes different genetic backgrounds 80 H3S10ph-positive mitotic and post-mitotic nuclei per condition were analysed for nuclear defects and calculated as percentage of the total number of H3S10ph nuclei. Slides were previously randomized and analysed in a blinded manner.

γH2AX signalling after HDAC inhibitor treatment was quantified using *FIJI* by calculating the integrated density of the nuclear γH2AX signal of three random areas of the coverslip. The replicate values were averaged and compared with an unpaired two-tailed t-test. Gaussian distribution was assumed.

To calculate the percentage of binucleated cells treated with the HDAC inhibitor MS-275 compared to PBS treated control cells, three random areas of the same size on the coverslip were chosen for each concentration and binucleated cells were counted in a blinded manner. The percentage of binucleated cells compared to the total number of normal nuclei was calculated for each area. The triplicate values were averaged and analysed using ordinary one-way ANOVA. The Sidak multiple comparison test was used to locate significant differences between selected means. The confidence levels of all statistical analyses were set to 95% (*$p<0.05$; **$p<0.01$; ***$p<0.001$; ns means not significant). All data are plotted as mean and SEM.

3. Results

3.1 Generation of mice with epidermal expression of the HDAC1 variants HDAC1^{Ci} and HDAC1^{2S}

To study the specific catalytic and scaffolding functions of HDAC1 in the context of epidermal morphogenesis and homeostasis, we replaced endogenous HDAC1 with different HDAC1 variants specifically in keratinocytes. Therefore, mice with lox P sites flanking exon 6 (*Hdac1*$^{f/f}$) were crossed with mice expressing FLAG-tagged HDAC1 H141A (*Hdac1*$^{Ci/+}$ or *Hdac1* $^{Ci/Ci}$) or HDAC1 S421A, S423A (*Hdac1* $^{2S/+}$ or *Hdac1* $^{2S/2S}$) from the safe harbour locus Rosa 26. Mice were also crossed with a strain expressing the cre-recombinase enzyme under the bovine Keratin 5 promotor, enabling keratinocyte specific deletion of endogenous *Hdac1* with simultaneous expression of catalytic inactive *Hdac1* (*Hdac1* $^{\Delta/\Delta ep\ Ci/+}$). In addition, using this genetic setting, mice were generated in which endogenous HDAC1 was replaced with a catalytically inactive HDAC1 protein variant that is unable to integrate into co-repressor complexes (*HDAC1*$^{\Delta/\Delta ep\ 2S/+}$). Mice obtained in the breeding for catalytically inactive HDAC1 variant had the following genotypes *Hdac1*$^{\Delta ep/+\ Ci/+}$; *Hdac1*$^{\Delta ep/+\ Ci/Ci}$; *Hdac1*$^{\Delta/\Delta ep\ Ci/+}$; *Hdac1* $^{\Delta/\Delta ep\ Ci/Ci}$. Mice obtained in the breeding for the 2S variant had the following genotypes *Hdac1*$^{\Delta ep/+\ 2S/+}$; *Hdac1* $^{\Delta ep/+\ 2S/2S}$; *Hdac1* $^{\Delta/\Delta ep\ 2S/+}$; *Hdac1* $^{\Delta/\Delta ep\ 2S/2S}$. In this project we mainly focused on the phenotypical *Hdac1*$^{\Delta/\Delta ep\ Ci/+}$ strain as well as the new *Hdac1*$^{\Delta/\Delta ep\ 2S/+}$ strain and utilized wildtype mice and a mouse strain with keratinocyte-specific knockout of *Hdac1* (*Hdac1* $^{\Delta/\Delta ep}$) controls.

3.1.1 Validation of mice carrying different epidermal *Hdac1* variants

Before dissection and analysis of the mice, we aimed to confirm the expression of the transgenes as well as the knockout of endogenous *Hdac1* on the DNA and on the protein level. For validation on the DNA level, we used several different PCR reactions. Figure 8A shows an agarose gel with genotyping results from one litter. Knockout of endogenous *Hdac1* is assessed by the HD1 flox PCR resulting in a 900bp fragment if an endogenous *Hdac1* allele is floxed out and an 850bp fragment if at least 1 wildtype allele is present. The presence of a single band at ~1240 bp after the HDAC1 screen PCR implies that this mouse carries at least one transgenic allele. In case, that no transgene is inserted into the Rosa26 locus R26wt PCR resulted in a product of 915 bp. Mice were found to be cre-recombinase positive when the Cre-PCR generated a product of 1000 bp. Finally, HDAC1 Δ PCR produced a 600 bp PCR product only when at least one allele of the transgene and the *cre*-recombinase are present. The red box indicates a *Hdac1* $^{\Delta/\Delta ep\ Ci/+}$ mouse (Figure 8A).

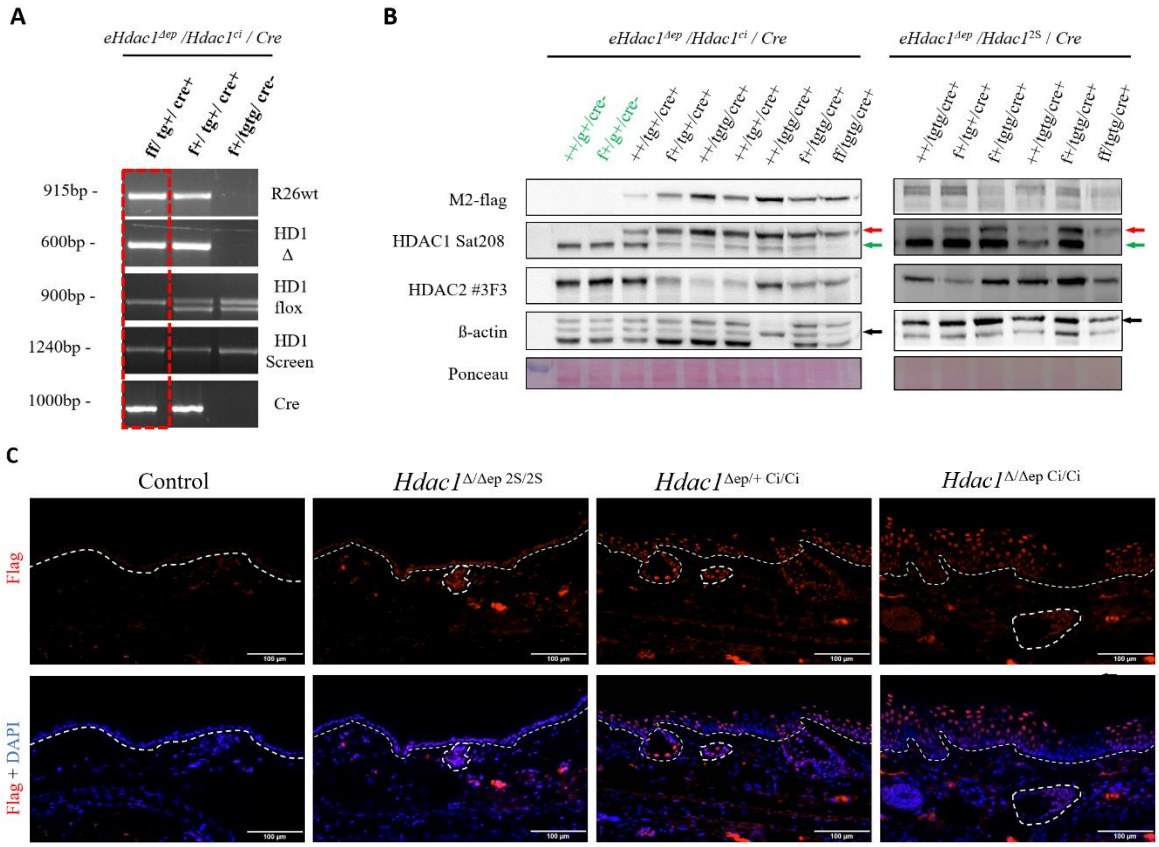

Figure 8: Validation of HDAC^{CI} and HDAC1^{2S} mice on DNA, protein and immunohistology levels. (A) Genotyping PCR products were separated on a 2% agarose gel. Mice expressing at least one wildtype allele of *Hdac1* show one band at 915bp after the R26wt PCR. Mice showing a band after the HD1Δ PCR carry at least one transgene in a Cre-positive background. The HD1 flox PCR produces a 900bp fragment in mice with at least one floxed *Hdac1* allele and an additional 850bp fragment if at least 1 wildtype allele is present. The HD1 Screen PCR results in a single band at 1240bp if at least one transgene is present in the mouse. An example for a *Hdac1*$^{\Delta/\Delta ep\ Ci/+}$ mouse is highlighted as a red box. (B) Western blot analysis showing the expression of endogenous (green arrow) and transgenic (red arrow) HDAC1 protein. Protein lysates of tail epidermis of all genotype combinations were separated on a 10% SDS gel. Anti-M2-FLAG and anti-HDAC1 antibodies were used to detect the respective proteins. ß-actin was visualized with the ab8227 antibody and served as loading control. Whole protein Ponceau staining served as a control for equal loading and blot integrity. (C) Immunofluorescence staining of back skin sections from Cre-negative (control), *Hdac1* $^{\Delta/\Delta ep\ 2S/2S}$, *Hdac1* $^{\Delta ep/+\ Ci/Ci}$ and *Hdac1* $^{\Delta/\Delta ep\ Ci/Ci}$ mice. The tissues were stained an anti-M2flag specific antibody and the nuclei were counterstained with DAPI. Upper panel depicts the Flag-signal, lower panel depicts overlay of Flag and DAPI signals. Dashed line indicates dermal -epidermal border and hair follicles, respectively, scale bar indicates 100µm.

The ablation of the endogenous HDAC1 protein as well as the expression of HDAC1 variants were additionally validated by immunoblotting of protein lysates of the tail epidermis. As a control, samples of *Cre* negative mice were used. The simultaneous ablation of the endogenous HDAC1 protein and the expression of the transgenic HDAC1 was validated with an HDAC1-specific antibody. The transgenic HDAC1 proteins contain an additional FLAG-tag resulting in a higher band compared to endogenous HDAC1. The protein levels of the transgenes were also validated by using an M2-FLAG specific antibody. As depicted in Figure 8B, all strains expressing the cre recombinase also express the FLAG-tagged mutant HDAC1 version. We observed that protein

levels of transgenic HDAC1 are similar to endogenous HDAC1 when only a single allele of transgenic *Hdac1* is expressed while expression of two alleles of *Hdac1* ^{Ci} displayed overexpression of the transgenic protein compared to wildtype HDAC1. To avoid dose dependent effects that might be caused by the overexpression of *Hdac1*^{Ci}, we mostly focused on mice heterozygous for catalytically inactive *Hdac1* for the majority of our comparative analysis.

Some mice with two floxed endogenous *Hdac1* alleles still displayed a band of the size of endogenous HDAC1 which could be due to residual immune cells in the epidermis still expressing endogenous HDAC1. Preliminary Ponceau staining and ß-actin antibody detection were used as loading controls (Figure 8B). We additionally assessed the expression of the transgenic proteins by immunofluorescence analysis (Figure 8C). Co-staining of dorsal skin biopsies with a FLAG-specific antibody and the DNA dye DAPI confirmed expression of the FLAG-tagged transgenic protein HDAC1^{2S} and HDAC1^{Ci} in the epidermis and in hair follicles while in wildtype mice (*Cre* negative) no M2-FLAG signal was detected. Furthermore, the staining revealed that the expression of the HDAC1^{Ci} protein seems to be patchy (80~90% FLAG-positive keratinocytes) in some mice, indicating a negative selection or suppression of the HDAC1^{Ci} variant in some keratinocytes.

3.1.2 Assessment of Mendelian ratios indicate gene dosage-dependent mortality of mice when endogenous HDAC1 is replaced by catalytic inactive HDAC1

To analyse pre- and post-natal lethality of mice expressing catalytic inactive HDAC1, offspring of different crossings were counted after an age of 2 months and compared to the theoretical Mendelian ratio. For analysis of the mortality of mice expressing one allele of *Hdac1* H141A 7 litters with 67 mice born were assessed. Of this, 14 *Hdac1*$^{\Delta/\Delta ep\ Ci/+}$ mice reached the age of 2 months and no dead animal was found. In addition, the number of mice closely matched the number of mice theoretically born (15.4) indicating that replacing endogenous *Hdac1* with an allele of catalytically inactive *Hdac1* does not result in increased perinatal and postnatal lethality. In contrast, out of 100 offspring (10 litters) with a predicted number of 14 *Hdac1* $^{\Delta/\Delta ep\ Ci/Ci}$ mice, only 4 were born and of these only 2 survived to two months of age. This indicates that the level of catalytically inactive HDAC1 protein is relevant to increased mortality in the absence of functional endogenous HDAC1. Protein measurements of mice carrying the transgene showed an overexpression when two alleles of *Hdac1* ^{Ci} were present which could indicate a dominant effect of the transgenic HDAC1 over endogenous compensation via HDAC2.

3.1.3 Keratinocyte-specific expression of catalytic inactive HDAC1 results in skin abnormalities

After confirming the knockout of endogenous *Hdac1* and the expression of the transgenes we first analysed the macroscopic phenotype of mice carrying the transgenes and compared them to wildtype and *Hdac1* $^{\Delta/\Delta ep}$ mice. As already mentioned, only two *Hdac1* $^{\Delta/\Delta ep\ Ci/Ci}$ mice have been born so far and only one of them was analysed in the present thesis. Appropriately, this mouse displayed the most severe skin phenotype with partial alopecia and shaggy and greasy hair (Figure 9B). Likewise, the majority of mice carrying only one transgene of catalytically inactive *Hdac1* in the epidermal *Hdac1* knockout background also showed obvious phenotypical differences compared to the control strains (Figure 9B). In contrast, *Hdac1*-deficient mice with or without a single or two *Hdac1* ^{2S} alleles showed normal development and were indistinguishable from *Cre*-deficient control mice (Figure 9A, 9B). The absence of any phenotype changes in the *Hdac1* ^{2S}

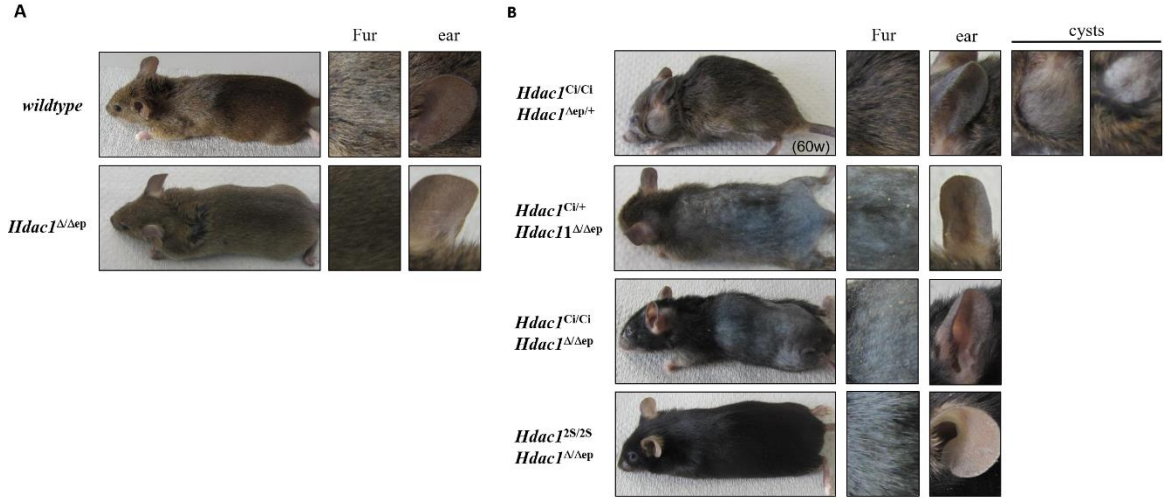

Figure 9: Macroscopic phenotype of control, *Hdac1*^{Ci} and *Hdac1*^{2s} mice. (A) images of Cre negative wildtype control mice (WT) and *Hdac1* knockout mice (*Hdac1*$^{\Delta/\Delta ep}$). **(B)** Representative pictures of phenotypical mice expressing the catalytically inactive *Hdac1*^{Ci} transgene (*Hdac1*$^{\Delta/\Delta ep\ Ci/+}$, *Hdac1*$^{\Delta/\Delta ep\ Ci/Ci}$; *Hdac1*$^{\Delta ep/+\ Ci/Ci}$) and a mouse of the HDAC1^{2S} (*Hdac1*$^{\Delta/\Delta ep\ 2S/2S}$) strain.

mutants suggests that the disruption of scaffolding functions of HDAC1 in keratinocytes does not have an obvious effect on epidermal morphogenesis and homeostasis. The timing and severity of the phenotype of *Hdac1* $^{\Delta/\Delta ep\ Ci/+}$ mice differed between individuals. In general, they developed more or less shaggy and less shiny hair indicating arising alopecia. Another observation was the thickening of the ears, which can be a sign for immune cell infiltration into the skin. Furthermore, we observed cyst formation in some older mice carrying at least one copy of catalytically inactive *Hdac1*.

3.1.4 Keratinocyte-specific inactivation of HDAC1 results in acanthosis, hyperkeratosis and differentiation defects of the epidermis

After assessing the macroscopic phenotype of the mice, we isolated samples from the ear and from dorsal skin and performed hematoxylin and eosin (H&E) staining from all mouse strains at different postnatal ages. The staining revealed several abnormalities in the structure of the skin of *Hdac1*$^{\Delta/\Delta ep\ Ci/+}$ mice compared to wildtype controls. As depicted in Figures 10A and 10B, the epidermal structure of *Hdac1*^{Ci} mice is characterized by an overall thickening of the epidermis (acanthosis; indicated by double headed arrows) and a thickened and compacted strateum corneum (hyperkeratosis; indicated by asterisk) indicating epidermal keratinocyte hyperproliferation. In the dermis, we observed an overall higher cellularity which can be a sign of inflammation due to infiltration of immune cells into the dermal compartment (indicated by hashtag). Moreover, sebaceous glands seemed to be enlarged (arrows). To further investigate a possible deregulation of the epidermal differentiation processes of our transgenic mice, we performed immunofluorescence staining on dorsal skin biopsies with an antibody specific for the late terminal differentiation marker Loricrin and for the activation marker Keratin 6. As depicted in Figure 11 A and B we observed a strong upregulation for both signals in *Hdac1*^{Ci} mice but not in the *Hdac1*^{2S} mice, when compared to wildtype mice. Immunolabeling for Loricrin in *Hdac1*^{Ci} mice not only showed higher signal intensity, but also extended to multiple epidermal layers, indicating a deregulation of the process of terminal keratinocyte differentiation. Likewise, Keratin 6 was found to be expressed in the *Hdac1*$^{\Delta/\Delta ep\ Ci/Ci}$ mouse, whereas it was absence in all other strains. Since epidermal keratinocytes express Keratin 6 only in skin diseases such as psoriasis or atopic dermatitis and during wound healing, our finding suggests that inhibition of HDAC1 leads to activation of keratinocytes, similar to skin pathologies. Next, we performed expression analysis of RNA isolated from tail-epidermis samples by qRT-PCR comparing mRNA levels of two different keratins and the endonuclease *Dnase1l2* of wildtype (control), *Hdac1*$^{\Delta/\Delta ep\ 2S/2S}$, *Hdac1*$^{\Delta/\Delta ep}$, *Hdac1*$^{\Delta/\Delta ep\ Ci/+}$, *Hdac1*$^{\Delta ep/+\ Ci/Ci}$ mice using primer pairs for. We observed a strong upregulation in the hyperkeratosis-associated Keratin 1 as well as in the activation and hyperproliferation associated keratin 6 in *Hdac1*$^{\Delta ep/+\ Ci/Ci}$ compared to wildtype controls which correlates with our IF results (Figure 11C). The expression levels of the endonuclease *Dnase1l2*, which correlates with late terminal differentiation, was not significantly affected for any of the mouse strains analysed.

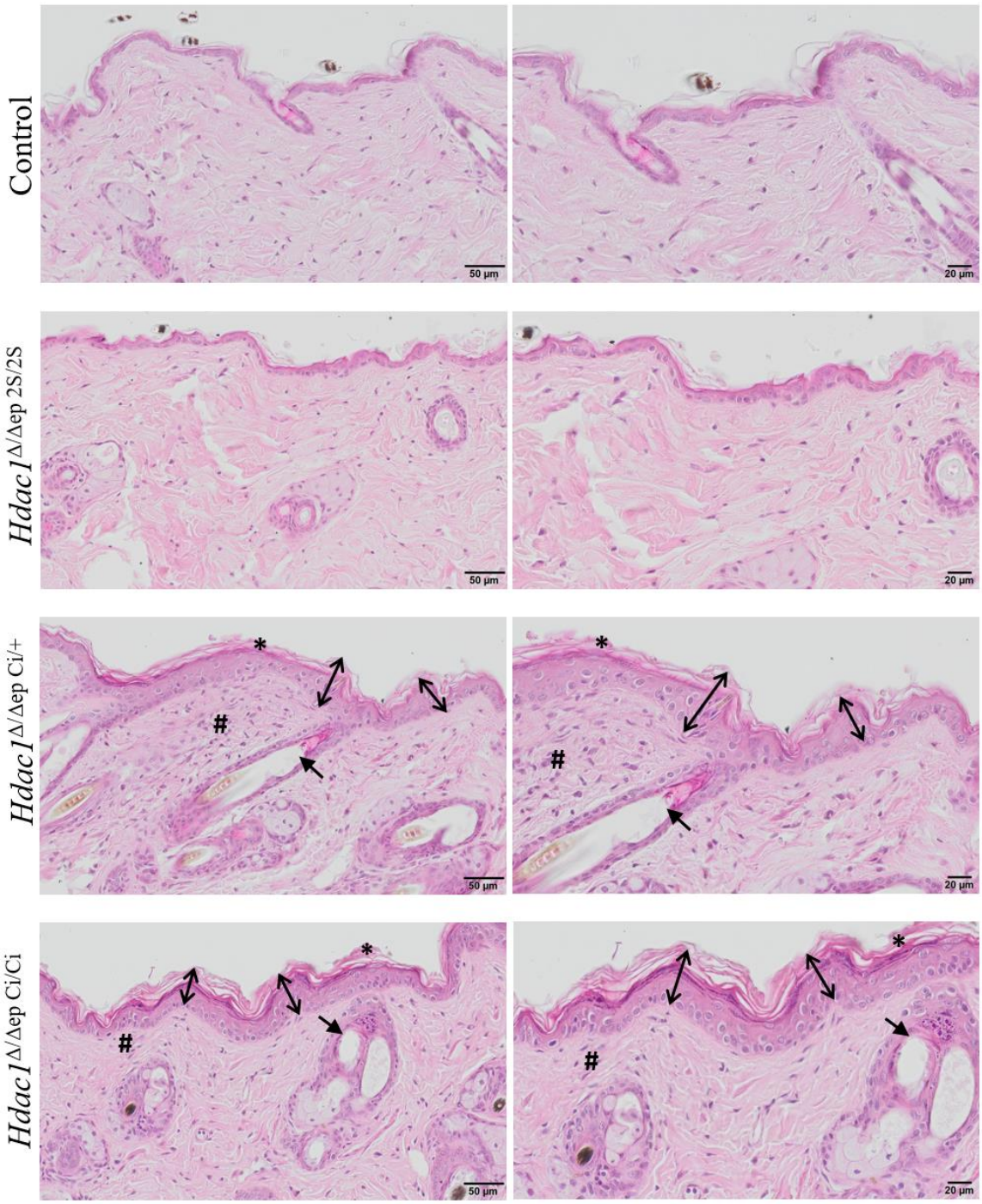

Figure 10A: Histopathology of dorsal skin sections of wildtype, *Hdac1*$^{\Delta/\Delta ep\ 2S/2S}$, *Hdac1*$^{\Delta/\Delta ep\ Ci/+}$and *Hdac1*$^{\Delta/\Delta ep+\ Ci/Ci}$mice. H&E staining of skin sections from the back of wildtype (control) *Hdac1*$^{\Delta/\Delta ep\ 2S/2S}$, *Hdac1*$^{\Delta/\Delta ep\ Ci/+}$and *Hdac1*$^{\Delta/\Delta ep+\ Ci/Ci}$ mice. Enlarged sections are indicated on the right. Dermatopathological alterations found are indicated, such asAcanthosis (double headed arrows), hyperkeratosis (asterisk), enlarged sebaceous glands (arrow) and immune cell infiltration in the dermis (hashtag).

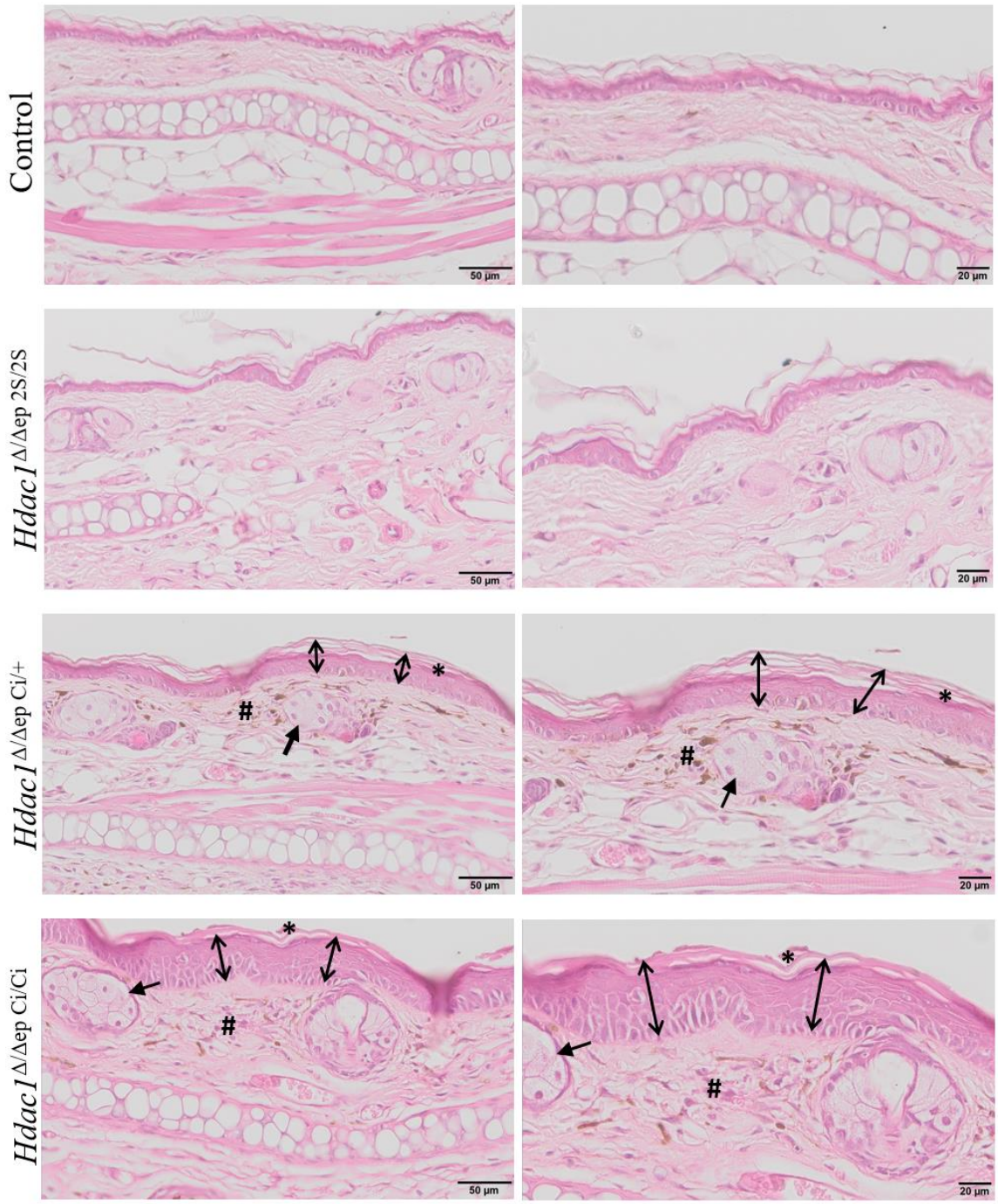

Figure 10B: Histopathology of ear skin sections of wildtype, *Hdac1*$^{\Delta/\Delta ep\ 2S/2S}$, *Hdac1*$^{\Delta/\Delta ep\ Ci/+}$and *Hdac1*$^{\Delta/\Delta ep+\ Ci/Ci}$mice. H&E staining of skin sections from the ear of wildtype (control) *Hdac1*$^{\Delta/\Delta ep\ 2S/2S}$, *Hdac1*$^{\Delta/\Delta ep\ Ci/+}$and *Hdac1*$^{\Delta/\Delta ep+\ Ci/Ci}$ mice. Enlarged sections are indicated on the right. Dermatopathological alterations found are indicated, such as Acanthosis (double headed arrows), hyperkeratosis (asterisk), enlarged sebaceous glands (arrow) and immune cell infiltration in the dermis (hashtag).

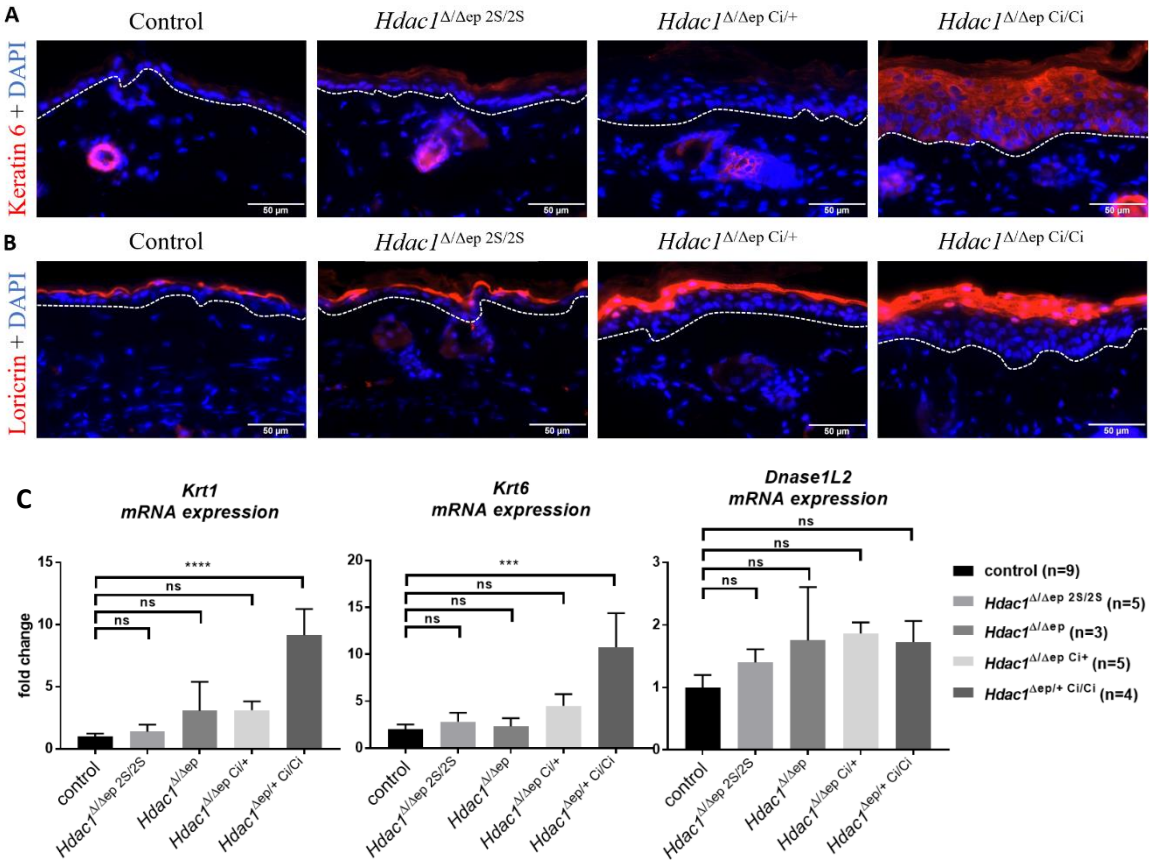

Figure 11: Deregulation of epidermal proliferation and differentiation in *Hdac1*$^{Ci/Ci}$ mice. **A&B**. Immunofluorescence staining of back skin sections from Cre-negative (control), *Hdac1*$^{\Delta/\Delta ep\ 2S/2S}$, *Hdac1*$^{\Delta/\Delta ep\ Ci/+}$and *Hdac1*$^{\Delta/\Delta ep\ Ci/Ci}$ mice. The tissues were stained with Keratin6 (**A**) or Loricrin (**B**) antibodies and nuclei were counterstained with DAPI. One representative picture for each genotype is shown. Scale bars indicate 50µm. **C.** RNA expression analyses by qRT-PCR of Cre-negative (control), *Hdac1*$^{\Delta/\Delta ep}$, *Hdac1*$^{\Delta/\Delta ep\ 2S/2S}$, *Hdac1*$^{\Delta/\Delta ep\ Ci/+}$and *Hdac1*$^{\Delta ep/+\ Ci/Ci}$ mice for different proliferation and differentiation markers. Expression levels were calculated relative to the expression of the house keeping gene beta-2-microglobulin and to the mean value of wildtype mice (ctrl), which was set to 1. Ordinary one-way-ANOVA and Sidak multiple comparison test were used to determine p-values. Data is blotted as mean ± s.d. ***p<0.001; ****p<0.0001; ns=not significant.

3.1.5 Immune cell infiltration and upregulation of immune genes in *Hdac1*^{Ci} mice

The increased cellularity in the skin as well as the apparent thickened ears we observed in our H&E staining in *Hdac1*^{Ci} mice and the upregulation of keratin 6 indicated an infiltration of immune cells. To investigate the hypothesis of invading immune cells, we subjected dorsal skin biopsies to additional staining's for leukocytes using a CD45-specific antibody. As depicted in Figure 12, we observed an increase of CD45-positive leukocytes in the skin of both *Hdac1*$^{\Delta/\Delta ep\ Ci/+}$ and *Hdac1*$^{\Delta/\Delta ep+\ Ci/Ci}$ mice compared to *Cre*-negative wildtype mice. The *Hdac1*$^{\Delta/\Delta ep\ Ci/Ci}$ mouse displayed the most severe increase of CD45-positive leukocytes in the skin. By contrast, the *Hdac1*$^{\Delta/\Delta ep\ 2S}$ mice did not show any increase of CD45 positive cells.

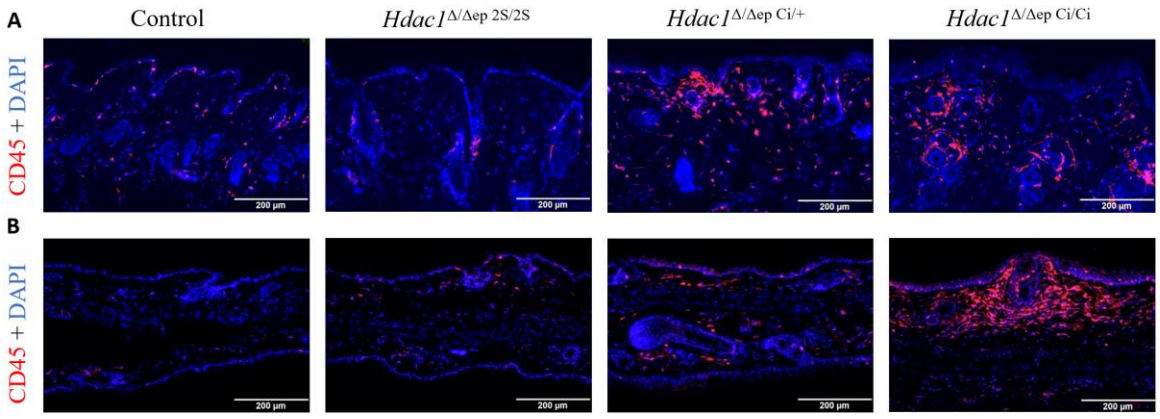

Figure 12: Dose-dependent Increase of CD45 positive leukocytes in the skin of mice expressing one or two alleles of catalytically inactive *Hdac1*. Immunofluorescence analysis of back skin (A) and ear (B) sections of *Hdac1*$^{\Delta ep/+\ Ci/Ci}$ *Hdac1*$^{\Delta/\Delta ep\ Ci/Ci}$ mice compared to Cre-negative control mice. The tissue was stained with an anti-CD45 antibody and nuclei were counterstained with DAPI. Scale bars indicate 200µm

To asses if the immune response in the *Hdac1*^{Ci} mice is regulated at the mRNA levels and to investigate which pathways might be involved in the upregulation of the immune system in our transgenic mice, we performed expression analysis of tail-epidermal samples by qRT-PCR. We compared mRNA levels of wildtype (control), *Hdac1*$^{\Delta/\Delta ep\ 2S/2S}$, *Hdac1*$^{\Delta/\Delta ep}$, *Hdac1*$^{\Delta/\Delta ep\ Ci/+}$, *Hdac1*$^{\Delta ep/+\ Ci/Ci}$ mice using primer pairs targeting selected interferon responsive and pro-inflammatory genes. Figure 13 depicts the results of the expression analysis, showing a significant upregulation in mRNA expression in most of the immune-related genes tested, including *Cxcl10*, *Oasl1*, *Ccl5* and *Tnf*. The pro-inflammatory cytokines *Cxcl10* and *Tnf* as well as the antiviral gene Oasl1 showed the strongest upregulation in *Hdac1*$^{\Delta ep/+\ Ci/Ci}$ mice. Likewise, the expression levels of the chemokine *Ccl5* were significantly elevated in mice overexpressing the catalytically inactive transgene. Interestingly, the interferon responsive gene *Isg15* was only upregulated in *Hdac1*$^{\Delta/\Delta ep\ Ci/+}$ mice but not in *Hdac1*$^{\Delta ep/+\ Ci/Ci}$ mice. The interferon induced protein *Ifit1* was the only gene that was not deregulated in any of the cell lines. Since we observed extranuclear DNA in the epidermis of one of our *Hdac1*$^{\Delta ep/+\ Ci/Ci}$ mice (not shown), we additionally analysed the expression of the cytosolic DNA sensor *cGAS* and observed a slight increase in its expression levels in *Hdac1*$^{\Delta/\Delta ep\ Ci/+}$ and *Hdac1*$^{\Delta ep/+\ Ci/Ci}$ mice. Interestingly, we also found a slight deregulation of some immune related genes in the *Hdac1*$^{\Delta/\Delta ep\ 2S/2S}$ mice including *Oasl1* and *Tnf.* No deregulation in any of the analysed immune-related genes was observed in the second control mouse strain *Hdac1*$^{\Delta/\Delta ep}$.

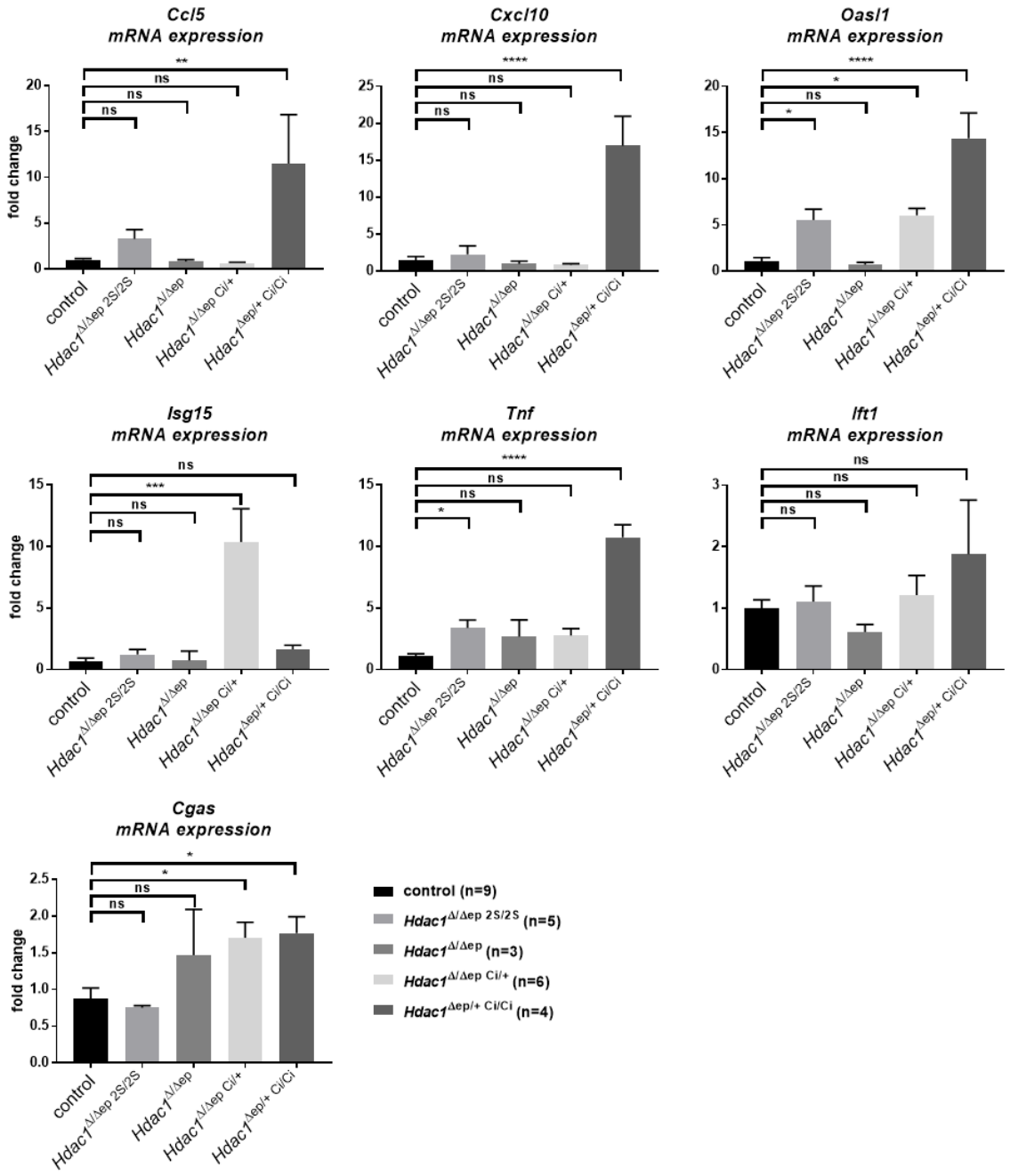

Figure 13: Altered Immune gene expression profile in *Hdac1*$^{\Delta ep/+\ Ci/Ci}$ mice. RNA was extracted from tail epidermis of Cre-negative control, *Hdac1*$^{\Delta/\Delta ep\ 2S/2S}$, *Hdac1*$^{\Delta/\Delta ep}$, *Hdac1*$^{\Delta/\Delta ep\ Ci/+}$ and *Hdac1*$^{\Delta ep/+\ Ci/Ci}$ mice. mRNA expression was measured by qRT-PCR. Expression levels were calculated relative to the expression of the housekeeping gene b2m as well as to the mean of wildtype mice (ctrl), which was set to 1. Ordinary one-way-ANOVA and Sidak multiple comparison test were used to determine p-values. Data is blotted as mean + s.d. *p≤0.05; **p≤0.01; ***p≤0.001; ****p≤0.0001; ns=not significant.

3.1.6 Defective epidermal barrier and increased epidermal stress in mice carrying a keratinocyte-specific inactivation of HDAC1

The histological characterization of *Hdac1*^{Ci} mice with infiltrating immune cells, hyperkeratosis and acanthosis together with the upregulation of certain immune genes and the key barrier alarmin keratin 6 in the epidermis were indications for a defective epidermal barrier. This prompted us to investigate the integrity of the epidermal barrier by performing trans-epidermal water loss (TEWL) measurements and comparing *Hdac1*$^{\Delta/\Delta ep}$ and *Hdac1*$^{\Delta/\Delta ep\ Ci/+}$ mice with wildtype control mice (Figure 14). We observed a significant increase in TEWL levels in *Hdac1*$^{\Delta/\Delta ep\ Ci/+}$ mice. In males, the increase in TEWL levels seems to be slightly higher, suggesting sex dependent differences in phenotype development. Taken together, histology and increased TEWL values suggest a defective epidermal barrier function in *Hdac1*$^{\Delta/\Delta ep\ Ci/+}$ mice.

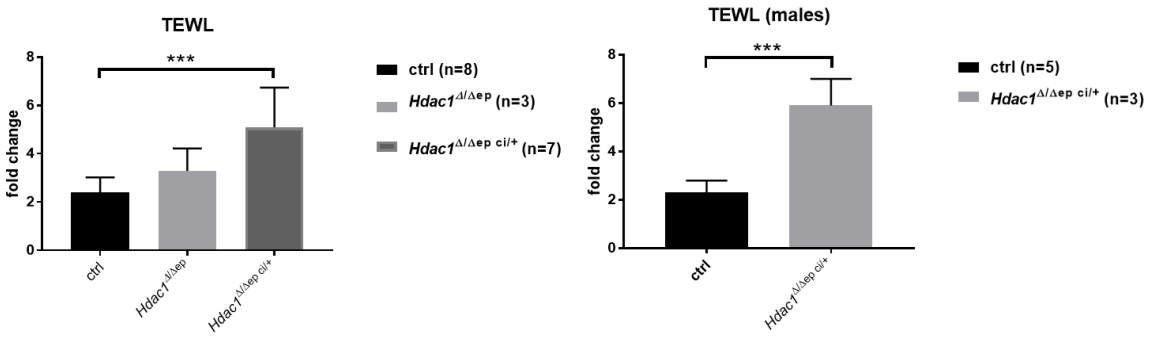

Figure 14: HDAC1^{Ci} mice display increased trans epidermal water loss (TEWL). Immediately after killing, the napes of the mice were shaved and the TEWL (g/m2/h) was measured. Measurements were repeated at least 3 times for each mouse. Ordinary one-way-ANOVA and Sidak multiple comparison test were used to determine p-values. Data is blotted as mean ± SEM ***p≤0.001; ns=not significant.

3.1.7 Evidence for increased DNA damage and presence of extranuclear DNA in the epidermis of the *Hdac1*$^{\Delta/\Delta ep\ Ci/Ci}$ mouse

Previous studies have shown that cells with simultaneous ablation of HDAC1 and HDAC2 exhibit micronucleation as well as increased hypersensitivity in response to DNA-damaging agents (Miller et al., 2010b); (Jamaladdin et al., 2014). Therefore, we performed immunofluorescence staining on dorsal skin biopsies with an antibody specific for γH2AX to compare the DNA damage response between *Hdac1*^{Ci} mice and our wildtype controls. The γH2AX antibody stains nuclear foci of DNA repair. As illustrated in Figure 15, we were able to observe an increased amount of DNA damage foci in our one *Hdac1*$^{\Delta/\Delta ep\ Ci/Ci}$ mutant mouse. However, increased DNA damage was not detected

in *Hdac1* knockout mice, expressing one allele of catalytic inactive *Hdac1* (*Hdac1*$^{\Delta/\Delta ep\ Ci/+}$).

As previously motioned, we observed anecdotal evidence of extranuclear DNA in the *Hdac1*$^{\Delta/\Delta ep\ Ci/Ci}$ mutant and an upregulation of the cytosolic DNA sensor *cGAS* in the qPCR results. Therefore, we also stained the dorsal skin samples with an antibody specific for *cGAS*. For this staining, we compared our *Hdac1*^{Ci} strains with our wildtype control as well as specific positive (*Dnmt*$^{\Delta/\Delta ep}$) and negative controls (*cGas*$^{\Delta/\Delta ep}$). As depicted in Figure 16 the epidermis of *Hdac1*$^{\Delta/\Delta ep\ Ci/Ci}$ mice exhibited a clear increase of *cGAS* signal compared to wildtype and *cGAS* knockout mice. No evidence of *cGAS* expression was observed in any of the other transgenic mouse strains (not shown).

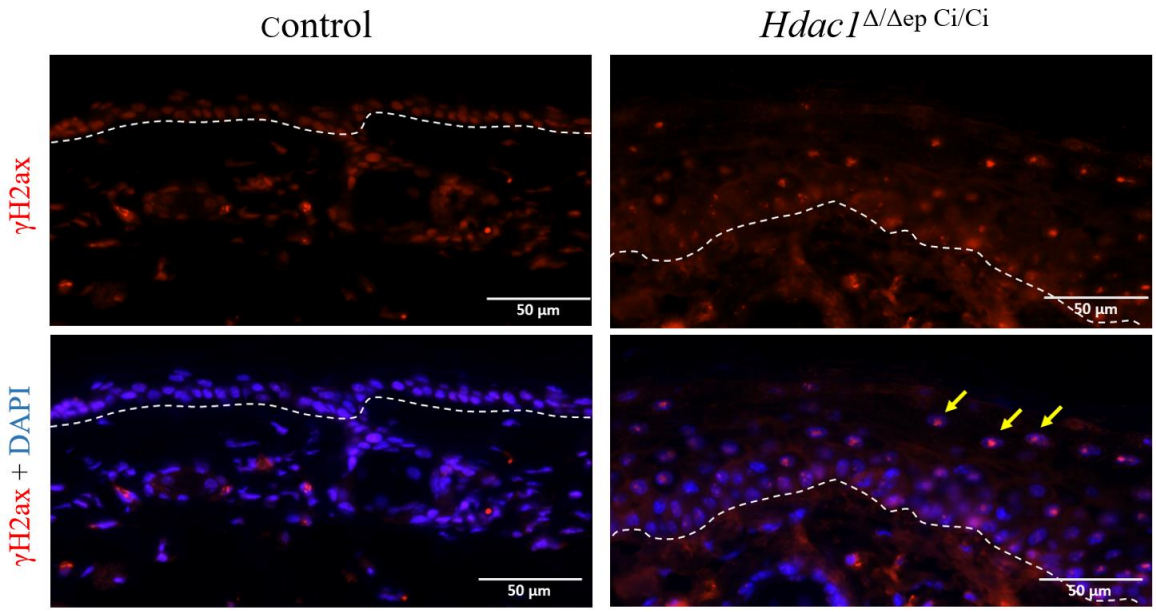

Figure 15: ***Hdac1*$^{/\Delta ep\ Ci/Ci}$ mice display increased DNA damage response.** Immunofluorescence analysis of back skin sections of *Hdac1*$^{\Delta/\Delta ep\ Ci/Ci}$ mice compared to Cre-negative control mice. The tissue was stained with an anti-γH2AX antibody and nuclei were counterstained with DAPI. Images were taken for γH2AX and γH2AX +DAPI. Dashed lines indicate epidermal/dermal border. Scale bars: 50µm.

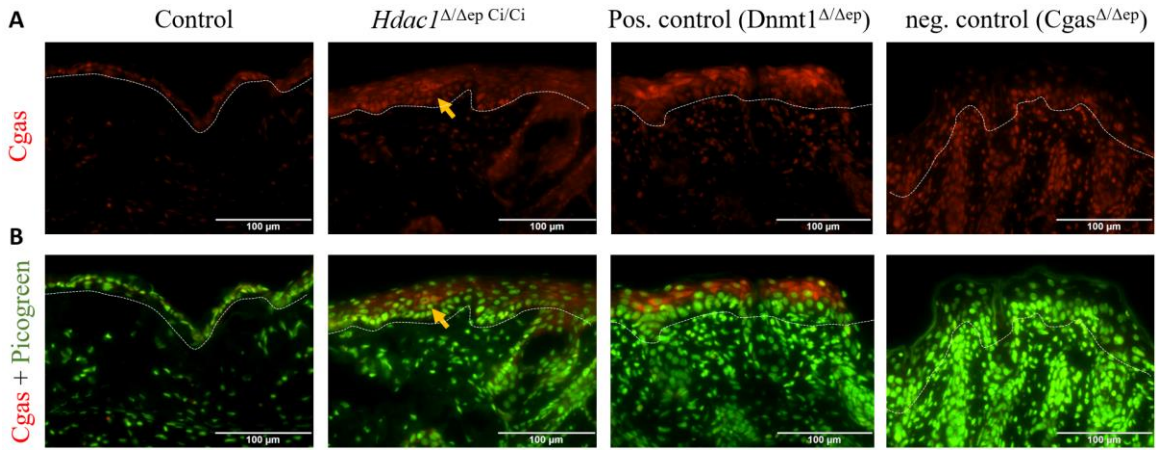

Figure 16: Upregulation of Cgas in the epidermis of *Hdac1*$^{\Delta/\Delta ep\ Ci/Ci}$ mice. Representative images of back skin sections of *Hdac1*$^{\Delta/\Delta ep\ Ci/Ci}$ mice compared to Cre-negative control mice. Skin sections from Dnmt1$^{\Delta/\Delta ep}$ mice were used as positive control and sections from Cgas$^{\Delta/\Delta ep}$ mice were used as negative control. The tissue was stained with an anti-Cgas antibody and nuclei were counterstained with Picogreen. Images were taken for Cgas (A) and Cgas + Picogreen (B). Yellow arrow marks increased Cgas expression. Dashed line indicates epidermal/dermal border. Scale bars: 100µm.

3.2 Analysis of immortalized human keratinocytes expressing wildtype HDAC1 and catalytic inactive HDAC1

In order to investigate the impact of inhibition of HDAC1 in a human cell system we used previously generated immortalized human keratinocyte derived cell lines which are described in the Master Thesis of Eva Zorec. Briefly, cDNAs coding for either FLAG–tagged HDAC1 wildtype (*HDAC1*^{wt}) or catalytic inactive (*HDAC1*^{Ci}) were cloned downstream of the EF1a promoter and integrated into the save harbour AAVS locus of immortalized human keratinocytes (NHEK SV-Tert 3-5) by using the CRISP/Cas9 method. In addition, endogenous *HDAC1* was knocked down by lentiviral-mediated shRNA to generate the following cell lines: *HDAC1*^{wt,HD1kd} and *HDAC1*^{ci,HD1kd}. Additionally, we treated and compared wildtype keratinocytes with different chemical HDAC inhibitors.

3.2.1 Validation of cell lines

We first aimed to confirm the expression of our transgenes as well as the specific knockdown of *HDAC1* in the different human keratinocyte cell lines on the protein level by immunoblotting. Figure 17A shows an immunoblot of all cell lines with different specific antibodies. All transgenic cell lines express the transgene coupled with a FLAG tag, indicated by an increase of the molecular size. Western blot analysis indicated that the cell lines used express FLAG-tagged HDAC1 at a similar or slightly higher level than compared to the endogenous HDAC1 expressed by wildtype

NHEK Sv-Tert cells. shRNA-mediated knockdown specifically of endogenous HDAC1 could be confirmed in both cell lines (*HDAC1*^{wt,HD1kd} and *HDAC1*^{ci,HD1kd}) However, expression of endogenous HDAC1 was not completely abolished, as shown by a remaining faint band. Additionally, we confirmed the purity of the cell lines and expression of the transgenes by immunofluorescence analysis staining using an M2-FLAG specific antibody (Figure 17B).

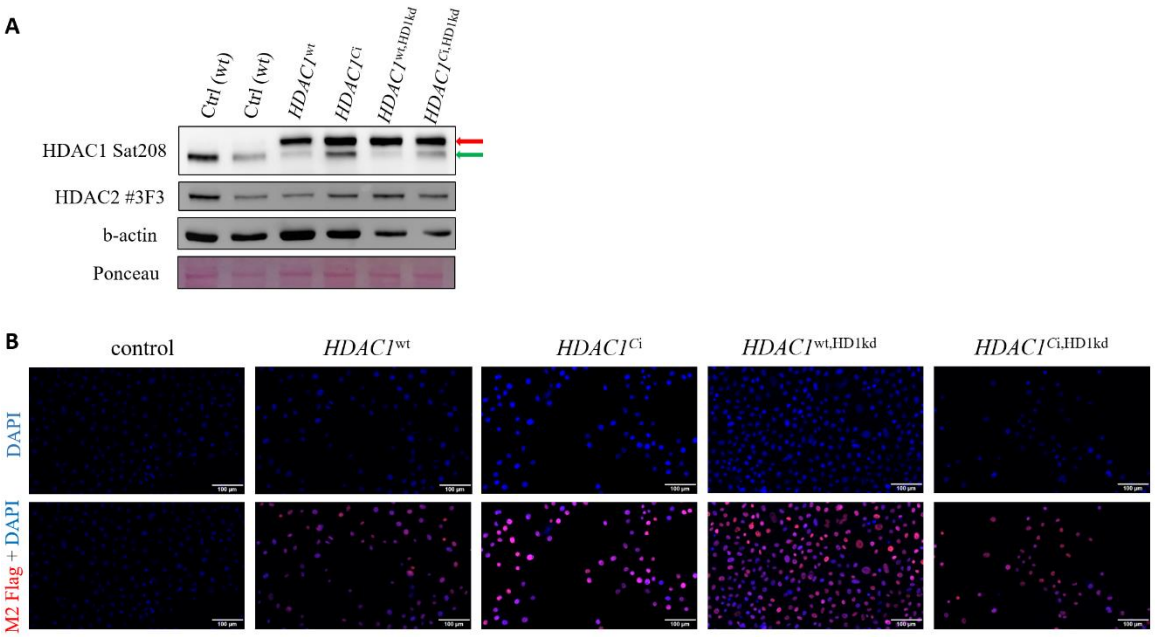

Figure 17: Validation of transgene expression in different human keratinocyte cell lines. (A) Immunoblot analysis. Lysates from cultivated keratinocytes were extracted at ~ 80% confluency and were separated on a 10% SDS gel. The HDAC1 immunoblot results in a band at 60 kDa for endogenous HDAC1 (green arrow) and a slightly higher band for the FLAG-tagged transgenic HDAC1^{Cl} (red arrow). An HDAC2 specific antibody was utilized to visualize the HDAC2 protein. ß-actin was visualized with the ab8227 antibody and served as loading control. Whole protein Ponceau staining served as additional loading and integrity control. **(B)** Immunofluorescence staining of different keratinocyte cell lines with an anti-FLAG antibody. Nuclei were counterstained with DAPI. Scale bar indicates 100µm.

3.2.2 Increased abnormal mitosis in human keratinocytes expressing inactive HDAC1

Recent studies of our lab showed that DNMT1 inhibition leads to defective mitosis, which causes formation of micronuclei and activation of the *cGAS/Sting* pathway (Beck et al., 2021a). As we identified an upregulation of *cGAS* in the epidermis of our *Hdac1*$^{\Delta/\Delta ep\ Ci/Ci}$ mouse and as it was previously shown that HDAC1 and 2 are also essential for a correct mitotic process in other cell lines (Jamaladdin et al., 2014) we sought out to investigate and compare the mitotic stability of our different cell lines. Here we aimed to stain the keratinocyte cell line with an antibody specific for the mitotic histone variant H3S10ph and the ultra-sensitive DNA dye Picogreen. After staining, cell lines were randomized and analysed in a blinded manner with regard to nuclear abnormalities during different stages of mitosis as exemplified in Figure 18A. In a preliminary experiment with

our different cell lines, almost 25% of the cells undergoing mitosis showed nuclear abnormalities in the cell line in which endogenous *HDAC1* was knocked down and catalytic inactive *HDAC1* (HDAC1^{CI}) was expressed (*HDAC1*^{ci,HD1kd}). Whereas, in all other cell lines the percentage of abnormal mitotic cells did not exceed 15%. Interestingly, the *HDAC1*^{wt} cell line overexpressing two additional alleles of endogenous *HDAC1* displayed a decrease in abnormal mitotic cells (Figure 8B and C).

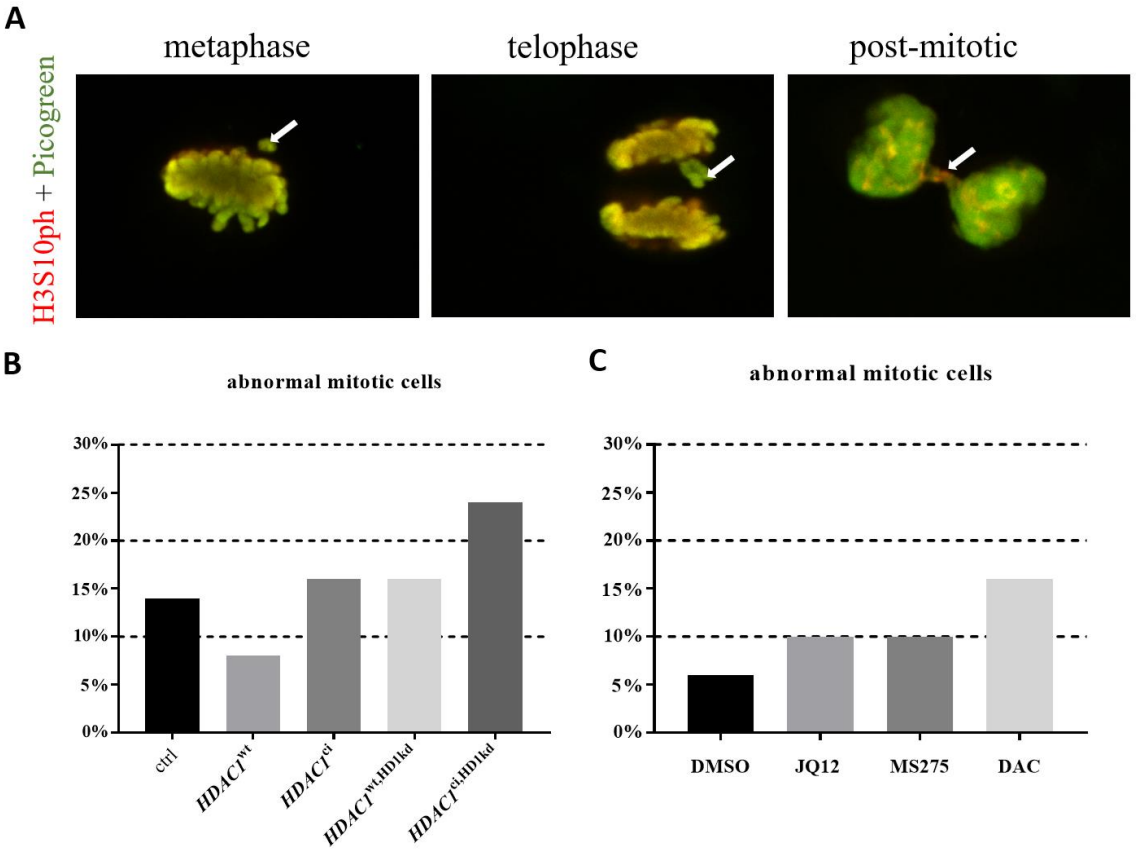

Figure 18: Human keratinocytes expressing catalytically inactive HDAC1 in an endogenous HDAC1 knockdown background display increased amount of abnormal mitotic cells. (A) Immunofluorescence staining of *HDAC1*$^{-/-\ ci/ci}$ keratinocytes displaying mitotic abnormalities (marked by white arrow) in different stages of mitosis. Cells were stained with an anti-H3S10ph antibody and nuclei were counterstained with Picogreen. Arrows point to nuclear abnormalities. (B) Quantification of abnormal mitotic cells in different keratinocyte cell lines compared to wildtype keratinocytes (preliminary). About 80 H3S10ph-positive mitotic and post-mitotic nuclei per condition and cell line were analysed for nuclear defects and calculated as percentage of the total number of H3S10ph nuclei. Only one well per cell line was analysed. (C) Analysis of abnormal mitotic wildtype keratinocytes after treatment for 24h with either MS275 (2µM), JQ12 (2µM), DAC (2µM) or DMSO as a control in the same way as described for B.

Furthermore, we also treated wildtype human immortalized keratinocytes with different HDAC inhibitors for 48h to see if chemical HDAC inhibition would also cause mitotic abnormalities in keratinocytes. As a positive control we used cells treated with a DNMT1 inhibitor which has been previously shown by our lab to induce abnormal mitotic behaviour in keratinocytes (Beck et al.,

2021a). In our control cells treated with DMSO we observed about 5% abnormal mitotic events, whereas inhibition of class I HDAC by MS-275 or JQ-12 resulted in 10 % abnormal nuclei. The proportion of mitotic errors increased to 15 % in keratinocytes treated with deoxy-5-azacytidine (DAC). All together these results indicate, that catalytic inhibition of HDAC1 has an impact on mitotic integrity.

3.2.3 Chemical HDAC1 inhibition leads to DNA damage induction & an increase of binucleated cells

Since we observed an increase of DNA damage in the epidermis of the *Hdac1*$^{\Delta/\Delta ep\ Ci/Ci}$ mouse (see chapter 3.1.6) we treated wildtype human keratinocytes with the HDAC inhibitor ms-275 for 24h and 48h and subsequently stained them with a gH2Ax-specific antibody. As illustrated in Figure 19A, microscopic analyses of cells stained with a γH2Ax specific antibody indicated an increase of DNA damage foci after HDAC inhibitor treatment. Quantification and integrated density analysis of the stained cells revealed a significant increase of DNA damage foci after 48h of treatment with already a slight increase after 24h (Figure 19B).

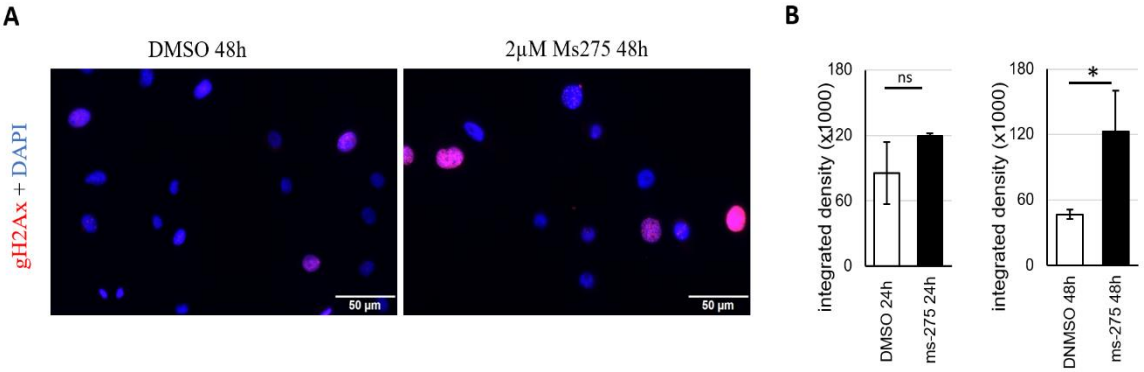

Figure 19: Increased DNA damage in Keratinocytes upon treatment with HDAC inhibitor Ms275. (A) Immunofluorescence analysis of wildtype keratinocytes treated with 2µm ms275 or DMSO for 24h or 48h using anti-γH2ax antibody. Nuclei were counterstained with DAPI. Scale bars: 50µm (B) Quantification of γH2ax labelling by calculation of the integrated density using FIJI. The mean of the integrated density of the biological replicates (2 for 24h and 3 for 48h) was blotted ± SEM.

Aberrant mitosis can lead to incomplete cytokinesis, which is manifested in the formation of binucleated cells. Therefore, we treated keratinocytes with different concentrations of ms-275 for 48h and determined the proportion of binucleated cells. As shown in figure 20, we observed a dose dependent increase of binucleated cells in keratinocytes in comparison to the PBS treated control, indicating that inhibition of class I HDAC can lead to defective mitosis in human keratinocytes.

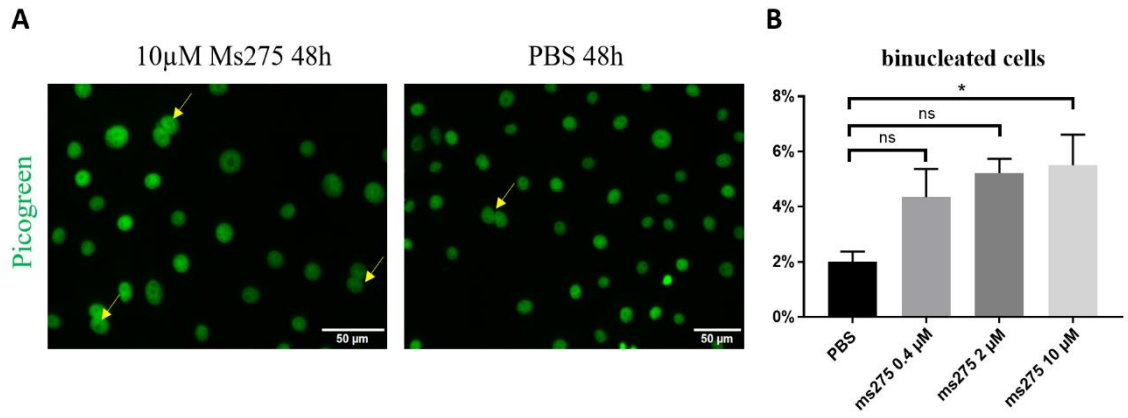

Figure 20: Keratinocytes treated with ms275 show dose-dependent increase of binucleated cells. Wildtype keratinocytes were treated with different concentrations of Ms275 (0,4µM, 2 µM, 10µM) or PBS as a control. **(A)** Nuclei of keratinocytes treated with 10µM Ms275 for 48h were stained with Picogreen. Yellow arrows mark binucleated cells. Scale bar indicates 50µM. **(B)** Percentage of binucleated cells in keratinocytes treated with different concentrations of Ms275 compared to cell treated with PBS. The total number of cells and the number of binucleated cells were counted in three areas of the same size for each concentration. The Percentage for each area was calculated and the triplicate values were averaged. Data is blotted as mean ± SEM from 3 biological replicas.

3.3 Single cell RNA sequencing additionally reveals significant gene expression differences in *Hdac1*^{Ci} mice

In the course of this work, we had the opportunity to perform single cell RNA sequencing on our different murine skin samples in cooperation with the lab of Michael Mildner. We aimed to compare the cell-specific gene expression levels in the whole skin of wildtype cre-negative mice to *Hdac1*$^{\Delta/\Delta ep\ Ci/+}$ mice and added *Hdac1*$^{\Delta/\Delta ep}$ mice as a secondary control. Samples from three mice per genotype were collected, pooled and further processed by the Mildner group as described in chapter 2.8 of this work and in more detail in Klas et al., 2021.

3.3.1 Validation of mice used for scRNAseq and overview of cell type distributions

Before collecting the samples from the mice used for the experiment, they were genotyped on the DNA level via PCR reactions to assure the correct genotypes. After collecting the samples for the Single cell RNA sequencing, we first aimed to validate the genotype specific expression of HDAC1 as well as the successful knockout of endogenous HDAC1 in our epidermal skin samples on a protein level by immunoblotting. Figure 21 shows the immunoblot of all nine mice used for scRNAseq. The wildtype control displays the expected band at 60 kDa for endogenous HDAC1. *Hdac1*$^{\Delta/\Delta ep\ Ci/+}$ mice only display a slightly higher band due to the FLAG-tag of the catalytically inactive HDAC1, showing that they only express the transgenic version of HDAC1. As expected, the *Hdac1*$^{\Delta/\Delta ep}$ mice display no band for endogenous or FLAG-tagged HDAC1.

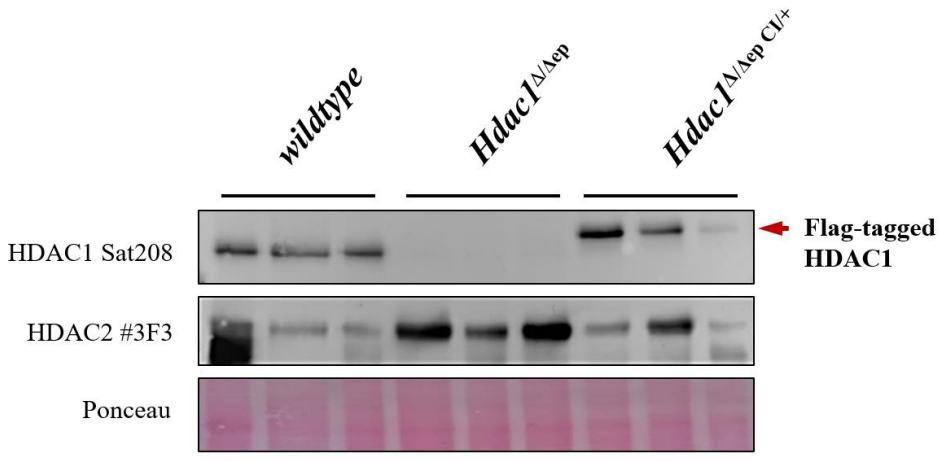

Figure 21: Genotype validation of mice used for scRNAseq experiment. Western blot analysis showing the expression of endogenous (lower HDAC1 band) and transgenic (red arrow) HDAC1 protein as well as HDAC2 expression. Protein lysates of tail epidermis samples of all genotypes were separated on a 10% SDS gel. Anti-HDAC1 and anti-HDAC2 antibodies were used to detect the respective proteins. Whole protein Ponceau staining served as a control for equal loading and blot integrity.

3.3.2 Overview of cell type distribution shows differences in proliferating and differentiating keratinocytes as well as hair follicle cells.

The first result we received from Katharina Klaas and Michael Mildner was an overview of the cell type distribution in our three different groups. Figure 22 shows a UMAP representation in which each point represents a cell, arranged in different clusters depending on their individual gene expression. Here we could already observe clear differences between the different genotypes. *Hdac1*$^{\Delta/\Delta ep\ Ci/+}$ mice (MUT) show a clear increase of sevarel types of proliferating keratinocytes (prol KC 2), type 2,3 and 5 hair follicle cells (HF2, HF3, HF5) as well as differentiating keratinocytes type 3 (diff KC3) as indicated by the dotted red circle. On the other hand, they also display a decrease of differentiating keratinocytes types 2, 4 and 1. Next, we looked at the overall numbers of cells corresponding to the different groups of cells for each genotype (Figure 23). Compared to the wildtype control (WT), *Hdac1*$^{\Delta/\Delta ep\ Ci/+}$ mice (MUT) showed a decrease in overall fibroblasts, basal keratinocytes (basal KC) and differentiated keratinocytes (diff KC) but an increase in hair follicle cells and proliferating keratinocytes (prol KC). The *Hdac1*$^{\Delta/\Delta ep}$ mouse strain (KO) showed a similar but less pronounced trend of cell type distribution as the MUT strain with a slight increase in prol KC and hair follicle cells as well a slight decrease in the number of fibroblasts and diff KC.

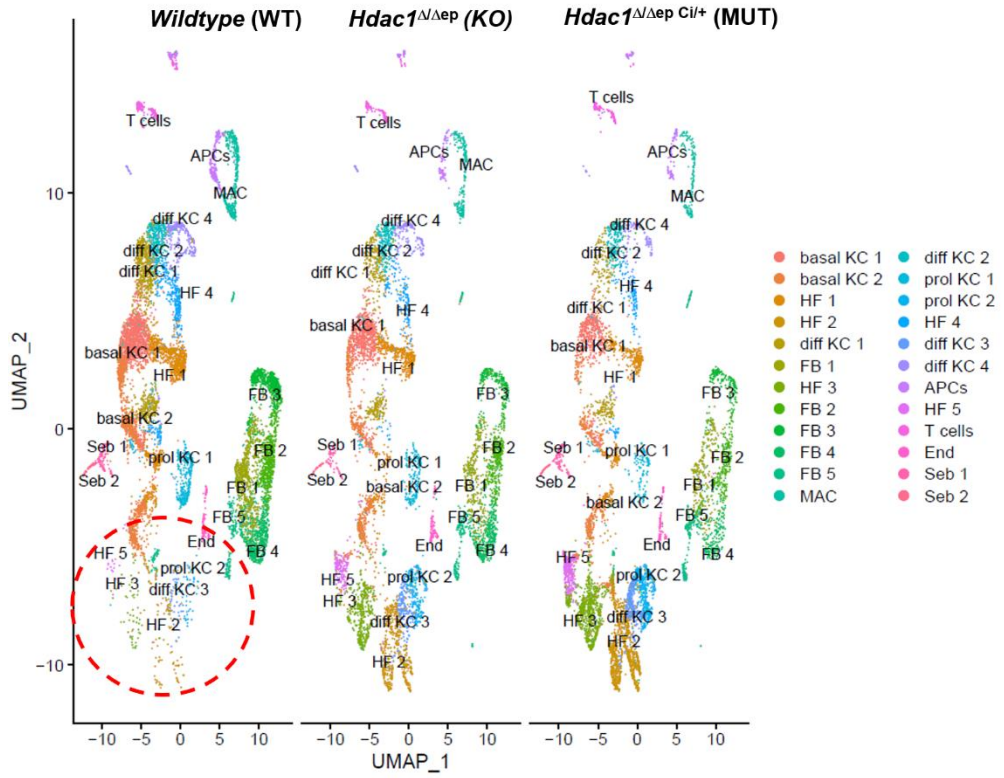

Figure 22: Comparison of cell populations. UMAP-plots comparing all identified cell populations in *Hdac1*$^{\Delta/\Delta ep\ Ci/+}$ (n=3) and *Hdac1*$^{\Delta/\Delta ep}$ mice (n=3) to cell populations of wildtype controls mice (n=3). Representative population difference indicated with red dashed circle. (Figure generated in cooperation with Katharina Klas)

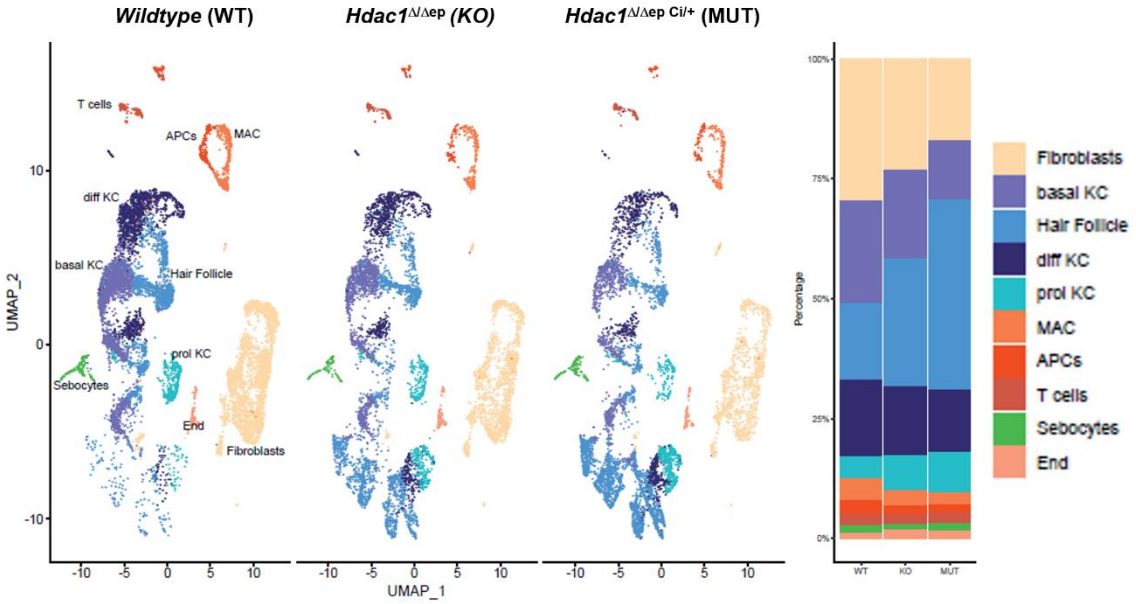

Figure 23: Comparison of cell type distribution. UMAP-plots comparing the relative distribution of grouped cell populations in *Hdac1*$^{\Delta/\Delta ep\ Ci/+}$ (n=3) and H *Hdac1*$^{\Delta/\Delta ep\ mice}$ (n=3) compared to wildtype control mice (n=3). Figure generated in cooperation with Katharina Klas.

3.3.3 Analysis of *Hdac1* expression by scRNAseq

Another analysis was performed for the expression of *Hdac1* specifically in keratinocytes (Figure 24). The analysis did not distinguish between endogenous *Hdac1* and catalytically inactive *Hdac1*. As expected, the *Hdac1* knockout mice show a strong reduction of HDAC1 expression in all keratinocytes compared to the wildtype control. The MUT strain displayed an overall increase of *Hdac1* expression, especially for hair follicle types 2,3 and 5 (HF 2, HF 3, HF 5) as well as for proliferating keratinocytes 2 (prol KC 2) and differentiating keratinocytes type 3(diff KC 3). The graph on the right-hand side of the figure shows that the total expression of *Hdac1* is stronger in the MUT genotype group compared to the wildtype control (WT), which is mainly due to keratinocytes derived from the hair follicle and from the proliferating compartment. The *Hdac1*$^{\Delta/\Delta ep}$ (KO) group seems to still have some small residual *Hdac1* mRNA expression in some keratinocyte cell types.

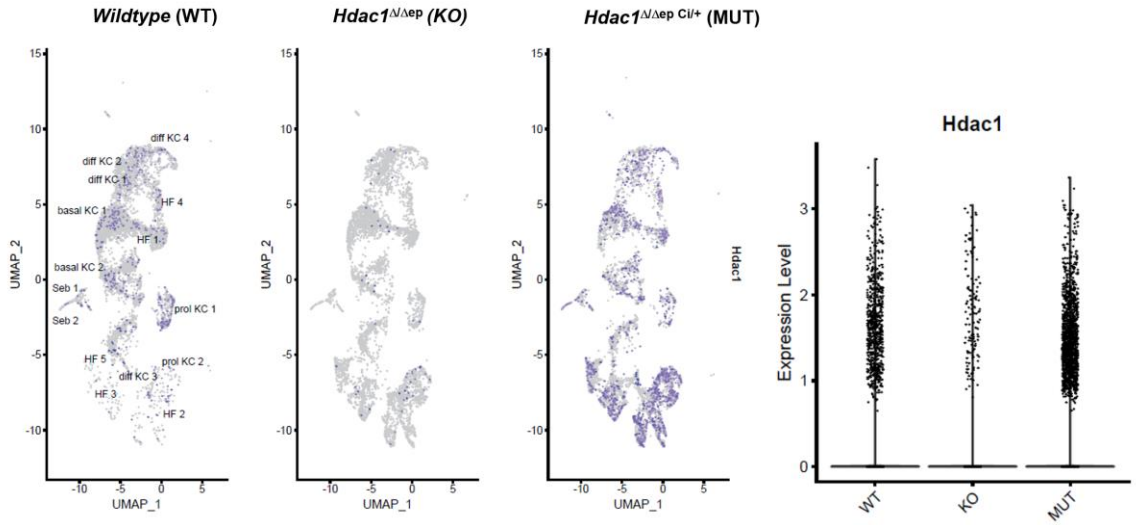

Figure 24: Comparison of *Hdac1* expression in keratinocytes. UMAP-plot representing *Hdac1* expression in the different cell types (left panel) and overall expression analysis of *Hdac1* (right panel). (Figure generated in cooperation with Katharina Klas)

3.3.4 HDAC1 inactivation correlates with deregulation of keratinocyte differentiation

In order to identify which biological processes and molecular functions are implicated in the phenotype of MUT mice, gene ontology analysis was done on the data generated by the single cell sequencing using the free online tool Metascape. Figure 18A displays a GO-term analysis of differentiated keratinocytes which shows the strongest deregulation in genes playing a role in the formation of the cornified envelope and also a slight deregulation in genes involved in skin development. To further investigate the deregulated genes in detail, the scRNAseq data was used to generate violin plots (in cooperation with Katharina Klas) for specific genes displaying the specific expression levels of these genes in each cell type for all three genotypes. We observed a decrease of the early keratinocyte differentiation marker *keratin10* in the MUT mice and in the KO mice but the effect was about twice as prominent in the MUT mice then in the KO (Figure 25B). Simultaneously we found an upregulation in the gene expression of the late keratinocyte differentiation marker Loricrin (*Lor),* which correlates with our previous findings in our immunofluorescence staining of the LOR protein (chapter 3.1.3).

Furthermore, to confirm the deregulation of differentiation on an mRNA level we performed qRT-PCR on tail epidermis samples of the mice used for the single cell RNA sequencing experiment. The qRT-PCR results confirmed a significant deregulation of Keratin10 in both *Hdac1*$^{\Delta/\Delta ep\ Ci/+}$ and *Hdac1*$^{\Delta/\Delta ep}$ mice. For Loricrin we could just observe a tendency towards a higher expression in *Hdac1*$^{\Delta/\Delta ep\ Ci/+}$ mice which was not statistically significant. Since we used RNA of total epidermis, these qPCRs might not be able to perfectly replicate the deregulations shown in the scRNAseq data, because our samples contain all keratinocytes and in addition other cell types like immune cells which would impact the measured mRNA levels. We additionally analysed the expression of some other genes involved in keratinocyte differentiation and the formation of the cornified envelope (Figure 26). We found that the mRNA levels of Claudin 3 (Clau3) were significantly upregulated in the *Hdac1*$^{\Delta/\Delta ep\ Ci/+}$ group and only indicated a small upregulation in the *Hdac1*$^{\Delta/\Delta ep}$ group. *Clau3* is involved in bicellular tight junction assembly and epithelial cell morphogenesis and plays a role in the correct development of the cornified envelope and in epithelial development and therefore important for the integrity of the epidermal barrier. The serine peptidase inhibitor *Spink5*, which is involved epidermal homeostasis and cell differentiation, was found to significantly downregulated in both the *Hdac1*$^{\Delta/\Delta ep\ Ci/+}$ and *Hdac1*$^{\Delta/\Delta ep}$ mice. We also compared mRNA levels for the proliferation marker *Epgn* but couldn't find any significant deregulations. These results are consistent with the previous finding, that mice expressing catalytically inactive HDAC1 in keratinocytes have a defective epidermal barrier and a deregulated differentiation process.

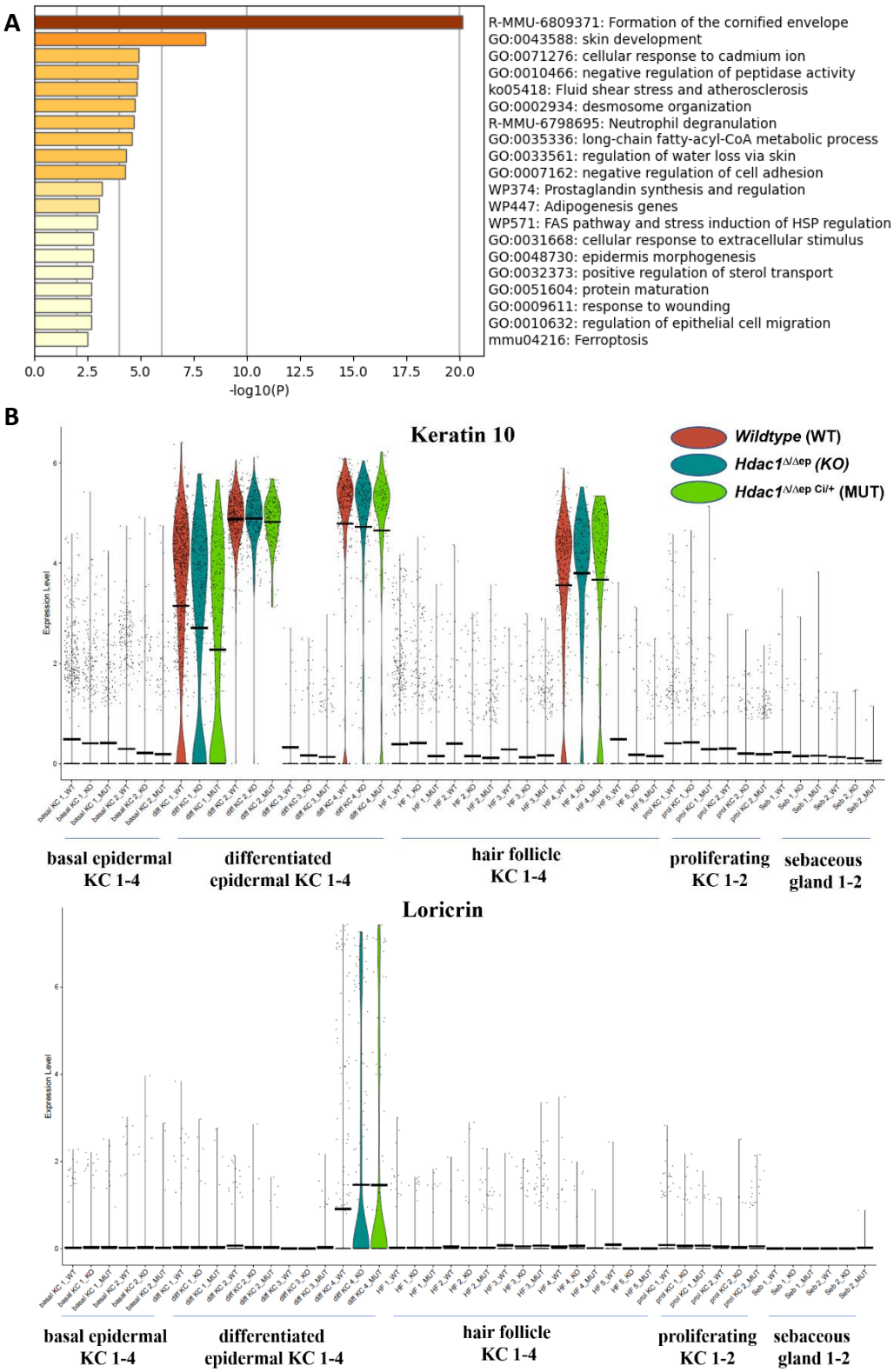

Figure 25: Differentiated keratinocytes of *Hdac1*$^{\Delta/\Delta ep\ Ci/+}$ mice display deregulations in differentiation processes. (A) Gene Ontoloy (GO) term analysis results using Metascape. Genes with a differential expression fold change of >1.5 or <0.6 were assigned to GO terms. (B) Violin plots of gene expression profiles for Keratin 10 (upper panel) and Loricrin (lower panel) for different cell cluster. Violin plots show gene expression levels. The crossbar of violin plots depicts mean expression values, the vertical lines show maximum expression. The width of the violins represents the frequency of cells at the corresponding expression levels. (Figure generated in cooperation with Katharina Klas)

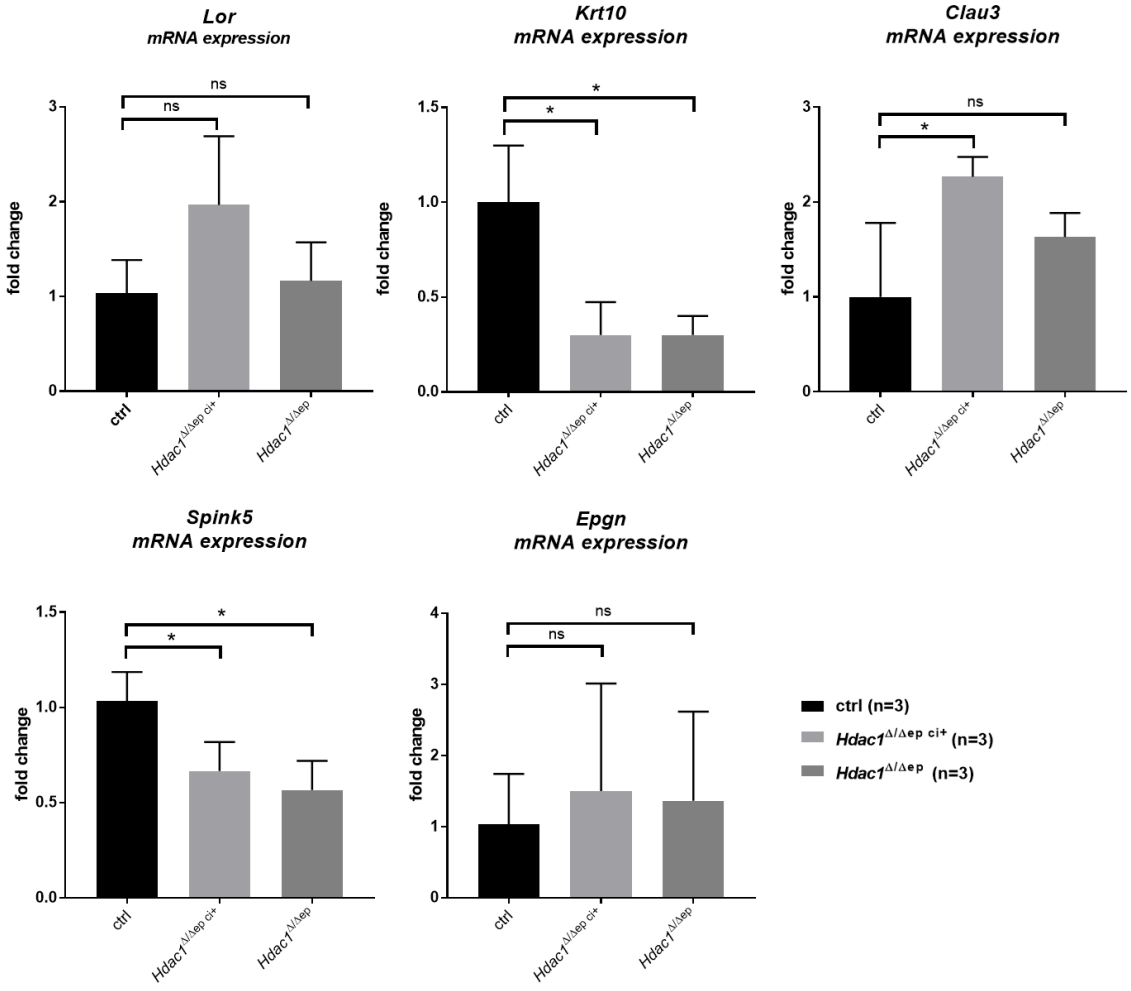

Figure 26: Expression analysis of differentiation associated genes. RNA was extracted from tail epidermis of Cre-negative control, *Hdac1*$^{\Delta/\Delta ep}$ and *Hdac1*$^{\Delta/\Delta ep\ Ci/+}$ mice. mRNA expression was measured by qRT-PCR. Expression levels were calculated relative to the expression of the housekeeping gene b2m as well as to the mean of wildtype mice (ctrl), which was set to 1. Ordinary one-way-ANOVA and Sidak multiple comparison test were used to determine p-values. Data is blotted as mean ± SEM *p≤0.05; ns=not significant.

3.3.5 HDAC1 inactivation correlates with deregulation of lipid associated genes

Another GO-term analysis was performed for the data on sebaceous glands (Seb2) in wildtype versus MUT mice. As displayed in Figure 27 the fatty acid metabolic process is the most deregulated process in sebaceous gland cells (seb2) in *Hdac1*$^{\Delta/\Delta ep\ Ci/+}$ mice. The steroid metabolic processes and the metabolism of lipids in sebaceous gland cells also shows strong deregulations in gene expression between wildtype and *Hdac1*$^{\Delta/\Delta ep\ Ci/+}$ mice. Furthermore, violin plots were generated from the scRNAseq data to compare the expression of genes associated with lipid metabolism. Figures 28A and B shows the violin plot for the ceramide synthase 4 (Cers4) and the serine palmitoyl transferase long chain base subunit1 (sptlc1), which are both deregulated in sebaceous glands type 1 and 2 (Seb1 and Seb2). Cers4 expression seems to be downregulated in Seb1 but upregulated in Seb2 in wildtype mice compared to *Hdac1*$^{\Delta/\Delta ep\ Ci/+}$ mice. The expression of Sptlc1 is downregulated in *Hdac1*$^{\Delta/\Delta ep\ Ci/+}$ mice compared to the wildtype control. To further investigate and validate the deregulations of the fatty acid and lipid metabolism processes we also performed qRT-PCR on RNA samples extracted from the tail epidermis from the mice used for the scRNAseq experiment (Figure 28C). The results showed that the mRNA expression levels for none of the tested genes we tested were significantly deregulated. Since the GO-term analysis was performed only on seb2 cells and the deregulation of for example Cers4 was also only found in sebaceous glands the deregulation of the lipid metabolism seems to be exclusive for sebaceous gland cells. This could explain why these qPCR results did not show any significant deregulations since we worked with whole epidermal RNA including all cell types within the epidermis.

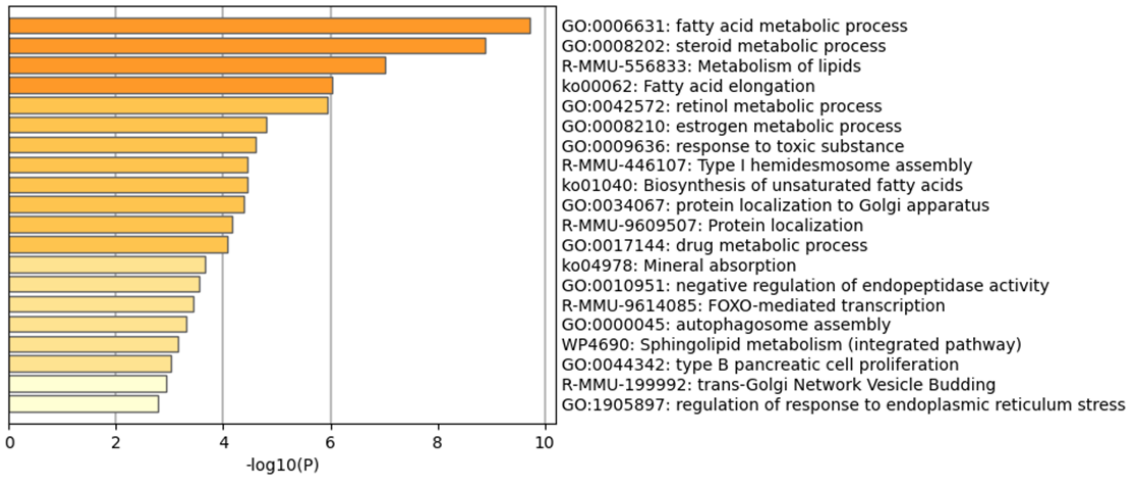

Figure 27: Deregulation of lipid and fatty acid matbolic processes. GO-term analysis of sebaceous glands 2. Gene Ontoloy (GO) term analysis results using Metascape. Genes with a differential expression fold change of >1.5 (control compared versus *Hdac1*$^{\Delta/\Delta ep\ Ci/+}$ mice) were used.

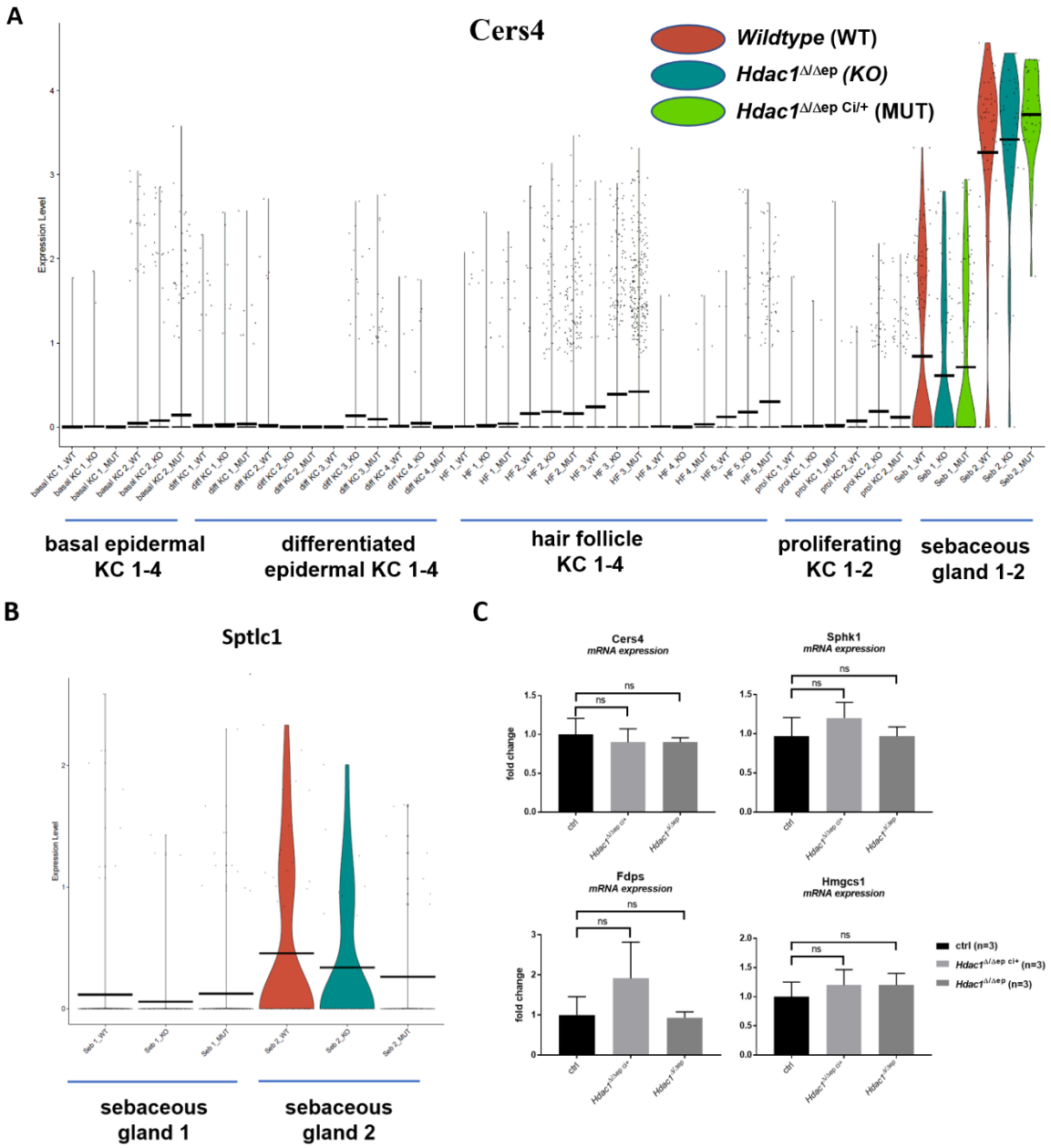

Figure 28: Deregulation of lipid metabolism associated genes in the sebaceous gland 2 cell cluster. (A) Violin plots for Cers4 expression in all cell clusters for all genotypes. (B) Violin plot for Sptlc1 in the cell clusters for sebaceous glands 1 and 2. The crossbar of violin plots depicts mean expression values; the vertical lines show maximum expression. The width of the violins represents the frequency of cells at the corresponding expression levels. (C) mRNA expression analysis of lipid metabolism associated genes via qRT-PCR. RNA was extracted from tail epidermis and measured by qRT-PCR. Expression levels were calculated relative to the expression of the housekeeping gene b2m as well as to the mean of wildtype mice (ctrl), which was set to 1. Ordinary one-way-ANOVA and Sidak multiple comparison test were used to

3.3.6 HDAC1 inactivation correlates with activation of antigen presenting cells

Further utilizing the scRNAseq data, GO-term analysis was performed on differentiated keratinocytes with the focus on antigen presenting cells (APCs). The data plotted in Figure 29 displays the deregulated processes in *Hdac1*$^{\Delta/\Delta ep\ Ci/+}$ mice compared to wildtype controls. Several immune related processes were deregulated in *Hdac1*$^{\Delta/\Delta ep\ Ci/+}$ mice including leukocyte differentiation, NF-κB signalling, and an increase in inflammatory response.

For further investigation we decided to compare the different expression patterns of some immune genes in APCs, macrophages and T-cells in all three genotype groups. The violin plots in Figure 29B show a slight upregulation of the pro-inflammatory cytokine interleukin 1 beta (*IL1b*) in APCs in *Hdac1* $^{\Delta/\Delta ep\ Ci/+}$ mice and a downregulation in *Hdac1*$^{\Delta/\Delta ep}$ mice compared to wildtype mice. The tumor necrosis factor (*Tnf*) which is mainly expressed in macrophages shows a slight upregulation in both *Hdac1*$^{\Delta/\Delta ep\ Ci/+}$ and *Hdac1*$^{\Delta/\Delta ep}$ mice but also displays in increased expression in APCs of *Hdac1*$^{\Delta/\Delta ep\ Ci/+}$ mice.

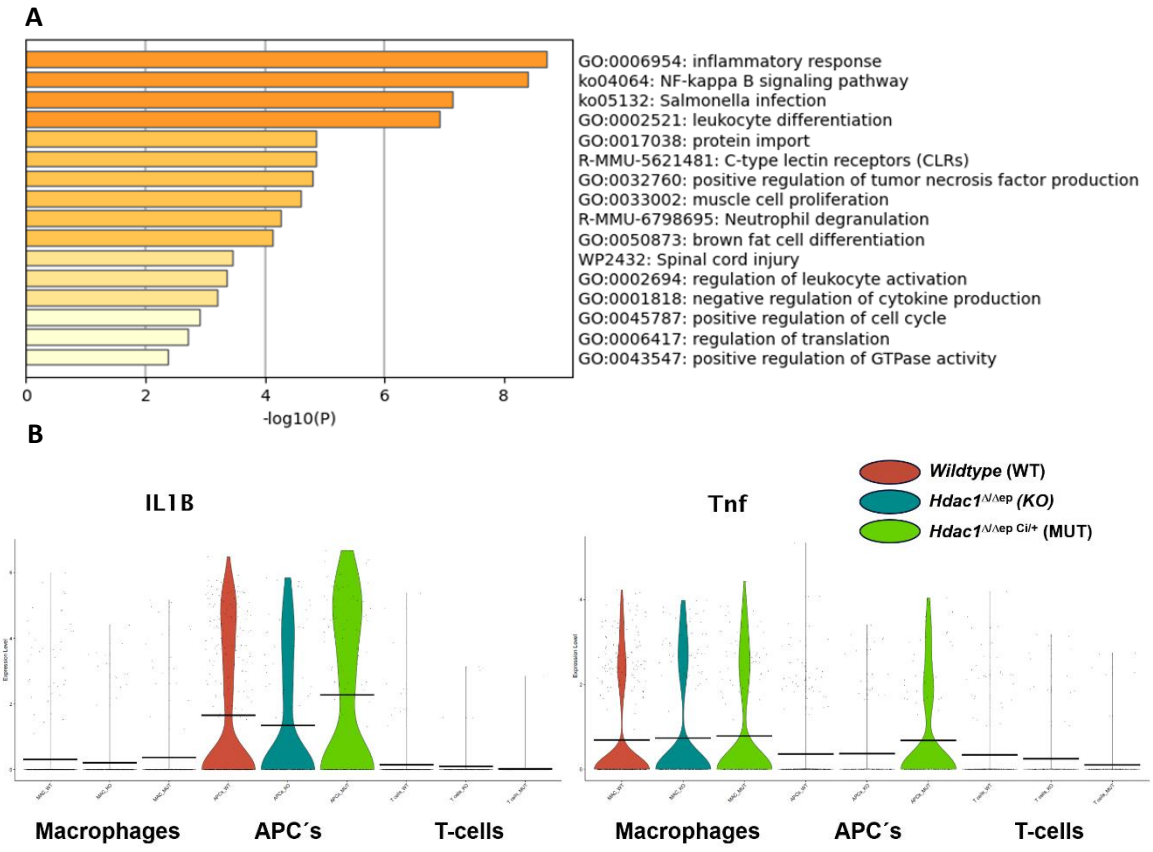

Figure 29: Deregulation of immune related processes in *Hdac1*$^{\Delta/\Delta ep\ Ci/+}$ **mice. (A)** GO-term analysis of Antigen presenting cells. Gene Ontology (GO) term analysis results using Metascape. Genes with a differential expression fold change of >1.5 (*Hdac1*$^{\Delta/\Delta ep\ Ci/+}$ compared to control mice) were used **(B)** Violin plots for IL1B (left panel) and Tnf (right panel) gene expression profiles in macrophages, APCs and T-cells. The crossbar of violin plots depicts mean expression values, the vertical lines show maximum expression. The width of the violins represents the frequency of cells at the corresponding expression levels. (Figure generated in cooperation with Katharina Klas)

Additionally, we performed mRNA expression analysis on RNA of isolated tail epidermis samples of the mice used to the scRNAseq experiment to further investigate which immune pathways might be involved in the increased inflammatory response. We investigated the expression of several immune genes by qRT-PCR which is depicted in Figure 30. We were not able to see any significant difference in mRNA expression for all of our tested genes except for the less studied Lymphocyte antigen 6 complex locus G6c (*Ly6g6c*) which is interesting since it is assumed to also be involved in bacterial response processes. However, we can still observe a tendency of increased inflammation related genes in *Hdac1*$^{\Delta/\Delta ep\ Ci/+}$ mice including *Ccl5*, *Cxcl10* and *Isg15*. The mRNA levels of *Tnf* also seem to increase for both *Hdac1*$^{\Delta/\Delta ep\ Ci/+}$ mice and *Hdac1*$^{\Delta/\Delta ep}$ mice but the standard deviation between the biological replicas was too big to determine any significant changes. The interferon gamma (*Ifng*) and the lymphocyte antigen 6 complex locus D (*Ly6D*) also did not display any significant deregulations in our tested genotypes. The PR domain containing 1 (PRDM1) mRNA expression showed a tendency of downregulation in both *Hdac1*$^{\Delta/\Delta ep\ Ci/+}$ mice and *Hdac1*$^{\Delta/\Delta ep}$ mice but here we also had the problem of a standard deviation between the biological replicas that was too high to achieve statistical significance.

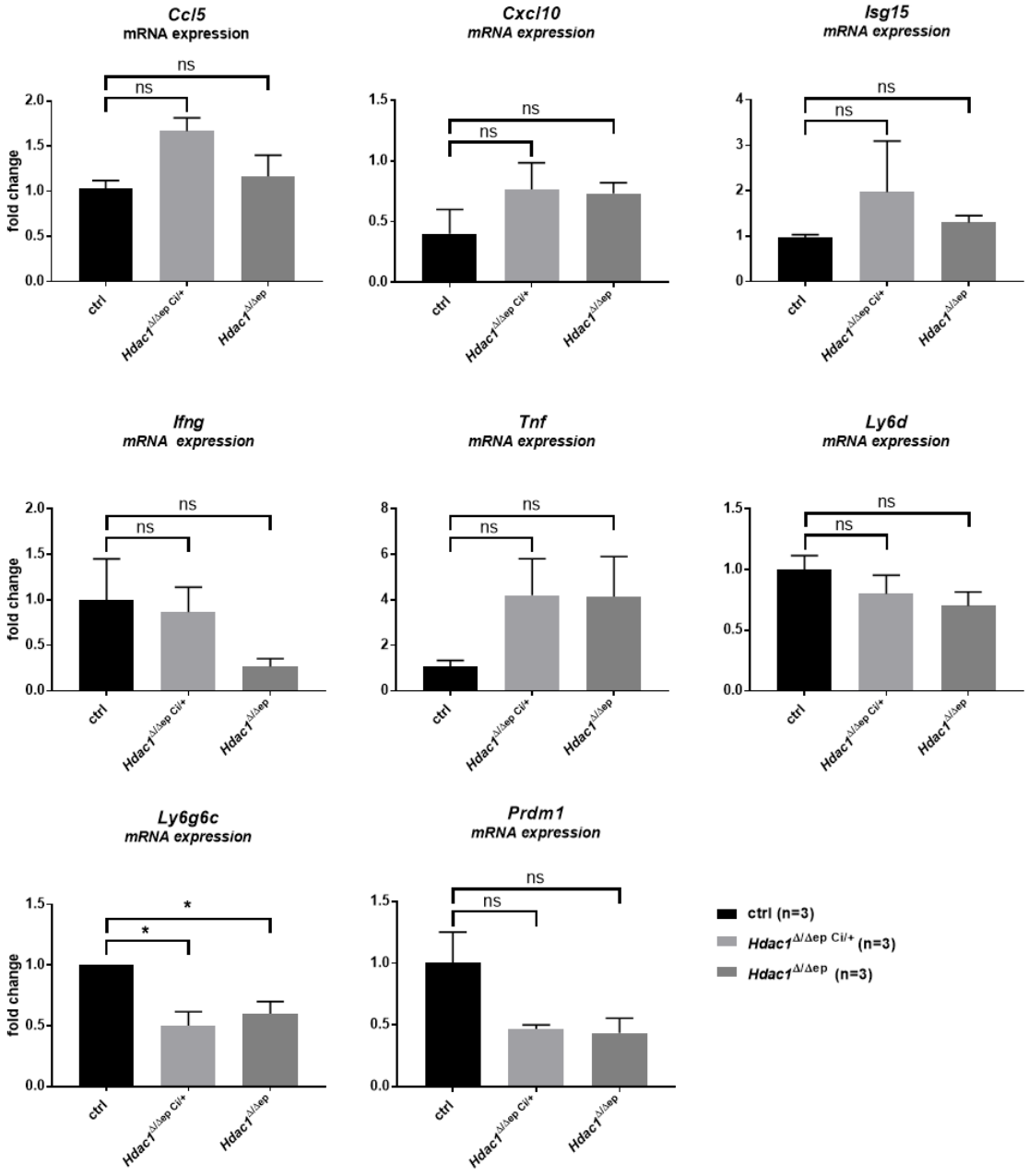

Figure 30: No significant changes in mRNA expression profiles of immune related genes. RNA was extracted from tail epidermis and measured by qRT-PCR. Expression levels were calculated relative to the expression of the housekeeping gene b2m as well as to the mean of wildtype mice (ctrl), which was set to 1. Ordinary one-way-ANOVA and Sidak multiple comparison test were used to determine p-values. Data is blotted as mean ± SEM *p≤0.05; ns=not significant

4.Discussion

4.1 Keratinocyte specific expression of HDAC1 variants in mice in epidermal *Hdac1* knockout background

Since the germline deletion of *Hdac1* is embryonically lethal in mice (Lagger et al., 2002b), conditional tissue specific deletions of *Hdac1* and the inhibition of different functions of HDAC1 are essential for dissecting the specific catalytically and non-catalytically functions of the HDAC1 protein. Furthermore, the genetic deletion of *Hdac1* leads to a compensatory upregulation of its homologue *Hdac2*, making it difficult to dissect the functions of both class I HDACs. Previous studies of our lab using mice with keratinocyte specific deletion of *Hdac1* and/or *Hdac2* revealed a pre-dominant function of HDAC1 in the murine epidermal development since only a single allele of *Hdac1* but not of *Hdac2* is sufficient for the correct epidermal development (Winter et al., 2013b). To investigate the functions of HDAC1 independently of HDAC2 and to determine its influence on the epidermal proliferation and differentiation processes we replaced the HDAC1 wildtype enzyme in the epidermis by a catalytically inactive isoform. To this end, we combined the epidermal specific deletion of endogenous *Hdac1* (*Hdac1*$^{\Delta/\Delta ep}$) with the introduction of a catalytically inactive *Hdac1* transgene (*Hdac1*$^{Ci/+}$) expressed from the Rosa26 locus specifically in keratinocytes using the Cre-recombinase system. The *Hdac1*^{Ci} transgene harbours the point mutation H141A rendering it catalytically inactive but still capable of incorporation into co-repressor complexes (Hagelkruys et al., 2016b; Hassig et al., 1998). Additionally, we investigated an HDAC1 mutant called HDAC1 2S (*Hdac1*$^{2S/+}$) which cannot be phosphorylated at S421 and S423 rendering it incapable of forming complexes as well as abolishing its enzymatic activity (Pflum et al., 2001). On the DNA level, we were able to confirm the deletion of exon 6 of the endogenous *Hdac1* gene as well as the deletion of the stop cassette 5´ to mutated *Hdac1* transgenes within the Rosa26 locus, resulting in the expression of FLAG-tagged HDAC1 variants (Figure. 8A). Likewise, on the protein level we could confirm expression of both transgenes as well as the abolished or downregulated expression of endogenous HDAC1 considering the respective genotypes (Figure 8B). Some mice with epidermal deletion of endogenous *Hdac1* still showed some HDAC1 protein expression in Western blot analysis which could be due to the conditional knockout strategy, which only applies to epidermal keratinocytes expressing the K5-promotor. Therefore, other cell types residing in the epidermis like immune cells can still harbour and express endogenous *Hdac1* which would be detected on the western blot analysis of epidermal samples.

To test this possibility, one could co-stain epidermal skin biopsies with antibodies specific for endogenous HDAC1 and CD45-positive cells and investigate co-localization signals.

4.2 Mice expressing two *Hdac1*^{Ci} alleles display increased perinatal and postnatal lethality and a severe epidermal skin phenotype

Since only four of the expected 14 *Hdac1*$^{\Delta/\Delta ep\ Ci/Ci}$ mice were born and just two reached the age of 2 months, whereas the *Hdac1*$^{\Delta/\Delta ep\ Ci/+}$ mice reached the expected rates of birth with no observed perinatal and postnatal lethality, we hypothesize that the gene dosage of catalytically inactive HDAC1 protein plays an important role in the increased mortality in the absence of functional endogenous HDAC1. Additionally, the macroscopic analysis revealed that the majority of mice carrying at least one transgene of catalytically inactive *Hdac1* in the epidermal *Hdac1* knockout background showed obvious phenotypical differences compared to the control strains but timing and severity of the phenotype of *Hdac1*$^{\Delta/\Delta ep\ Ci/+}$ mice differed between individuals (Figure 9). During the time of this project only one of the two *Hdac1*$^{\Delta/\Delta ep\ Ci/Ci}$ mice was analysed but the observations are in line with our hypothesis of a dose-dependent effect of HDAC1 since this mouse also displayed the most severe skin phenotype. With the dominant effect of HDAC1 over HDAC2 in the epidermal development in mind this could indicate that HDAC1 and HDAC2 compete for the binding sites at corepressor complexes. Therefore, enhanced expression of *Hdac1*^{il}, might lead to a higher incorporation ratio of HDAC1^{Ci} proteins compared to HDAC2 proteins in an endogenous *Hdac1* knockout background just by a higher abundance of HDAC1^{Ci} proteins. Thus resulting in a more severe impairment of the deacetylation activity of these co-repressor complexes, which could be the cause for the perinatal lethality we observed, which would be in line with the perinatal lethality reported by LeBoeuf et al., 2010 after epidermal double knockout of *Hdac1* and *Hdac2*.

Interestingly mice expressing the HDAC1^{2S} variant in the epidermal HDAC1 knockout background do not show any phenotypical changes (Figure 9). In these mice, the loss of active HDAC1 might be compensated to a certain extent by HDAC2, as Western blot analysis revealed a slight upregulation of HDAC2. This finding indicates that the catalytically activity of HDAC1 in keratinocytes might only be relevant for murine epidermal development and homeostasis if it can be incorporated into co-repressor complexes. Therefore, if catalytically inactive HDAC1 is present but cannot be incorporated into co-repressor complexes, more HDAC2 molecules would be able to join the multiprotein complexes compensating for the dysfunctional HDAC1 variant. Moreover, in mice expressing *Hdac1*^{2S}, the transgenic protein was found to be present at lower amounts

compared to the epidermis of mice expressing *Hdac1*^{Ci}. This might indicate that free HDAC1, which is not present in any co-repressor complex, might be susceptible to proteolytic degradation.

Since all available HDAC1 inhibitors act also on other class I HDACs, our model could be used to mimic the application of an isoform-specific HDAC1 inhibitor at various settings. For instance, the influence of the catalytically activity of HDAC1 for initiation and growth of skin tumours could be investigated by application of a chemical carcinogenesis protocol. In addition, when *Hdac1*$^{\Delta/\Delta ep\ Ci/Ci}$ mice are used together with an inducible keratin 5 cre system (ERcre), the impact of specific HDAC1-inhibition on tumour regression could be determined. The resulting insights of such studies could provide a basis and the motor to develop isoform-specific HDAC1 inhibitors for clinical applications.

4.3 *Hdac1*$^{\Delta/\Delta ep\ Ci/+}$ mice display abnormal skin morphology caused by deregulated differentiation and proliferation processes

The expression of *Hdac1*^{Ci} in an epidermal endogenous *Hdac1* knockout background results in similar, but less severe, epidermal abnormalities as the *Hdac1*$^{\Delta/\Delta ep}$ *Hdac2*$^{\Delta/+ep}$ phenotype described by Winter et al., 2013. HDAC1^{Ci} mice display acanthosis and hyperkeratosis as well as abnormal dermal morphology with an infiltration of immune cells and enlarged sebaceous glands as we observed in our histological examination by H&E staining of back and ear skin biopsies (Figure 10). Since Winter and colleagues (Winter et al., 2013b) identified epidermal proliferation and differentiation to be controlled by HDAC1/2 co-repressor complexes, we decided to further investigate if these processes were deregulated in our model using several approaches.

Single cell RNA sequencing revealed a deregulation of proliferating keratinocytes type 2,3 and 5 as well as deregulation of differentiating keratinocytes type 1,2,3 and 4 in *Hdac1*$^{\Delta/\Delta ep\ Ci/+}$ mice compared to wildtype (Figure 22). In regards to total cell type numbers scRNAseq showed an overall decrease of differentiating keratinocytes but an increase in proliferating keratinocytes as well as a higher expression rate of *Hdac1* which was shown to be mainly due to the increased number of proliferating keratinocytes and hair follicle cells (Figure 23).

Analysis of the mRNA expression *via* qRT-PCR of the activation marker *Krt1* and *Krt6* revealed strong upregulation in *Hdac1*$^{\Delta ep/+\ Ci/Ci}$ mice**.** The activation of the hyperkeratosis associated *Krt1* and the hyperproliferation associated *Krt6* supports our hypothesis of a deregulated differentiation process upon expression of catalytically inactive HDAC1. In addition, scRNAseq

data and qRT-PCR results revealed a decrease of the early keratinocyte differentiation marker *Krt10* in *Hdac1*$^{\Delta/\Delta ep\ Ci/+}$ mice. Furthermore, mRNA expression analysis of the *Spink5* gene, which is encoding the putative 15-domain serine protease inhibitor LEKTI and is a marker for epithelial differentiation (Galliano et al., 2005), was significantly downregulated in mice carrying the catalytically inactive *Hdac1* version. Utilizing immunofluorescence staining's of back skin biopsies we were able to show that the signal of the late terminal differentiation marker LORICRIN, which is important for formation of the cornified envelope and therefore for the establishment of the barrier function (Kalinin et al., 2001), was amplified in mice expressing at least one allele of *Hdac1*^{Ci} in the *Hdac1* knockout background. This upregulation was further proven and specified in the scRNAseq experiment showing an upregulation of *Lor* specifically in differentiating keratinocytes type 4 in *Hdac1*$^{\Delta/\Delta ep\ Ci/+}$ mice. qRT-PCR analysis of samples extracted from the mice used for the scRNAseq experiment did not show a significant upregulation in *Lor* which can be explained by the fact that for qRT-PCR a mixture of whole epidermis was used including several cell layers where expression of LORICRIN is absent and thereby obscuring its upregulation. These results taken together point toward a slowed down differentiation process in combination with an upregulation in proliferation which is in line with the thickened epidermis and stratum corneum and with keratinocytes not fully differentiating while hyperproliferating. Previous findings of an anti-proliferative role of HDAC1 in the development of the epidermis (Mirjam A Moser, 2015) would support this theory.

4.4 Keratinocyte-specific expression of *Hdac1*^{Ci} causes activation of the innate immune system

By H&E staining we observed a higher cellularity in the skin of *Hdac1*$^{\Delta/\Delta ep\ Ci/+}$ mice (Figure 10), indicating the infiltration of immune cells. Indeed, CD45-staining of the back skin section showed more CD45 positive leukocytes compared to control mice (Figure 12). We decided to further investigate the immune phenotype by analysing whole epidermis mRNA expression of several immune genes to further elucidate the source of the immune cell activation. Interestingly, the qRT-PCR results revealed a strong upregulation of several proinflammatory genes like Ccl5,Cxcl10, Oasl and Tnf but only in *Hdac1*$^{\Delta ep/+\ Ci/Ci}$ mice and not in *Hdac1*$^{\Delta/\Delta ep\ Ci/+}$ mice. This could be explained by a higher abundance of HDAC1^{Cl} compared to endogenous HDAC1 in these mice resulting in more catalytically inactive HDAC1 proteins being incorporated into the co-repressor complexes inhibiting their deacetylase activity. The fact that the upregulation of immune genes in

Hdac1$^{\Delta/\Delta ep\ Ci/+}$ mice was significantly less pronounced but still clearly observable in some genes further underpins the hypothesis of a dose dependent effect of catalytically inactive HDAC1. With the compensatory mechanism of HDAC2 in mind this could also mean that deregulation caused by the expression of only one allele of *Hdac1*^{Ci} can still be contained by *Hdac*2 expression and its incorporation into the co-repressor complexes. One could test this theory of competing HDAC1 versions by immunoprecipitation using specific antibodies for endogenous HDAC1 and/or HDAC2 and pulling down HDAC1 together with the attached multiprotein complex and then subsequently compare the incorporation rate to the different HDAC1 variants in the different genotypes. Acetylome studies of promotor regions for these genes would additionally be of interest to investigate wether the upregulation of immune genes was caused by hyperacetylated promotors or upstream regulators.

The scRNAseq data further confirmed the deregulated immune activity in *Hdac1*$^{\Delta/\Delta ep\ Ci/+}$ mice with the inflammatory response and NF-kappaB signalling pathway showing the most severe deregulations (Figure 29). The comparison of the immune gene expression in different immune cells revealed an increase of *Tnf* and *IL1*-β in antigen presenting cells. Both inflammatory mediators, *Tnf* and *IL1*-β were previously shown to be crucial for the development of the human autoimmune skin disease psoriasis which goes along with epidermal hyperproliferation and a disrupted epidermal barrier function (L. J. Zhang, 2019).

We tried to confirm these results via qRT-PCR of samples from the mice used for the scRNAseq experiment but could not show significant induction of mRNA expression in any immune gene we tested except for the neutrophil marker *Ly6g*. Neutrophils are one of the first responding immune cells upon epidermal barrier breach by microorganism like bacteria and viruses and were previously shown to activate keratinocytes to produce psoriasis-related Inflammatory mediators (Liu et al., 2022). The scRNAseq expression data showed a deregulation of immune genes only in APCs and to some extent macrophages. This could explain our qPCR results since we used whole epidermis samples for the RNA extraction, so our results are probably influenced by the other cell types residing in the epidermis. The upregulation of some immune genes in keratinocytes could be explained by a defective epidermal barrier which leads to the recruitment of immune cells and neutrophils which in turn activate the immune gene expression in keratinocytes resulting in a phenotype similar to the one observed in early psoriasis and atopic dermatitis (Kobayashi et al, 2019 immunity; Hawerkamp, 2022 Skin health and disease).

4.5 The Phenotype of *Hdac1*^{Ci} mice might be caused by a disrupted epidermal barrier

As the barrier function of the epidermis is maintained and controlled by a balance of proliferation and differentiation of keratinocytes (L. Zhang, 2018) and since some of the gene we found to be deregulated, are directly or indirectly involved in the integrity of the epidermal barrier, we decided to further investigate the function of the epidermal barrier in mice expressing *Hdac1*^{Ci}. We measured the trans epidermal water loss of *Hdac1*$^{\Delta/\Delta ep\ Ci/+}$ mice compared to wildtype controls and revealed that, especially in *Hdac1*$^{\Delta/\Delta ep\ Ci/+}$ males, the TEWL was significantly increased. This confirmed our hypothesis of an epidermal barrier defect.

Further underlining the defective barrier, the previously described downregulation of *Spink5* in *Hdac1*^{Ci} mice also points towards a defective epidermal barrier since *Spink5* null mutants develop a lethal, severe ichthyosis with a loss of skin barrier function caused by spontaneous detachment of the strateum corneum (Hewett et al., 2005). Furthermore, the mRNA expression level of *Claudin3*, which is important for tight junction formation and therefore important for the integrity of the epidermal barrier, was upregulated in *Hdac1*^{Ci} mice. It was previously suggested that overexpression of *Claudin3* may be an attempt to overcompensate for the loss of cell adhesion due to other molecular changes (Heinzelmann-Schwarz et al., 2004). The single cell analysis additionally revealed a deregulation in lipid associated genes (Figure 27). As lipids are a core component of the physical epidermal barrier, changes in lipid composition were also previously shown to correlate with a defective epidermal barrier (Van Smeden & Bouwstra, 2016). The observed upregulation of *Cers4* is also a distinct indicator for a defective barrier, since Ito et al., 2017 showed a correlation between Cers4 upregulation in human patients with atopic dermatitis related impairment of the epidermal barrier function. In general most reports of an impaired epidermal barrier function are related to abnormalities in ceramide synthesis which have been shown to be a hallmark of atopic dermatitis (A. Y. Lee, 2020).

Furthermore, immunohistological staining of back skin biopsies in *Hdac1*$^{\Delta/\Delta ep\ Ci/Ci}$ mice revealed an activation of *Krt6* in the epidermis. Its upregulation was previously shown to be involved in several cellular processes like alteration of proliferation, cell adhesion, migration and inflammatory features of keratinocytes but also functions as a key early barrier alarmin and is an indicator for a defective barrier as its upregulation contributes to hyperproliferation and innate immune activation of keratinocytes in response to epidermal barrier breaches. *Krt6* is also considered as a biomarker psoriasis (Zhang et al., 2019). Our mouse model also displays two of the three main histological features of psoriasis with epidermal hyperproliferation and dermal leukocyte

infiltration. Immune related diseases like psoriasis and autoimmune blistering diseases (AIBDs) can cause an overactivation of the immune system which results in a defective epidermal barrier (Jiang et al., 2015; Stevens et al., 2019) but *vice versa* a defective epidermal barrier also causes the activation of the immune system as it is considered the initial step in the development of atopic dermatitis, a chronic inflammatory skin disease (B. E. Kim & Leung, 2018).

4.6 catalytically Genetic or pharmacological inhibition of HDAC1 in keratinocytes might cause mitotic errors and increased DNA damage

By immunolabeling of the skin of the *Hdac1*$^{\Delta/\Delta ep\ Ci/Ci}$ mouse, we observed higher levels of cGAS and increased DNA damage when compared to control samples. The finding correlates with previous studies showing that *cGas* expression can occur upon failed mitosis (Beck et al., 2021b) and after aging related accumulation of DNA damage (Lan et al., 2019). HDAC1 and HDAC2 inhibition has been previously shown to impair the correct mitotic process and cell cycle progression in different cell types (Senese et al., 2007; Wu et al., 2020; Xie et al., 2012). Furthermore, several studies were able to show that HDAC1 has a direct impact on the DNA damage response of the cell and that HDAC1 depleted cells are hypersensitive to DNA damaging agents (Miller et al., 2010a; Pao et al., 2020; Wu et al., 2020). In accordance with these studies our results suggest that overexpression of catalytically inactive HDAC1 also directly impacts mitotic and genomic stability of keratinocytes. To further elucidate this hypothesis, we switched to an *in vitro* system of human immortalized keratinocytes. Here we were able to validate the expression of the different transgenes as well as the knockdown of endogenous *HDAC1* (Figure 21) and investigated the different genotypes and treated wildtype keratinocytes with different HDAC inhibitors. Preliminary experiments, observing different transgenic keratinocyte cell lines stained with an antibody specific for mitotic cells, showed an increase of defective mitotic events in cells expressing catalytically inactive HDAC1 while endogenous HDAC1 is knocked down. A similar trend could be shown after the treatment of wildtype human keratinocytes with different HDAC1 inhibitors with a slight increase of abnormal mitotic cells. Treatment of wildtype keratinocytes with the HDAC inhibitor MS-275 additionally led to the increase in DNA damage foci which is in line with previous reports of DNA damage induction upon HDAC1 inhibition (J. H. Lee et al., 2010; Pao et al., 2020).

Furthermore, HDAC inhibition *via* MS-275 led to an increase of binucleated cells in human keratinocytes which could be interpreted as another indicator for dysfunctional mitosis upon HDAC1 inhibition since binucleated cells were shown to be formed mainly after failed cytokinesis. The vast majority of cells that fail to undergo cytokinesis undergo apoptosis instead of forming a

binucleated cell. The clinical relevance of binucleated cells is still controversial, since they are often accumulated in malignant tumours, but also occur in normal tissues (Nishimura et al., 2016).

Taken together, our results of inhibition of HDAC1 in human immortalized keratinocytes suggest that catalytically activity of HDAC1 directly impacts mitosis and the DNA damage response in keratinocytes, which would be consistent with the literature on catalytically inhibition in other cell types.

4.7 Conclusion and outlook

In this work we were able to establish a mouse model, where specifically in keratinocytes HDAC1 was replaced by catalytically inactive HDAC1 variants. Whereas the exchange by HDAC1 2S did not lead to skin abnormalities, the expression of catalytically inactive HDAC1 H141A (HDAC1^{Ci}) led to a deregulation of the differentiation and proliferation processes of keratinocytes. Disturbed epidermal homeostasis was characterized by hyperproliferation of keratinocytes, deregulation of genes and proteins involved in the process of differentiation and cornified envelope formation, as well as by an increase of the transepidermal water loss, indicating a barrier defect. We also showed an activation of the innate immune system in murine keratinocytes expressing *Hdac1*^{Ci} which is reminiscent of inflammatory skin diseases like psoriasis and atopic dermatitis. Moreover, we revealed that the deregulated epidermal differentiation process as well as the upregulation of the immune system correlate with a defective epidermal barrier in *Hdac1*^{CI} mice. Whether the expression of catalytically inactive HDAC1 directly causes an epidermal barrier dysfunction by deregulating epidermal differentiation and proliferation processes which results in an upregulation of the immune system or if the HDAC1 variant is directly responsible for the activation of the immune system which then in turn could be the cause of a disrupted epidermal barrier development remains unknown. An approach to test the hypothesis could be to cross the *Hdac1*$^{\Delta/\Delta ep\ Ci/+}$ mice into an immunosuppressed mouse strain such as *Rag1*$^{-/-}$. Alternatively, *Hdac1*$^{\Delta/\Delta ep\ Ci/+}$ mice could be treated with immunosuppressive agents such as corticosteroids or calcineurin inhibitors. These experiments could help clarify whether the immune system is directly involved in response to HDAC1 inhibition or just a consequence. Furthermore, we found evidence of increased DNA damage induction and the activation of the extranuclear DNA sensor *cGas* in our *Hdac1*$^{\Delta/\Delta ep\ Ci/Ci}$ mouse indicating a role of the catalytically activity of HDAC1 in mitotic and genomic integrity. Further pilot experiments with different transgenic human keratinocytes lines and the treatment of wildtype keratinocytes with HDAC inhibitors are also in line with these findings suggesting that the expression of catalytically inactive HDAC1 also has an impact on the DNA

damage response and the mitotic integrity of human keratinocytes. To further substantiate the link between HDAC1 inhibition and aberrant mitosis, affected genome stability and expression of pro-inflammatory cytokines, future experiments are necessary. Thereby, both human keratinocytes expressing catalytically inactive HDAC1 as well as keratinocytes isolated from *Hdac1*$^{\Delta/\Delta ep\ Ci/Ci}$ mice could be used to investigate nuclear morphology during mitosis, as well as to perform transcriptome analyses.

It still remains to be elucidated if and how our findings can be translated to the human epidermal system and what they imply about autoinflammatory skin diseases like atopic dermatitis or psoriasis. To tackle this objective our lab plans to establish a 3D keratinocyte culture. It has been previously shown that primary and immortalized human keratinocytes together with a dermal compartment including immune cells can be used to establish *in vitro* differentiated and immunocompetent organotypic skin equivalent models (Van Den Bogaard et al., 2014; Wagner et al., 2018). This could be helpful to investigate if the results obtained in our mouse system are translatable into the human model. A 3D organoid model additionally allows targeted adjustments in complexity by adding or removing certain defined cell types to the organotypic skin (J. Kim et al., 2020). These experiments could be complemented by analyses of human skin diseases, where the expression levels of HDAC1 and HDAC2 could be determined by immunolabeling and correlated with disease severity.

5. References

Alberts, B., Johnson, A. D., Lewis, J., Morgan, D., Raff, M., Roberts, K., & Walter, P. (2014). *Molecular Biology of Cell*. *5*, 591–595.

Allis, C. D., & Jenuwein, T. (2016). The molecular hallmarks of epigenetic control. *Nature Reviews Genetics 2016 17:8*, *17*(8), 487–500. https://doi.org/10.1038/nrg.2016.59

Alonso, L., & Fuchs, E. (2003). Stem cells of the skin epithelium. *Proceedings of the National Academy of Sciences*, *100*(suppl 1), 11830–11835. https://doi.org/10.1073/PNAS.1734203100

Bannister, A. J., & Kouzarides, T. (2011). Regulation of chromatin by histone modifications. *Cell Research 2011 21:3*, *21*(3), 381–395. https://doi.org/10.1038/cr.2011.22

Baroni, A., Buommino, E., De Gregorio, V., Ruocco, E., Ruocco, V., & Wolf, R. (2012). Structure and function of the epidermis related to barrier properties. *Clinics in Dermatology*, *30*(3), 257–262. https://doi.org/10.1016/j.clindermatol.2011.08.007

Beck, M. A., Fischer, H., Grabner, L. M., Groffics, T., Winter, M., Tangermann, S., Meischel, T., Zaussinger-Haas, B., Wagner, P., Fischer, C., Folie, C., Arand, J., Schöfer, C., Ramsahoye, B., Lagger, S., Machat, G., Eisenwort, G., Schneider, S., Podhornik, A., … Seiser, C. (2021a). DNA hypomethylation leads to cGAS-induced autoinflammation in the epidermis. *The EMBO Journal*, *40*(22), e108234. https://doi.org/10.15252/EMBJ.2021108234

Beck, M. A., Fischer, H., Grabner, L. M., Groffics, T., Winter, M., Tangermann, S., Meischel, T., Zaussinger-Haas, B., Wagner, P., Fischer, C., Folie, C., Arand, J., Schöfer, C., Ramsahoye, B., Lagger, S., Machat, G., Eisenwort, G., Schneider, S., Podhornik, A., … Seiser, C. (2021b). DNA hypomethylation leads to cGAS-induced autoinflammation in the epidermis. *The EMBO Journal*, *40*(22), e108234. https://doi.org/10.15252/EMBJ.2021108234

Bernstein, B. E., Meissner, A., & Lander, E. S. (2007). The mammalian epigenome. *Cell*, *128*(4), 669–681. https://doi.org/10.1016/J.CELL.2007.01.033

Biterge, B. (2016). A mini review on post-translational histone modifications. *MOJ Cell Science & Report*, *Volume 3*(Issue 1). https://doi.org/10.15406/MOJCSR.2016.03.00047

Biterge, B., & Schneider, R. (2014). Histone variants: key players of chromatin. *Cell and Tissue Research*, *356*(3), 457–466. https://doi.org/10.1007/S00441-014-1862-4

Blanpain, C., & Fuchs, E. (2009). Epidermal homeostasis: a balancing act of stem cells in the skin. *Nature Reviews. Molecular Cell Biology*, *10*(3), 207. https://doi.org/10.1038/NRM2636

Bowman, G. D., & Poirier, M. G. (2015). Post-Translational Modificationsof Histones ThatInfluence Nucleosome Dynamics. *Chemical Reviews*, *115*(6), 2274. https://doi.org/10.1021/CR500350X

Brunmeir, R., Lagger, S., & Seiser, C. (2009). Histone deacetylase 1 and 2-controlled embryonic development and cell differentiation. *International Journal of Developmental Biology*, *53*(2–3), 275–289. https://doi.org/10.1387/IJDB.082649RB

Cavalli, G., & Heard, E. (2019). Advances in epigenetics link genetics to the environment and disease. *Nature*, *571*(7766), 489–499. https://doi.org/10.1038/S41586-019-1411-0

Chambers, E. S., & Vukmanovic-Stejic, M. (2020). Skin barrier immunity and ageing. *Immunology*, *160*(2), 116. https://doi.org/10.1111/IMM.13152

Chen, H. P., Zhao, Y. T., & Zhao, T. C. (2015). Histone deacetylases and mechanisms of regulation of gene expression. *Critical Reviews in Oncogenesis*, *20*(1–2), 35–47. https://doi.org/10.1615/CRITREVONCOG.2015012997

Chiocca, S., & Segré, C. V. (2011). Regulating the regulators: the post-translational code of class I HDAC1 and HDAC2. *Journal of Biomedicine & Biotechnology*, *2011*. https://doi.org/10.1155/2011/690848

Choudhary, C., Kumar, C., Gnad, F., Nielsen, M. L., Rehman, M., Walther, T. C., Olsen, J. V., & Mann, M. (2009). Lysine acetylation targets protein complexes and co-regulates major cellular functions. *Science (New York, N.Y.)*, *325*(5942), 834–840. https://doi.org/10.1126/SCIENCE.1175371

Dawson, M. A., & Kouzarides, T. (2012). Cancer epigenetics: from mechanism to therapy. *Cell*, *150*(1), 12–27. https://doi.org/10.1016/J.CELL.2012.06.013

Dupont, C., Armant, D. R., & Brenner, C. A. (2009). Epigenetics: Definition, Mechanisms and Clinical Perspective. *Seminars in Reproductive Medicine*, *27*(5), 351. https://doi.org/10.1055/S-0029-1237423

Ellmeier, W., & Seiser, C. (2018). Histone deacetylase function in CD4+ T cells. *Nature Reviews Immunology 2018 18:10*, *18*(10), 617–634. https://doi.org/10.1038/s41577-018-0037-z

Felsenfeld, G. (2014). A brief history of epigenetics. *Cold Spring Harbor Perspectives in Biology*,

6(1). https://doi.org/10.1101/CSHPERSPECT.A018200

Fuchs, E., & Horsley, V. (2008). More than one way to skin . . . *Genes & Development*, *22*(8), 976. https://doi.org/10.1101/GAD.1645908

Galliano, M. F., Roccasecca, R. M., Descargues, P., Micheloni, A., Levy, E., Zambruno, G., D'Alessio, M., & Hovnanian, A. (2005). Characterization and expression analysis of the Spink5 gene, the mouse ortholog of the defective gene in Netherton syndrome. *Genomics*, *85*(4), 483–492. https://doi.org/10.1016/J.YGENO.2005.01.001

Gibney, E. R., & Nolan, C. M. (2010). Epigenetics and gene expression. *Heredity*, *105*(1), 4–13. https://doi.org/10.1038/HDY.2010.54

Gonzales, K., & Fuchs, E. (2017). Skin and Its Regenerative Powers: An Alliance between Stem Cells and Their Niche. *Developmental Cell*, *43*(4), 387–401. https://doi.org/10.1016/J.DEVCEL.2017.10.001

Greer, E. L., & Shi, Y. (2012). Histone methylation: a dynamic mark in health, disease and inheritance. *Nature Reviews. Genetics*, *13*(5), 343. https://doi.org/10.1038/NRG3173

Hagelkruys, A., Mattes, K., Moos, V., Rennmayr, M., Ringbauer, M., Sawicka, A., & Seiser, C. (2016a). Essential Nonredundant Function of the Catalytic Activity of Histone Deacetylase 2 in Mouse Development. *Molecular and Cellular Biology*, *36*(3), 462. https://doi.org/10.1128/MCB.00639-15

Hagelkruys, A., Mattes, K., Moos, V., Rennmayr, M., Ringbauer, M., Sawicka, A., & Seiser, C. (2016b). Essential Nonredundant Function of the Catalytic Activity of Histone Deacetylase 2 in Mouse Development. *Molecular and Cellular Biology*, *36*(3), 462. https://doi.org/10.1128/MCB.00639-15

Hassig, C. A., Tong, J. K., Fleischer, T. C., Owa, T., Grable, P. G., Ayer, D. E., & Schreiber, S. L. (1998). A role for histone deacetylase activity in HDAC1-mediated transcriptional repression. *Proceedings of the National Academy of Sciences of the United States of America*, *95*(7), 3519–3524. https://doi.org/10.1073/PNAS.95.7.3519

Heath, W. R., & Carbone, F. R. (2013). The skin-resident and migratory immune system in steady state and memory: innate lymphocytes, dendritic cells and T cells. *Nature Immunology 2013 14:10*, *14*(10), 978–985. https://doi.org/10.1038/NI.2680

Heerboth, S., Lapinska, K., Snyder, N., Leary, M., Rollinson, S., & Sarkar, S. (2014). Use of

Epigenetic Drugs in Disease: An Overview. *Genetics & Epigenetics*, *6*(6), 9. https://doi.org/10.4137/GEG.S12270

Heinzelmann-Schwarz, V. A., Gardiner-Garden, M., Henshall, S. M., Scurry, J., Scolyer, R. A., Davies, M. J., Heinzelmann, M., Kalish, L. H., Bali, A., Kench, J. G., Edwards, L. S., Vanden Bergh, P. M., Hacker, N. F., Sutherland, R. L., & O'Brien, P. M. (2004). Overexpression of the Cell Adhesion Molecules DDR1, Claudin 3, and Ep-CAM in Metaplastic Ovarian Epithelium and Ovarian Cancer. *Clinical Cancer Research*, *10*(13), 4427–4436. https://doi.org/10.1158/1078-0432.CCR-04-0073

Henikoff, S., & Smith, M. M. (2015). Histone Variants and Epigenetics. *Cold Spring Harbor Perspectives in Biology*, *7*(1). https://doi.org/10.1101/CSHPERSPECT.A019364

Hess, L. (2017). *Dissection of catalytic and non-catalytic functions of HDAC1 and HDAC2*. University of Vienna.

Hewett, D. R., Simons, A. L., Mangan, N. E., Jolin, H. E., Green, S. M., Fallon, P. G., & McKenzie, A. N. J. (2005). Lethal, neonatal ichthyosis with increased proteolytic processing of filaggrin in a mouse model of Netherton syndrome. *Human Molecular Genetics*, *14*(2), 335–346. https://doi.org/10.1093/HMG/DDI030

Hodawadekar, S. C., & Marmorstein, R. (2007). Chemistry of acetyl transfer by histone modifying enzymes: structure, mechanism and implications for effector design. *Oncogene*, *26*(37), 5528–5540. https://doi.org/10.1038/SJ.ONC.1210619

Holoch, D., & Moazed, D. (2015). RNA-mediated epigenetic regulation of gene expression. *Nature Reviews. Genetics*, *16*(2), 71–84. https://doi.org/10.1038/NRG3863

Hrabeta, J., Stiborov, M., Adam, V., Kizek, R., & Eckschlager, T. (2014). Histone deacetylase inhibitors in cancer therapy. A review. *Biomedical Papers of the Medical Faculty of the University Palacky, Olomouc, Czechoslovakia*, *158*(2), 161–169. https://doi.org/10.5507/BP.2013.085

Ito, S., Ishikawa, J., Naoe, A., Yoshida, H., Hachiya, A., Fujimura, T., Kitahara, T., & Takema, Y. (2017). Ceramide synthase 4 is highly expressed in involved skin of patients with atopic dermatitis. *Journal of the European Academy of Dermatology and Venereology : JEADV*, *31*(1), 135–141. https://doi.org/10.1111/JDV.13777

Jamaladdin, S., Kelly, R. D. W., O'Regan, L., Dovey, O. M., Hodson, G. E., Millard, C. J., Portolano, N., Fry, A. M., Schwabe, J. W. R., & Cowley, S. M. (2014). Histone deacetylase

(HDAC) 1 and 2 are essential for accurate cell division and the pluripotency of embryonic stem cells. *Proceedings of the National Academy of Sciences of the United States of America*, *111*(27), 9840–9845. https://doi.org/10.1073/PNAS.1321330111

Jiang, S., Hinchliffe, T. E., & Wu, T. (2015). Biomarkers of An Autoimmune Skin Disease—Psoriasis. *Genomics, Proteomics & Bioinformatics*, *13*(4), 224. https://doi.org/10.1016/J.GPB.2015.04.002

Jurkin, J., Zupkovitz, G., Lagger, S., Grausenburger, R., Hagelkruys, A., Kenner, L., & Seiser, C. (2011). Distinct and redundant functions of histone deacetylases HDAC1 and HDAC2 in proliferation and tumorigenesis. *Cell Cycle (Georgetown, Tex.)*, *10*(3), 406–412. https://doi.org/10.4161/CC.10.3.14712

Kalinin, A., Marekov, L. N., & Steinert, P. M. (2001). Assembly of the epidermal cornified cell envelope. *Journal of Cell Science*, *114*(17), 3069–3070. https://doi.org/10.1242/JCS.114.17.3069

Khier, H., Bartl, S., Schuettengruber, B., & Seiser, C. (1999). Molecular cloning and characterization of the mouse histone deacetylase 1 gene: integration of a retrovirus in 129SV mice. *Biochimica et Biophysica Acta*, *1489*(2–3), 365–373. https://doi.org/10.1016/S0167-4781(99)00203-1

Kim, B. E., & Leung, D. Y. M. (2018). Significance of Skin Barrier Dysfunction in Atopic Dermatitis. *Allergy, Asthma & Immunology Research*, *10*(3), 207. https://doi.org/10.4168/AAIR.2018.10.3.207

Kim, J. K., Samaranayake, M., & Pradhan, S. (2008). Epigenetic mechanisms in mammals. *Cellular and Molecular Life Sciences 2008 66:4*, *66*(4), 596–612. https://doi.org/10.1007/S00018-008-8432-4

Kim, J., Koo, B. K., & Knoblich, J. A. (2020). Human organoids: model systems for human biology and medicine. *Nature Reviews Molecular Cell Biology 2020 21:10*, *21*(10), 571–584. https://doi.org/10.1038/s41580-020-0259-3

Klas, K., Copic, D., Direder, M., Laggner, M., Prucksamas, P. S., Gruber, F., Ankersmit, H. J., & Mildner, M. (2021). Transcriptional differences in lipid-metabolizing enzymes in murine sebocytes derived from sebaceous glands of the skin and preputial glands. *International Journal of Molecular Sciences*, *22*(21). https://doi.org/10.3390/IJMS222111631/S1

Klug, W. S., Cummings, M. R., Spencer, C. A., Palladino, M. A., & Killian, D. (2019). *Concepts*

of Genetics. Pearson Education Canada.

Kouzarides, T. (2007). Chromatin modifications and their function. *Cell*, *128*(4), 693–705. https://doi.org/10.1016/J.CELL.2007.02.005

Lagger, G., O'Carroll, D., Rembold, M., Khier, H., Tischler, J., Weitzer, G., Schuettengruber, B., Hauser, C., Brunmeir, R., Jenuwein, T., & Seiser, C. (2002a). Essential function of histone deacetylase 1 in proliferation control and CDK inhibitor repression. *EMBO Journal*, *21*(11), 2672–2681. https://doi.org/10.1093/EMBOJ/21.11.2672

Lagger, G., O'Carroll, D., Rembold, M., Khier, H., Tischler, J., Weitzer, G., Schuettengruber, B., Hauser, C., Brunmeir, R., Jenuwein, T., & Seiser, C. (2002b). Essential function of histone deacetylase 1 in proliferation control and CDK inhibitor repression. *The EMBO Journal*, *21*(11), 2672–2681. https://doi.org/10.1093/EMBOJ/21.11.2672

Lan, Y. Y., Heather, J. M., Eisenhaure, T., Garris, C. S., Lieb, D., Raychowdhury, R., & Hacohen, N. (2019). Extranuclear DNA accumulates in aged cells and contributes to senescence and inflammation. *Aging Cell*, *18*(2). https://doi.org/10.1111/ACEL.12901

LeBoeuf, M., Terrell, A., Trivedi, S., Sinha, S., Epstein, J. A., Olson, E. N., Morrisey, E. E., & Millar, S. E. (2010). Hdac1 and Hdac2 act redundantly to control p63 and p53 functions in epidermal progenitor cells. *Developmental Cell*, *19*(6), 807. https://doi.org/10.1016/J.DEVCEL.2010.10.015

Lee, A. Y. (2020). Molecular Mechanism of Epidermal Barrier Dysfunction as Primary Abnormalities. *International Journal of Molecular Sciences*, *21*(4). https://doi.org/10.3390/IJMS21041194

Lee, J. H., Choy, M. L., Ngo, L., Foster, S. S., & Marks, P. A. (2010). Histone deacetylase inhibitor induces DNA damage, which normal but not transformed cells can repair. *Proceedings of the National Academy of Sciences of the United States of America*, *107*(33), 14639–14644. https://doi.org/10.1073/PNAS.1008522107/SUPPL_FILE/PNAS.201008522SI.PDF

Li, B., Carey, M., & Workman, J. L. (2007). The role of chromatin during transcription. *Cell*, *128*(4), 707–719. https://doi.org/10.1016/J.CELL.2007.01.015

Li, E., & Zhang, Y. (2014). DNA Methylation in Mammals. *Cold Spring Harbor Perspectives in Biology*, *6*(5). https://doi.org/10.1101/CSHPERSPECT.A019133

Li, Zhaoyu, Gadue, P., Chen, K., Jiao, Y., Tuteja, G., Schug, J., Li, W., & Kaestner, K. H. (2012).

Foxa2 and H2A.Z Mediate Nucleosome Depletion during Embryonic Stem Cell Differentiation. *Cell*, *151*(7), 1608–1616. https://doi.org/10.1016/J.CELL.2012.11.018

Li, Zhiming, & Zhu, W. G. (2014). Targeting Histone Deacetylases for Cancer Therapy: From Molecular Mechanisms to Clinical Implications. *International Journal of Biological Sciences*, *10*(7), 757. https://doi.org/10.7150/IJBS.9067

Liu, X. T., Shi, Z. R., Lu, S. Y., Hong, D., Qiu, X. N., Tan, G. Z., Xiong, H., Guo, Q., & Wang, L. (2022). Enhanced Migratory Ability of Neutrophils Toward Epidermis Contributes to the Development of Psoriasis via Crosstalk With Keratinocytes by Releasing IL-17A. *Frontiers in Immunology*, *13*, 1094. https://doi.org/10.3389/FIMMU.2022.817040/BIBTEX

Ma, P., & Schultz, R. M. (2016). HDAC1 and HDAC2 in mouse oocytes and preimplantation embryos: Specificity versus compensation. *Cell Death & Differentiation*, *23*(7), 1119–1127. https://doi.org/10.1038/cdd.2016.31

Miller, K. M., Tjeertes, J. V., Coates, J., Legube, G., Polo, S. E., Britton, S., & Jackson, S. P. (2010a). Human HDAC1 and HDAC2 function in the DNA-damage response to promote DNA nonhomologous end-joining. *Nature Structural & Molecular Biology 2010 17:9*, *17*(9), 1144–1151. https://doi.org/10.1038/nsmb.1899

Miller, K. M., Tjeertes, J. V., Coates, J., Legube, G., Polo, S. E., Britton, S., & Jackson, S. P. (2010b). Human HDAC1 and HDAC2 function in the DNA-damage response to promote DNA nonhomologous end-joining. *Nature Structural & Molecular Biology*, *17*(9), 1144–1151. https://doi.org/10.1038/NSMB.1899

Mirabella, A. C., Foster, B. M., & Bartke, T. (2016). Chromatin deregulation in disease. *Chromosoma*, *125*(1), 75–93. https://doi.org/10.1007/s00412-015-0530-0

Moore, L. D., Le, T., & Fan, G. (2013). DNA methylation and its basic function. *Neuropsychopharmacology : Official Publication of the American College of Neuropsychopharmacology*, *38*(1), 23–38. https://doi.org/10.1038/NPP.2012.112

Moser, Mirjam A. (2011). *Master Thesis Mirjam Moster*.

Moser, Mirjam A. (2015). *Chromatin Modifiers as Regulator of Mouse Epidermal Development and Tumorgenisis*.

Moser, Mirjam Andrea, Hagelkruys, A., & Seiser, C. (2014). Transcription and beyond: the role of mammalian class I lysine deacetylases. *Chromosoma*, *123*(1), 67.

https://doi.org/10.1007/S00412-013-0441-X

Nakayama, J. I., & Hayakawa, T. (2011). Physiological roles of class I HDAC complex and histone demethylase. *Journal of Biomedicine & Biotechnology*, *2011*. https://doi.org/10.1155/2011/129383

Nestle, F. O., Di Meglio, P., Qin, J. Z., & Nickoloff, B. J. (2009). Skin immune sentinels in health and disease. *Nature Reviews. Immunology*, *9*(10), 679. https://doi.org/10.1038/NRI2622

Pao, P. C., Patnaik, D., Watson, L. A., Gao, F., Pan, L., Wang, J., Adaikkan, C., Penney, J., Cam, H. P., Huang, W. C., Pantano, L., Lee, A., Nott, A., Phan, T. X., Gjoneska, E., Elmsaouri, S., Haggarty, S. J., & Tsai, L. H. (2020). HDAC1 modulates OGG1-initiated oxidative DNA damage repair in the aging brain and Alzheimer's disease. *Nature Communications 2020 11:1*, *11*(1), 1–17. https://doi.org/10.1038/s41467-020-16361-y

Pflum, M. K. H., Tong, J. K., Lane, W. S., & Schreiber, S. L. (2001). Histone deacetylase 1 phosphorylation promotes enzymatic activity and complex formation. *The Journal of Biological Chemistry*, *276*(50), 47733–47741. https://doi.org/10.1074/JBC.M105590200

Portela, A., & Esteller, M. (2010a). Epigenetic modifications and human disease. *Nature Biotechnology 2010 28:10*, *28*(10), 1057–1068. https://doi.org/10.1038/nbt.1685

Portela, A., & Esteller, M. (2010b). Epigenetic modifications and human disease. *Nature Biotechnology 2010 28:10*, *28*(10), 1057–1068. https://doi.org/10.1038/nbt.1685

Ramazi, S., Allahverdi, A., & Zahiri, J. (2038). Review Evaluation of post-translational modifications in histone proteins: A review on histone modification defects in developmental and neurological disorders. *Journal of Biosciences*. https://doi.org/10.1007/s12038-020-00099-2

Saksouk, N., Simboeck, E., & Déjardin, J. (2015). Constitutive heterochromatin formation and transcription in mammals. *Epigenetics & Chromatin*, *8*(1). https://doi.org/10.1186/1756-8935-8-3

Sawicka, A., & Seiser, C. (2012). Histone H3 phosphorylation - a versatile chromatin modification for different occasions. *Biochimie*, *94*(11), 2193–2201. https://doi.org/10.1016/J.BIOCHI.2012.04.018

Sawicka, A., & Seiser, C. (2014). Sensing core histone phosphorylation — A matter of perfect timing. *Biochimica et Biophysica Acta (BBA) - Gene Regulatory Mechanisms*, *1839*(8), 711–

718. https://doi.org/10.1016/J.BBAGRM.2014.04.013

Senese, S., Zaragoza, K., Minardi, S., Muradore, I., Ronzoni, S., Passafaro, A., Bernard, L., Draetta, G. F., Alcalay, M., Seiser, C., & Chiocca, S. (2007). Role for Histone Deacetylase 1 in Human Tumor Cell Proliferation. *Molecular and Cellular Biology*, *27*(13), 4784. https://doi.org/10.1128/MCB.00494-07

Spange, S., Wagner, T., Heinzel, T., & Krämer, O. H. (2009). Acetylation of non-histone proteins modulates cellular signalling at multiple levels. *International Journal of Biochemistry and Cell Biology*, *41*(1), 185–198. https://doi.org/10.1016/J.BIOCEL.2008.08.027

Stevens, N. E., Cowin, A. J., & Kopecki, Z. (2019). Skin barrier and autoimmunity—mechanisms and novel therapeutic approaches for autoimmune blistering diseases of the skin. *Frontiers in Immunology*, *10*, 1089. https://doi.org/10.3389/FIMMU.2019.01089/BIBTEX

Tonna, S., El-Osta, A., Cooper, M. E., & Tikellis, C. (2010). Metabolic memory and diabetic nephropathy: potential role for epigenetic mechanisms. *Nature Reviews. Nephrology*, *6*(6), 332–341. https://doi.org/10.1038/NRNEPH.2010.55

Van Den Bogaard, E. H., Tjabringa, G. S., Joosten, I., Vonk-Bergers, M., Van Rijssen, E., Tijssen, H. J., Erkens, M., Schalkwijk, J., & Koenen, H. J. P. M. (2014). Crosstalk between keratinocytes and T cells in a 3D microenvironment: a model to study inflammatory skin diseases. *The Journal of Investigative Dermatology*, *134*(3), 719–727. https://doi.org/10.1038/JID.2013.417

Van Smeden, J., & Bouwstra, J. A. (2016). Stratum Corneum Lipids: Their Role for the Skin Barrier Function in Healthy Subjects and Atopic Dermatitis Patients. *Current Problems in Dermatology*, *49*, 8–26. https://doi.org/10.1159/000441540

Volle, C., & Dalal, Y. (2014). Histone variants: the tricksters of the chromatin world. *Current Opinion in Genetics & Development*, *25*(1), 8–14. https://doi.org/10.1016/J.GDE.2013.11.006

Waddington, C. H. (2012). The epigenotype. 1942. *International Journal of Epidemiology*, *41*(1), 10–13. https://doi.org/10.1093/IJE/DYR184

Wagner, T., Gschwandtner, M., Strajeriu, A., Elbe-Bürger, A., Grillari, J., Grillari-Voglauer, R., Greiner, G., Golabi, B., Tschachler, E., & Mildner, M. (2018). Establishment of keratinocyte cell lines from human hair follicles. *Scientific Reports*, *8*(1). https://doi.org/10.1038/S41598-018-31829-0

Waterland, R. A. (2006). Epigenetic mechanisms and gastrointestinal development. *The Journal of Pediatrics*, *149*(5 Suppl). https://doi.org/10.1016/J.JPEDS.2006.06.064

Wickett, R. R., & Visscher, M. O. (2006). Structure and function of the epidermal barrier. *American Journal of Infection Control*, *34*(10), S98–S110. https://doi.org/10.1016/J.AJIC.2006.05.295

Winter, M., Moser, M. A., Meunier, D., Fischer, C., Machat, G., Mattes, K., Lichtenberger, B. M., Brunmeir, R., Weissmann, S., Murko, C., Humer, C., Meischel, T., Brosch, G., Matthias, P., Sibilia, M., & Seiser, C. (2013a). Divergent roles of HDAC1 and HDAC2 in the regulation of epidermal development and tumorigenesis. *The EMBO Journal*, *32*(24), 3176–3191. https://doi.org/10.1038/EMBOJ.2013.243

Winter, M., Moser, M. A., Meunier, D., Fischer, C., Machat, G., Mattes, K., Lichtenberger, B. M., Brunmeir, R., Weissmann, S., Murko, C., Humer, C., Meischel, T., Brosch, G., Matthias, P., Sibilia, M., & Seiser, C. (2013b). Divergent roles of HDAC1 and HDAC2 in the regulation of epidermal development and tumorigenesis. *The EMBO Journal*, *32*(24), 3176–3191. https://doi.org/10.1038/EMBOJ.2013.243

Wu, C.-C., Jin, L.-W., Wang, I.-F., Wei, W.-Y., Ho, P.-C., Liu, Y.-C., & Tsai, K.-J. (2020). HDAC1 dysregulation induces aberrant cell cycle and DNA damage in progress of TDP-43 proteinopathies. *EMBO Molecular Medicine*, *12*(6), e10622. https://doi.org/10.15252/EMMM.201910622

Xie, H. J., Noh, J. H., Kim, J. K., Jung, K. H., Eun, J. W., Bae, H. J., Kim, M. G., Chang, Y. G., Lee, J. Y., Park, H., & Nam, S. W. (2012). HDAC1 Inactivation Induces Mitotic Defect and Caspase-Independent Autophagic Cell Death in Liver Cancer. *PLoS ONE*, *7*(4), 34265. https://doi.org/10.1371/JOURNAL.PONE.0034265

Yoon, S., & Eom, G. H. (2016). HDAC and HDAC Inhibitor: From Cancer to Cardiovascular Diseases. *Chonnam Medical Journal*, *52*(1), 1–11. https://doi.org/10.4068/cmj.2016.52.1.1

Zhang, L. (2018). Keratins in Skin Epidermal Development and Diseases. *Keratin*. https://doi.org/10.5772/INTECHOPEN.79050

Zhang, L. J. (2019). Type1 Interferons Potential Initiating Factors Linking Skin Wounds With Psoriasis Pathogenesis. *Frontiers in Immunology*, *10*(JUN), 1440. https://doi.org/10.3389/FIMMU.2019.01440

6. Table of Figures